[redacted] DECLASSIFIED

BNWL-117

C-93a, Advanced Concepts for Future Application–Reactor Experiments (M-3679, 41st Ed.)

COMPARISON OF PLUTONIUM, U^{233} AND U^{235} FUELING FOR THE 710 REACTOR

By

C. E. Leach

Reactor Engineering Section
Reactor and Materials Technology Department

and

W. W. Little, Jr., and L. L. Maas

Reactor Physics Section
Physics and Instruments Department

November, 1965

[redacted] This [redacted] Restricted Data [redacted] Atomic Energy Act [redacted] disclosure of its contents to an unauthorized person prohibited.

PACIFIC NORTHWEST LABORATORY
RICHLAND, WASHINGTON

TABLE OF CONTENTS

[redacted]

TABLE OF CONTENTS (contd)

COMPARISON OF PLUTONIUM, U^{233} AND U^{235} FUELING FOR THE 710 REACTOR

1.0 INTRODUCTION

This report presents the results of a comparative study of U^{235}, U^{233}, and plutonium fueling of a fast compact reactor. It is well known that the appreciably lower critical masses of plutonium and U^{233} fast reactor systems (compared to U^{235}) offer a potential for design improvements which might take the form of reductions in size and weight for given power and endurance, improved fuel stability through lowering of the fissile content, or improved endurances through greater control flexibility. It is also recognized that the magnitude of improvement which may actually be realized by fueling with plutonium or U^{233} fuel in a particular reactor type is subject to limitations imposed by the requirements for heat transfer, coolant flow, reactivity control, and fuel stability. Although some calculations have previously been made to compare fuels in generalized or simplified reactor models,[1, 2] a more specific evaluation of the effect of the subject fuels on reactor core design and performance was needed, for the purpose of (a) assessing the incentive for development of plutonium or U^{233} for use in fast compact reactors, (b) defining the technological problems unique to these fuels, and (c) determining deficiencies in current technology of the fuels and materials of interest.

The reactor chosen as the basis for this comparison was the 710 Test Reactor, a compact, high temperature, gas-cooled, nominally 10 MW_t fast reactor. The 710 Test Reactor is of sufficient power output to impose realistic engineering constraints on core size determination.

2.0 SCOPE OF STUDY

The 710 Test Reactor is a compact, cermet fueled, beryllium reflected, gas-cooled fast reactor controlled by rotating drums in the reflector. The fuel elements, with a nominal composition of 30 vol% $U^{235}O_2$ in tungsten matrix, are of hexagonal shape, pierced by circular

coolant passages uniformly spaced on a triangular lattice. Tantalum cladding is used. The coolant is a mixture of 90 vol% Ne–10 vol% He. Endurance of the initial 710 Test Reactor core is presently taken to be 1000 hr.

The principal objectives of this study were defined as:

- To determine the reductions in core size and weight, for equal power, endurance, and coolant pressure ratio, made possible by using plutonium or U^{233} fuel instead of U^{235}.
- To determine if an increase in endurance (i.e., available control span), for equal power, is made possible by using plutonium or U^{233} fuel instead of U^{235}.

Secondary objectives were to consider the performance of designs using more dilute cermet fuel and to consider the influence of the coolant pressure ratio on core design.

For the purpose of meeting the first objectives, three "design point" reactor cores were derived, to represent the three fuels. The design point conditions, which were held constant for this comparison, are given in Table 2.1.

TABLE 2.1

STUDY DESIGN POINT

Power	10 MW_t
Coolant	10 vol% He–90 vol% Ne
Inlet Temperature	635 °F
Exit Temperature	3500 °F
Inlet Total Pressure	833.3 psia
Plenum-To-Plenum Total Pressure Ratio	0.95
Minimum Bulk Average Reynolds Number	8000
Maximum Temperature of Average Tube	3800 °F
Cermet Composition	50 vol% fuel; 50 vol % W

In the case of both uranium fuels, the cermet composition was taken as UO_2-W. Because plutonium nitride appears to have a melting point comparable to that of uranium dioxide, whereas the more familiar stable plutonium oxide

materials melt near the operating temperature of the 710 reactor fuel, a PuN-W cermet was used for the plutonium fueled cores.

The study, however, was not limited to the design point conditions, but consisted of parametric nuclear analyses and thermal analyses from which the design point cores were derived and investigated in more detail. The approach used was to study a spectrum of unclad critical reactor cores over the following ranges of characteristics: L/D = 1, cermet composition 30 to 70 vol% fuel, core void fraction 0.2 to 0.5, with $U^{235}O_2$, $U^{233}O_2$, and PuN fuel. Since the volume fraction of tantalum clad is a function of core size, coolant tube size and number, and assumed fuel subdivision, the effect of tantalum was considered separately in the nuclear analysis.

Critical core sizes from the nuclear analyses were then transformed into engineering models for thermal analysis. The models used were subjected to several restrictions to reduce the scope of investigation to practical proportions. The restrictions are set forth in Table 2.2 as reasonable values which might be expected in a final design.

TABLE 2.2

GEOMETRIC DEFINITION OF CORE

- The fuel rod dimension across the flats is between 1.0 to 1.5 in. The final size is dictated with regard to the uniform distribution of coolant passages and an integral number of rods in the core.
- Tube wall thickness 0.008 in.
- Fuel rod clad 0.010 in. thick
- The cermets are 95% of theoretical density
- The spacing between rods is 4% of the flats dimension
- Coolant inlet loss coefficient is 1.5 channel velocity heads
- Coolant exit loss coefficient is 1.0 channel velocity heads
- The friction coefficient is 135% of that found in the literature

Other more detailed assumptions concerning the model are set forth in Appendix B.

[redacted]

The parametric engineering analyses were made using the simplifying assumption of uniform radial power distribution and uniform distribution of coolant tubes (spacing and size). The range of coolant pressure ratio considered was 0.75 to 1.0, and a Reynolds number of < 8000 was allowed, but the other fluid and thermal conditions of Table 2.1 were met. The analyses were performed utilizing two digital computer codes written for this work. [3, 4] To account for the effect of tantalum on the core designs, it was necessary to make an initial thermal analysis of unclad cores to determine the number and size of tubes required to meet all design conditions except total pressure ratio and cermet composition. The amount of tantalum in these cores was then determined, and its effect on critical size found by interpolation from the nuclear analyses. A second engineering analysis was then performed on the adjusted core sizes to establish core designs meeting both nuclear and thermal requirements.

For the design point cores, the models were modified from the parametric study to recognize the radial power shape and permit coolant tube size zoning to flatten the radial temperature distribution. Eight radial zones of coolant tube size were allowed.

Separate evaluations were made of the effectiveness of reflector control, of core endurance and control requirements, and of the reactivity coefficients of principal interest. An attempt was also made to define cores of size equal to the U^{235} fueled core, but with increased diluent (tungsten) in the cermet; however, this required in excess of 75 vol% tungsten and it was considered to be unlikely that a lower fuel concentration would be essential to achieving high fuel endurance. An attempt was also made to define a minimum size design point core on the basis of fuel decomposition at high temperature, but this could not be defined at tungsten content $\geq$ 30 vol% in the cermet because of the high thermal conductivity. At lower tungsten content, the thermal model of the cermet fuel becomes questionable.

3.0 RESULTS

3.1 SUMMARY OF MAJOR RESULTS

The principal results of this study are the comparisons of the "design point" cores for the three fuels, which serve to illustrate the incentives for

using plutonium or U^{233} fuel. These comparisons, in terms of core weight, volume, and diameter, are presented in Figures 3.1, 3.2, and 3.3, respectively, as plots versus the nonfueled core volume fraction (1 - cermet fraction). The design point cores with coolant distribution zoned to match radial power profile are shown as circles on these figures. Selected characteristics of these cores are listed in Table 3.1, and a more detailed description is presented in Section 3.2. The 0.95 pressure ratio line intersection in

TABLE 3.1

COMPARISON OF "DESIGN POINT" CORES

	PuN	$U^{233}O_2$	$U^{235}O_2$
Core Weight, lb	471	533	1370
Core Volume, ft^3	0.63	0.75	1.8
Core Diameter, ft	0.94	0.98	1.3
vol% Cermet	57	62	73
vol% Clad	14	12	7
vol% Void	29	26	20
kg, Fissile Material	65	64	168

the figures represents the corresponding uniform power and coolant distribution cores of the parametric study. The 710 Test Reactor design is shown as a triangle on Figure 3.3, and a comparison with this design is discussed in a later section of this report.

Inspection of Table 3.1 and these figures shows that a substantial reduction in size can be effected by using the alternate fuels. A 66 wt% saving is achieved with PuN and more than 60% with $U^{233}O_2$. The relatively small difference between the plutonium and U^{233} performance is attributable to the significant increase in coolant volume fraction dictated by the restriction that coolant pressure ratio be held constant at 0.95. However, if a lower pressure ratio (higher core pressure drop) were allowed, a greater savings in core size could be achieved by utilizing the higher density plutonium fuel, and the Reynolds number would be increased. In a reactor system designed for a specific application, it would be necessary

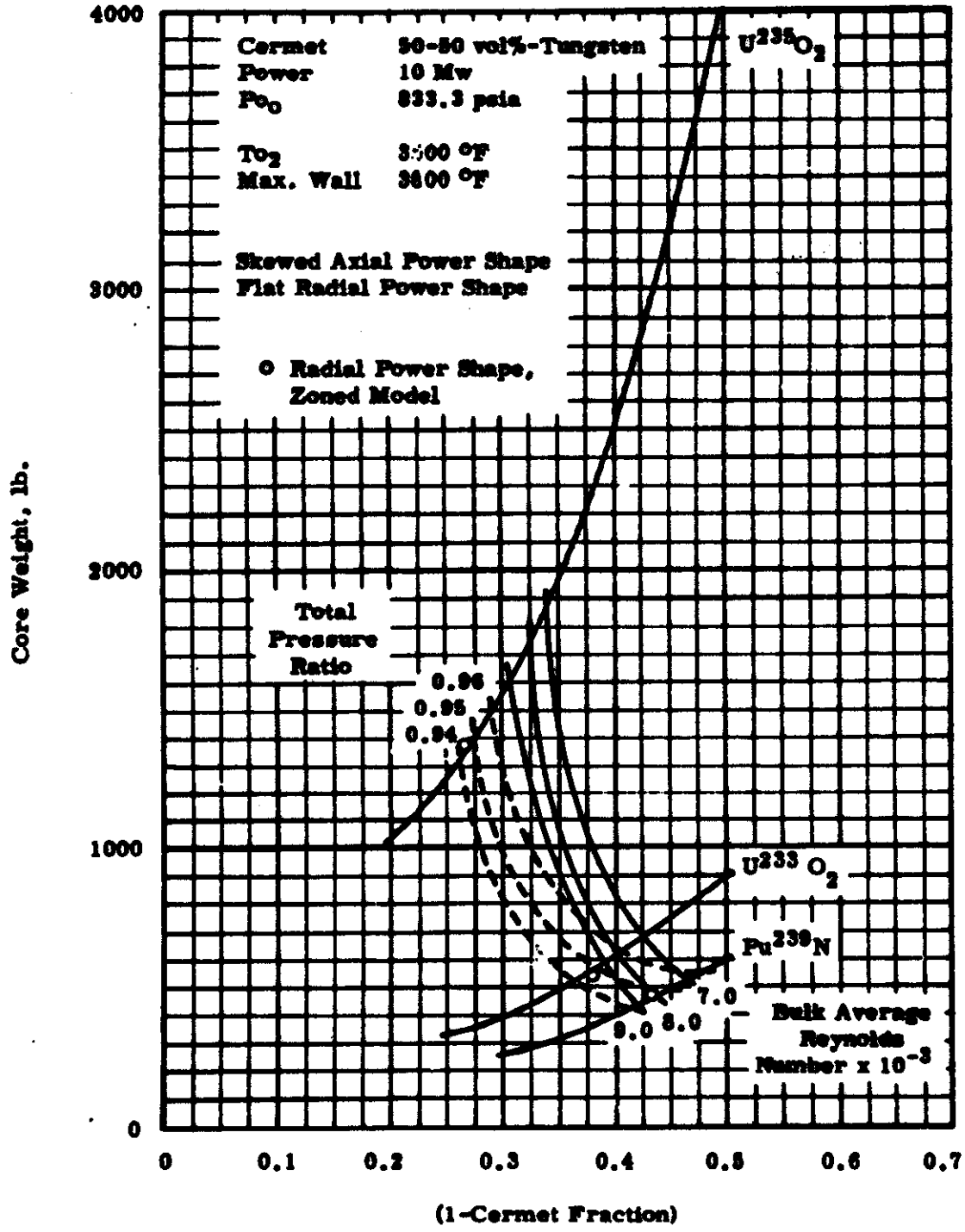

FIGURE 3.1

Fast Spectrum "Square" Core Weights, Total Pressure Ratio and Reynolds Number for Various Cermet Fractions

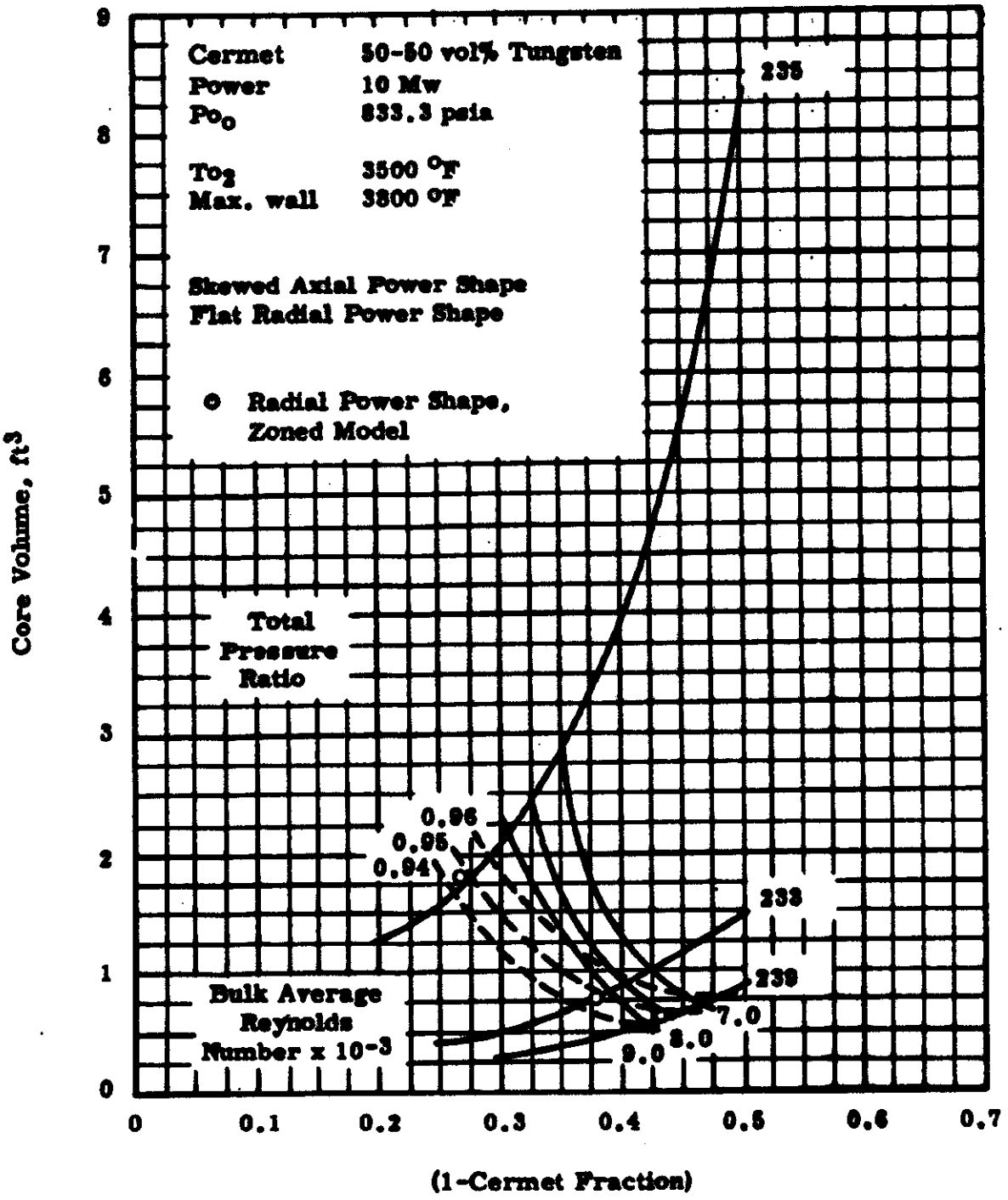

FIGURE 3.2

Fast Spectrum "Square" Core Volumes, Total Pressure Ratio and Reynolds Number for Various Cermet Fractions

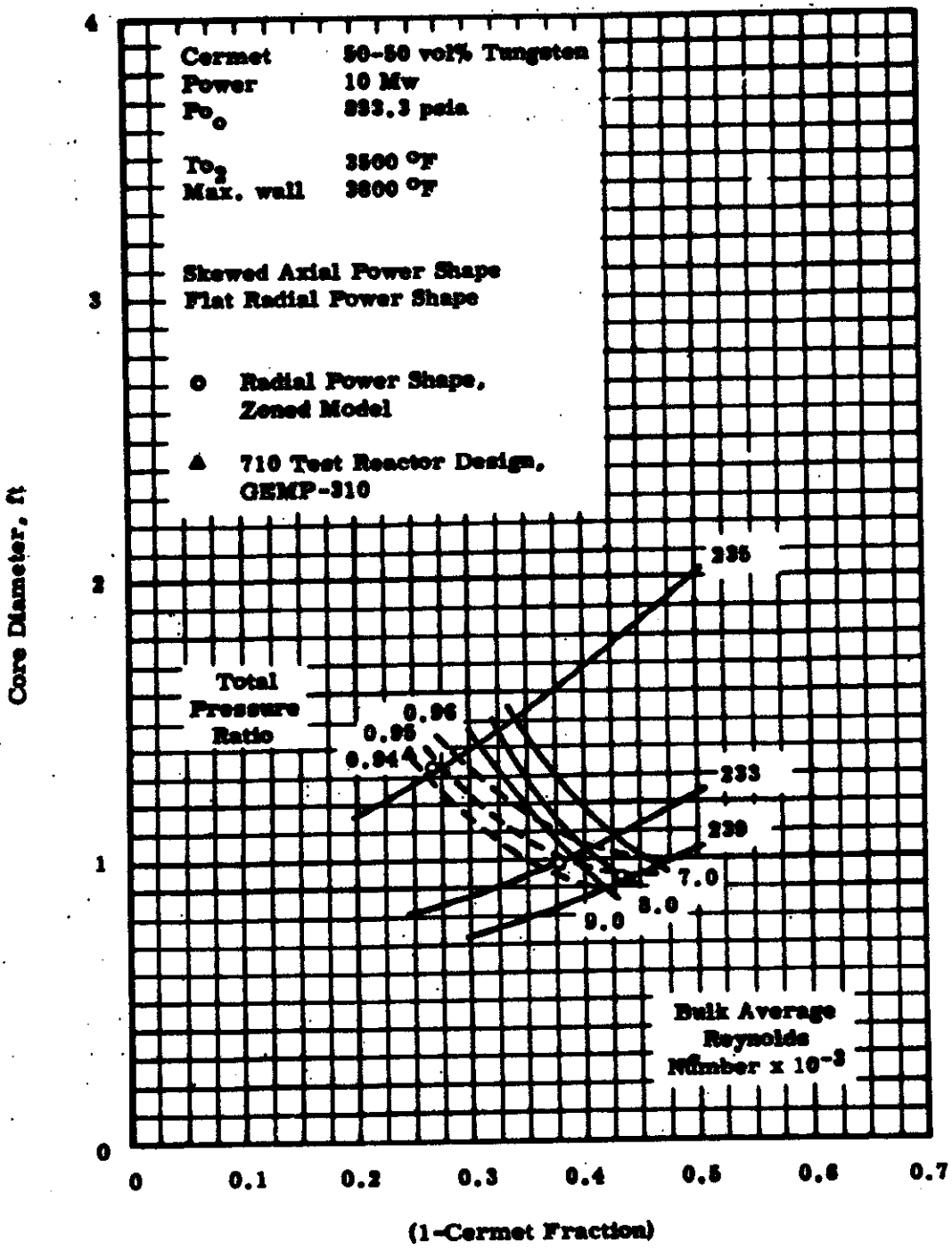

FIGURE 3.3

Fast Spectrum "Square" Core Diameters, Including the Effect of Tantalum on Critical Size, Total Pressure Ratio and Reynolds Number for Various Cermet Fractions

[redacted]

to make a system optimization study, considering pressure ratio and pumping power as variables, and determine an optimum pressure ratio for each of the three fuels. It is expected that this would result in a somewhat different ratio of core characteristics for the fuels.

A second major result is the evaluation of the effect of core size on reactor control strength and control span requirements. The smaller plutonium or U^{233} cores tend to have a control advantage vis-a-vis the U^{235} core, provided reflector control is accomplished by the physical removal of reflector sections. If, however, poison bearing reflector elements are used for control, the control advantage is rather small.

For a 1000 hr 710 Test Reactor core, the fuel burnups are small enough so that the difference in burnup control requirements between the U^{235} and plutonium or U^{233} cores is not significant. Hence, if the U^{235} core has sufficient control available, the plutonium fueled core should also have a sufficient control margin. On the other hand, if a 10,000 hr 710 core is considered, the increased fractional fuel burnup in the plutonium or U^{233} core and the consequent increased control requirements become important. If the U^{235} core is marginal in control, other control devices (e.g., reflector removal or fuel insertion) would have to be considered for the plutonium or U^{233} cores.

It is also possible to use a much more dilute cermet fuel if either U^{233} or plutonium is employed. At a constant reactor size and weight, a 30 vol% $U^{233}O_2$–70 vol% W cermet can be substituted for a 50 vol% $U^{235}O_2$–50 vol% W cermet. Although the survey was limited to 70 vol% W as a maximum, it can be estimated (from Figures 4.16 to 4.18) that a 25 vol% PuN–75 vol% W cermet could similarly be used. Should irradiation tests on 50 vol% fueled cermet fuel show that it is necessary to use more dilute cermets to achieve satisfactory endurance, it appears possible through use of plutonium or U^{233} to accomplish this either with a more modest reduction in reactor size or, at worst, without the penalty of a size increase.

[redacted]

Control requirements would be changed, however, because the fractional fuel burnup for equal core endurance would still increase substantially.

For reactors of lower power than the 710, the proportional savings in size or weight would be expected to be greater, since the coolant and clad would occupy a smaller fraction of the core volume and would diminish in importance in determining core size.

It can be seen from consideration of the above results that plutonium or U^{233} can be employed to greater advantage in this class of reactors if the reactor design is tailored to suit the nuclear as well as the physical characteristics of these fuels. It is insufficient to rely on developing a fuel materials technology on the basis that the fuel can be simply substituted in a reactor designed to utilize U^{235}. To use these fuels beneficially, technological developments must therefore be sought in several areas:

- Reactor nuclear analysis - more thorough understanding of the nuclear characteristics of plutonium and U^{233} in neutron spectra typical of this class of reactors is needed, and should be acquired through analysis and experimentation in fast critical assemblies.
- Reactor engineering - means of achieving greater available control span (e.g., by reflector or fuel movement) without significant penalty to total reactor size or weight must be developed. This work would require supporting design studies on reactor plants to make optimum use of these fuels, and determine the associated requirements for fuel and control system performance.
- Plutonium fuel materials - the physical properties of refractory plutonium compounds and their compatibility with structural materials must be determined. Performance limits of specific fuel designs must then be determined under typical operating conditions for specific power and endurance exceeding those for U^{235} fuels.
- U^{233} fuel materials - although the uranium materials technology is applicable, the performance of specific fuel designs must be determined since the specific power and endurance requirements exceed

[redacted]

those for U^{235} fuels. The technology of producing "clean" U^{233} and fuels must be demonstrated to insure that there are no major unforeseen technical or economic problems associated with this fuel.

3.2 DESIGN POINT CORE DATA

The detailed zoning results for the design point cores are given in Table 3.2. This information was derived by taking the design point based on the uniform core and admitting the radial power profiles shown in Figures 4.1, 4.2, and 4.3 to the analysis. Figures 3.4, 3.5, and 3.6 are profiles after zoning. As is evident from Table 3.2, upon comparison with other zones, temperature flattening is achieved by increasing or decreasing the core density (tube diameter, keeping the number of tubes constant) above or below the average, thereby increasing or decreasing the coolant flow and heat generated in the zone. This alters the power profile, as shown by Figures 3.4, 3.5, and 3.6 in comparison with Figures 4.1, 4.2, and 4.3. Although the zoned cores were found to have higher multiplication than the uniform cores (Table 3.2) because they are slightly larger in size, the difference in size of the zoned cores to achieve equal multiplication is small enough to be negligible.

To assess the validity of the uniform core parametric study, the three zoned core properties (weight, volume, and diameter) plotted on Figures 3.1, 3.2, and 3.3 may be compared with those of the uniform cores. The correspondence is seen to be within 1%. Since a close similarity exists between the zoned and homogeneous models, it is possible to make generally valid comparisons based on the parametric study without recognizing the radial power profile unless direct, more detailed, design quantities are desired.

TABLE 3.2

U^{235} Core

Zone	Outer Radius of Zone, ft	Volume Fraction in Zone 58-56 vol% Cermet	Volume Fraction of Ta in Zone	Void Fraction in Zone	Hydraulic Diameter of Coolant Tubes, in.	Number of Coolant Passages	Zone Power, MW	Exit Total Temperature, °F	Maximum Wall Temperature, °F	Total Pressure Ratio	Coolant Flow lb/hr	Bulk Average Reynolds Number
1	0.266	0.722	0.000	0.200	0.0762	662	1.770	3486	3700	0.9487	$8.04 \cdot 10^3$	12047
2	0.397	0.720	0.000	0.200	0.0732	827	2.946	3494	3800	0.9487	$9.13 \cdot 10^3$	11324
3	0.520	0.720	0.000	0.196	0.0706	1160	3.508	3504	3700	0.9486	$1.11 \cdot 10^4$	10182
4	0.606	0.742	0.000	0.198	0.0690	708	1.416	3547	3806	0.9487	$6.19 \cdot 10^3$	9648
5	0.612	0.740	0.000	0.194	0.0698	189	0.394	3582	3800	0.9488	$1.72 \cdot 10^3$	9600
6	0.620	0.727	0.000	0.197	0.0710	198	0.428	3511	3702	0.9487	$1.90 \cdot 10^3$	10072
7	0.645	0.720	0.000	0.202	0.0736	200	0.467	3468	3700	0.9488	$2.18 \cdot 10^3$	11147
8	0.661	0.702	0.072	0.226	0.0880	298	0.690	3378	3700	0.9488	$3.25 \cdot 10^3$	14686

Core Totals

Length, ft	In Core	In Core	In Core	Excess Mult. Factor		Total Power, MW	Average Temperature, °F	Coolant Flow, lb/sec	Core Weight, lb	Core Volume, ft^3
1.306	0.734	0.067	0.199	0.02	4137	9.757	3600	12.00	1370.55	1.736

[redacted]

TABLE 3.2 (Contd.)

U^{233} Core

Zone	Outer Radius of Zone, ft	Volume Fraction in Zone 50-50 vol% Cermet	Volume Fraction of Ta in Zone	Void Fraction in Zone	Hydraulic Diameter of Coolant Tubes, in.	Number of Coolant Passages	Zone Power, MW	Exit Total Temperature, °F	Maximum Wall Temperature, °F	Total Pressure Ratio	Coolant Flow lb/hr	Bulk Average Reynolds Number
1	0.197	0.611	0.121	0.260	0.0607	970	1.684	3463	3700	0.9476	$7.87 \cdot 10^3$	9704
2	0.266	0.620	0.119	0.261	0.0603	1210	1.973	3484	3800	0.9473	$8.81 \cdot 10^3$	9290
3	0.394	0.626	0.117	0.256	0.0681	1700	2.537	3506	3700	0.9473	$1.12 \cdot 10^4$	8668
4	0.443	0.632	0.116	0.252	0.0675	1000	1.492	3533	3810	0.9475	$6.57 \cdot 10^3$	8316
5	0.455	0.626	0.117	0.256	0.0681	276	0.414	3505	3700	0.9476	$1.84 \cdot 10^3$	8641
6	0.467	0.622	0.118	0.260	0.0680	288	0.444	3486	3700	0.9472	$1.98 \cdot 10^3$	8636
7	0.480	0.611	0.121	0.263	0.0607	298	0.513	3460	3806	0.9473	$2.30 \cdot 10^3$	9706
8	0.491	0.584	0.133	0.313	0.0601	298	0.764	3385	3790	0.9477	$3.00 \cdot 10^3$	13426

Core Totals

Length, ft	In Core	In Core	In Core	Excess Mult. Factor		Total Power, MW	Average Temperature, °F	Coolant Flow, lb/sec	Core Weight, lb	Core Volume, ft³
0.984	0.620	0.119	^.261	0.06	6062	9.881	3401	12.30	383.30	0.752

[redacted]

TABLE 3.3 (Contd.)

Pu^{239} Core

Zone	Outer Radius of Zone, ft	Volume Fraction in Zone 80-90 vol% Cermet	Volume Fraction of Ta in Zone	Void Fraction in Zone	Hydraulic Diameter of Coolant Tubes, in.	Number of Coolant Passages	Zone Power, MW	Exit Total Temperature, °F	Maximum Wall Temperature, °F	Total Pressure Ratio	Coolant Flow lb/hr	Bulk Average Reynolds Number
1	0.188	0.565	0.150	0.285	0.0650	1240	1.750	3477	3706	0.9473	$7.87 \cdot 10^3$	5560
2	0.282	0.565	0.147	0.288	0.0647	1880	2.072	3480	3700	0.9470	$9.20 \cdot 10^3$	5894
3	0.376	0.572	0.146	0.282	0.0636	2170	2.551	3502	3816	0.9460	$1.16 \cdot 10^4$	7060
4	0.428	0.570	0.144	0.277	0.0630	1320	1.581	3513	3700	0.9460	$6.66 \cdot 10^3$	7..4
5	0.435	0.570	0.144	0.277	0.0630	386	0.466	3513	3706	0.9470	$1.81 \cdot 10^3$	7280
6	0.446	0.577	0.144	0.271	0.0622	368	0.432	3512	3800	0.9475	$1.66 \cdot 10^3$	7312
7	0.458	0.568	0.147	0.285	0.0644	375	0.458	3498	3700	0.9470	$2.00 \cdot 10^3$	7712
8	0.469	0.531	0.156	0.314	0.0686	381	0.843	3428	3601	0.9466	$2.98 \cdot 10^3$	9048

Core Totals

Length, ft	In Core	In Core	In Core	Excess Mult. Factor		Total Power, MW	Average Temperature, °F	Coolant Flow, lb/sec	Core Weight, lb	Core Volume, ft^3
0.918	0.566	0.146	0.289	0.94	7758	9.946	3498	12.36	471.28	0.594

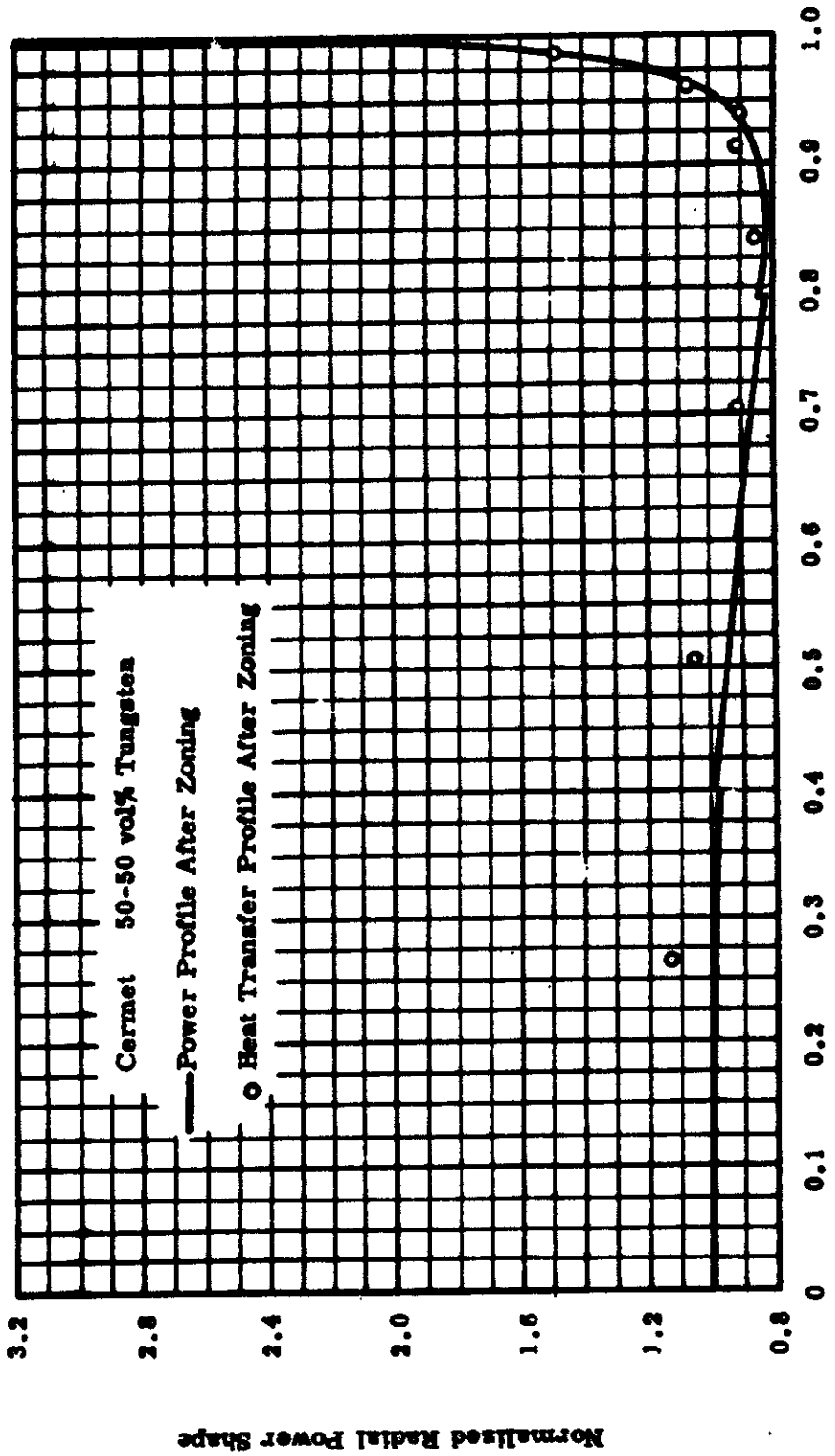

FIGURE 3.4
Normalised Radial Power Shape $U^{235}O_2$ Zoned Model

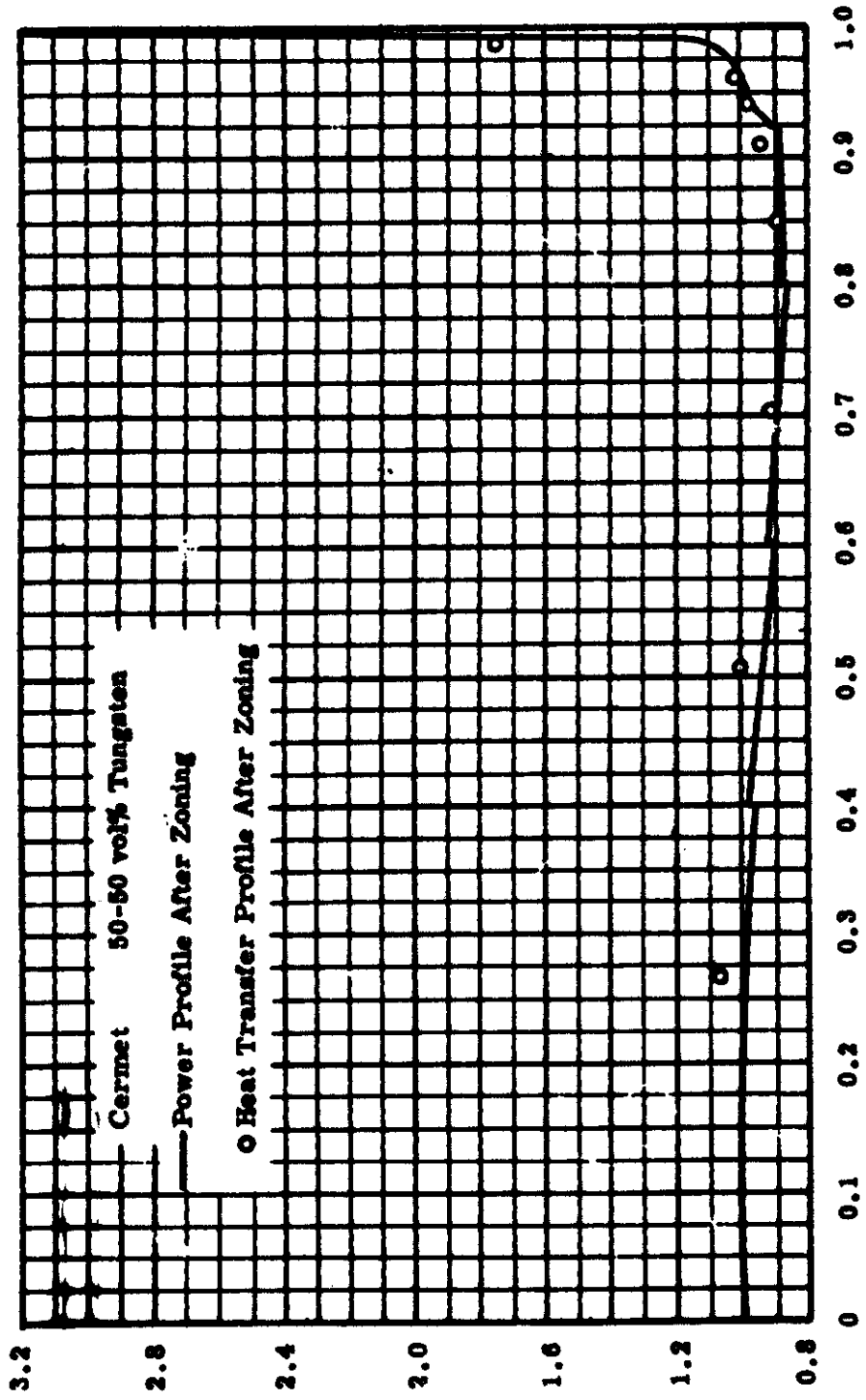

FIGURE 3.5
Normalized Radial Power Shape $U^{233}O_2$ Zoned Model

[redacted]

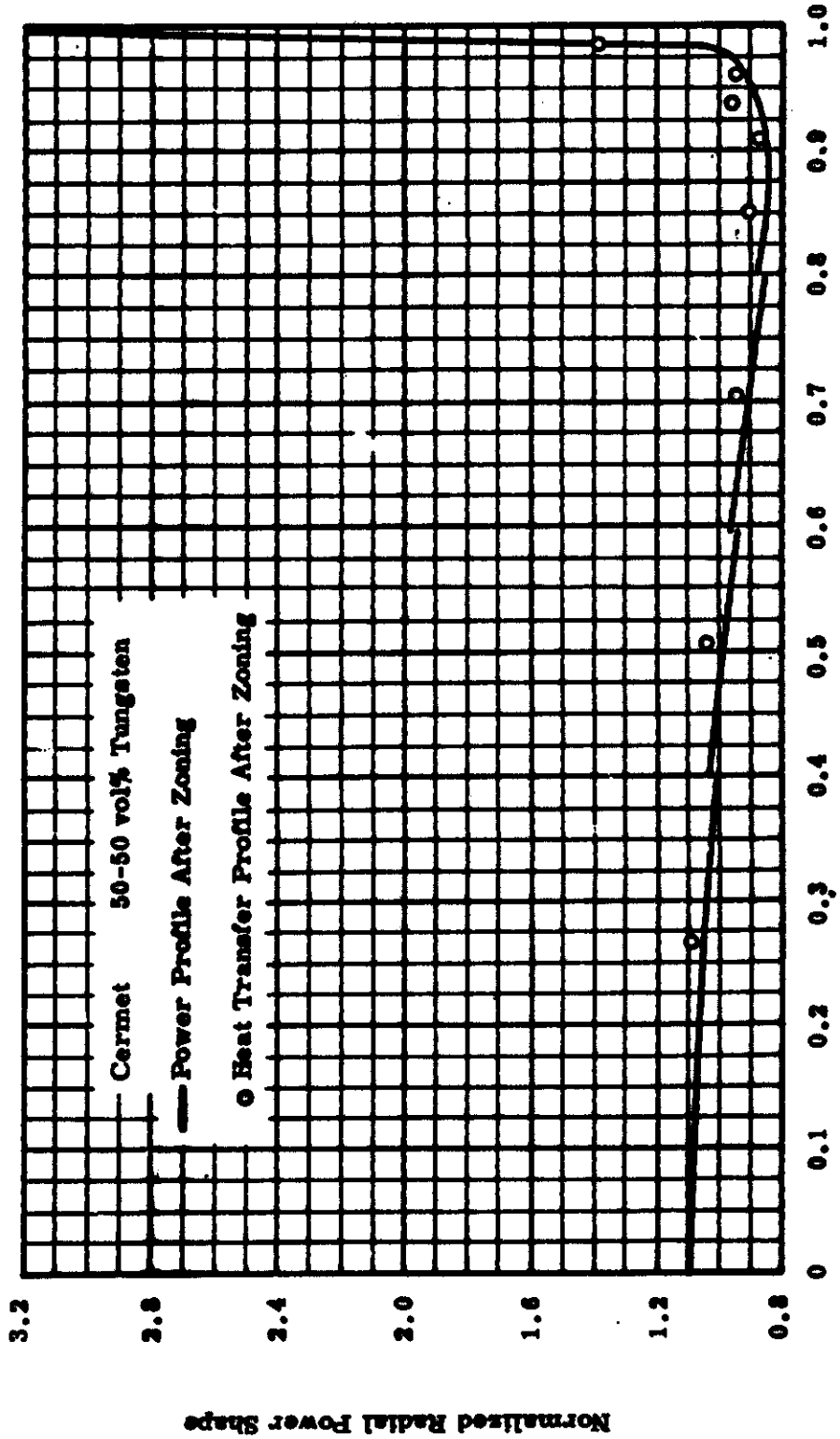

FIGURE 3.6

Normalized Radial Power Shape $Pu^{239}N$ Zoned Model

4.0 PARAMETRIC STUDY OF CORE HEAT TRANSFER AND FLUID FLOW

Previously, a class of cores restricted to a total pressure ratio of 0.95 and a fuel composed of 50-50 vol% cermets was considered. The first criterion was established by considerations external to the study while the second recognizes that the linear coefficient of expansion of 50-50 vol% W-UO_2 cermets closely approximate that of the tantalum clad. In addition, a parametric study was performed for two purposes: to define the proper area to meet the detailed design point mentioned above, and to look ahead to the advantages of higher fuel contents in the cermet if this is found to be feasible. In this study, the core power of 10 MW_t and clad temperature limitations of 3800 °F were retained; the only changes being cermet composition and core coolant total pressure ratio.

Including the preliminary study to determine the approximate amounts of tantalum in the cores, a total of 164 cases was considered. Total pressure ratios to as low as convergence would allow were obtained (≈0.3), and fuel volume in the cermet fractions varied from 30 to 70%. Results are presented for total pressure ratios down to 0.75.

4.1 POWER DISTRIBUTION

The homogeneous core normalized radial power ratio obtained from nuclear calculations is shown in Figures 4.1, 4.2, and 4.3 along with the axial power profiles. Since the axial profiles change slightly with core composition, length, and diameter, the effect on core heat transfer of two U^{235} profiles, obtained from 26 and 36 cm cores, was investigated. The effect on clad temperature was found to be negligible (several degrees F). The 36 cm U^{235} profile and those shown for the remaining fuel were used throughout the study. The computer program does not solve the compressible flow equation in a step-by-step manner but uses an integrated equation that presumes the power shape can be adequately represented by a general polynomial equation. The correspondence of the fit is shown as dotted lines in Figures 4.1 - 4.3.

 [redacted]

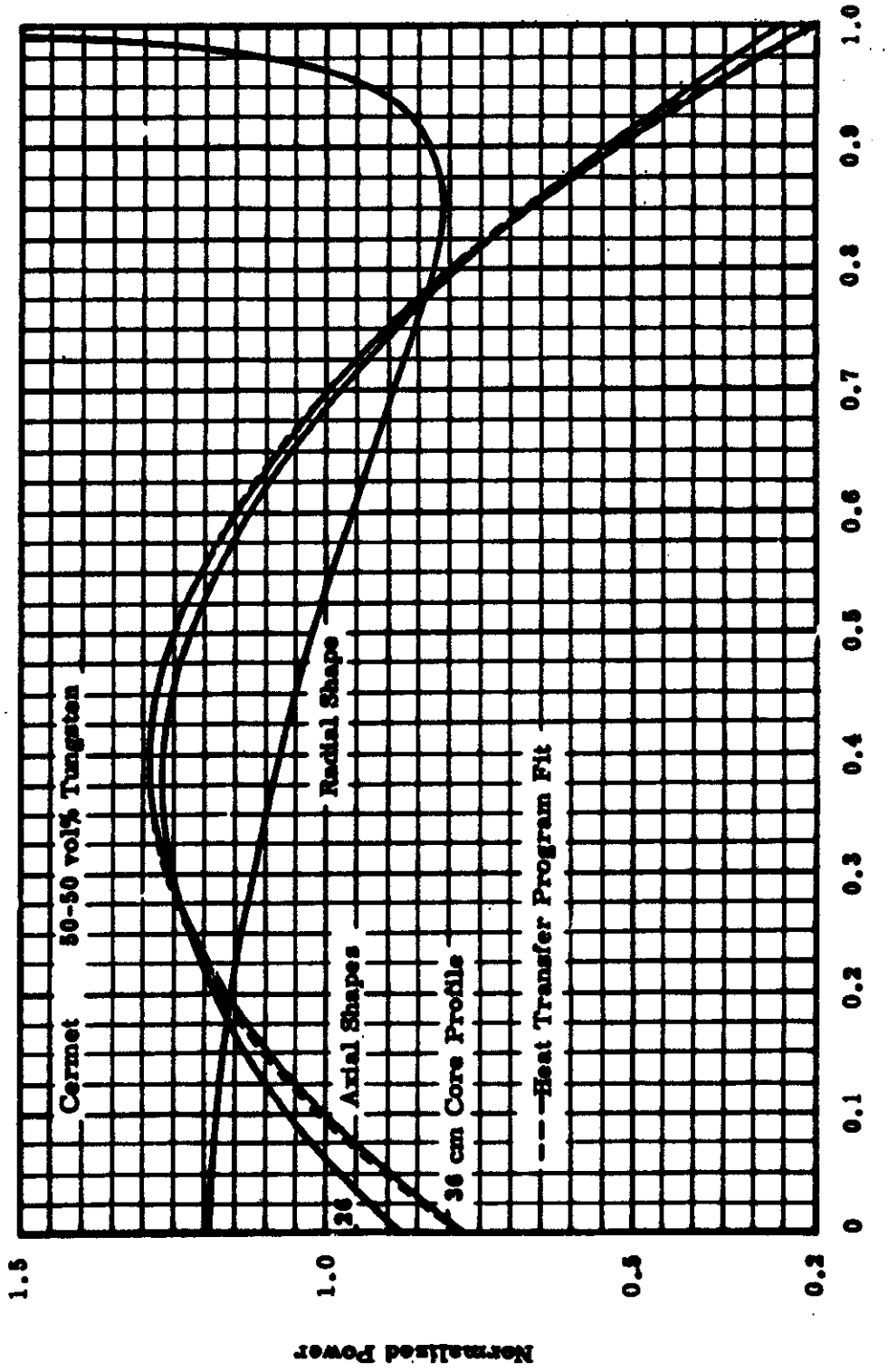

FIGURE 4.1

Uniform Core Power Shape $U^{235}O_2$

[redacted]

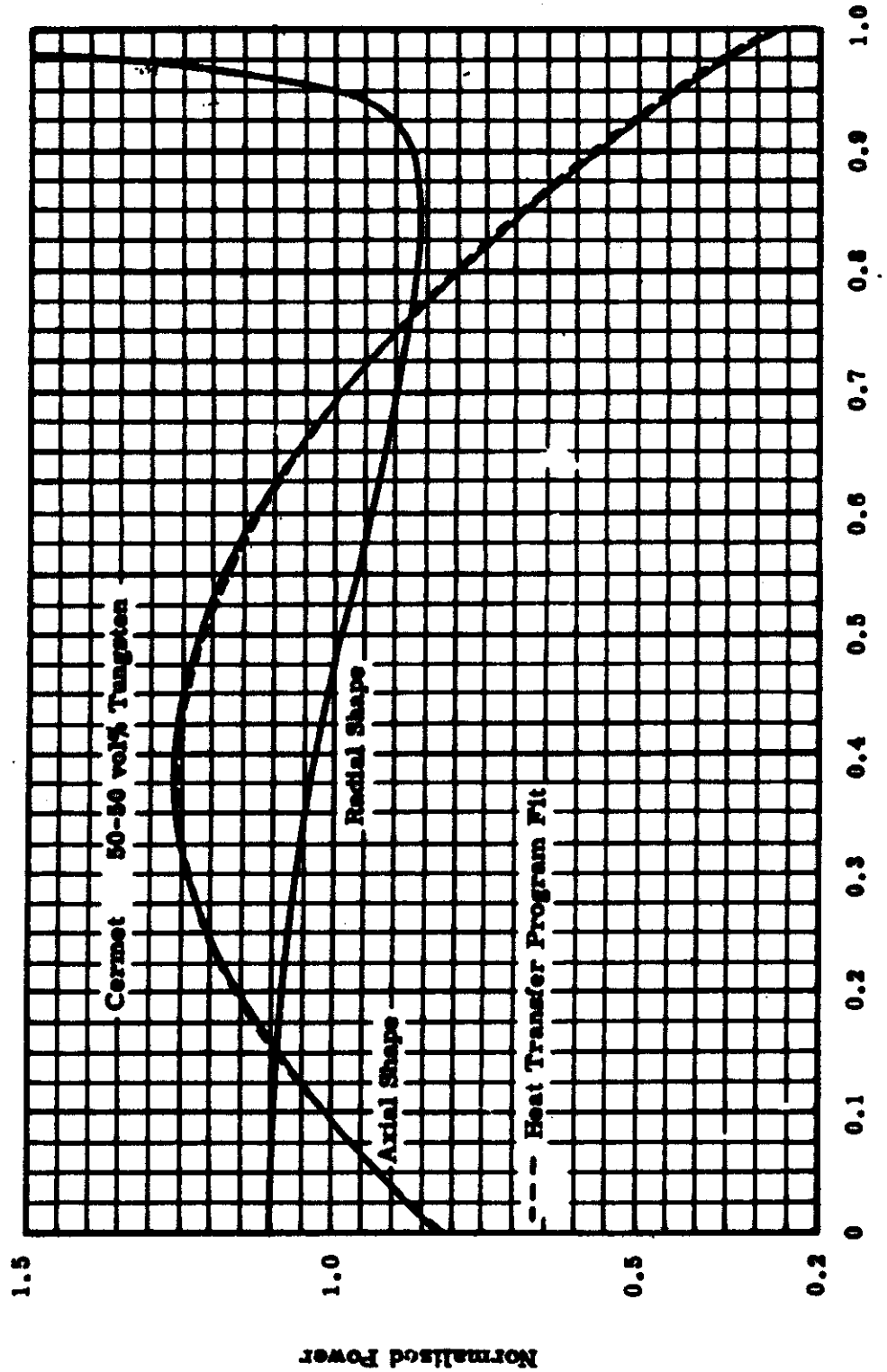

FIGURE 4.2

Uniform Core Power Shape $U^{233}O_2$

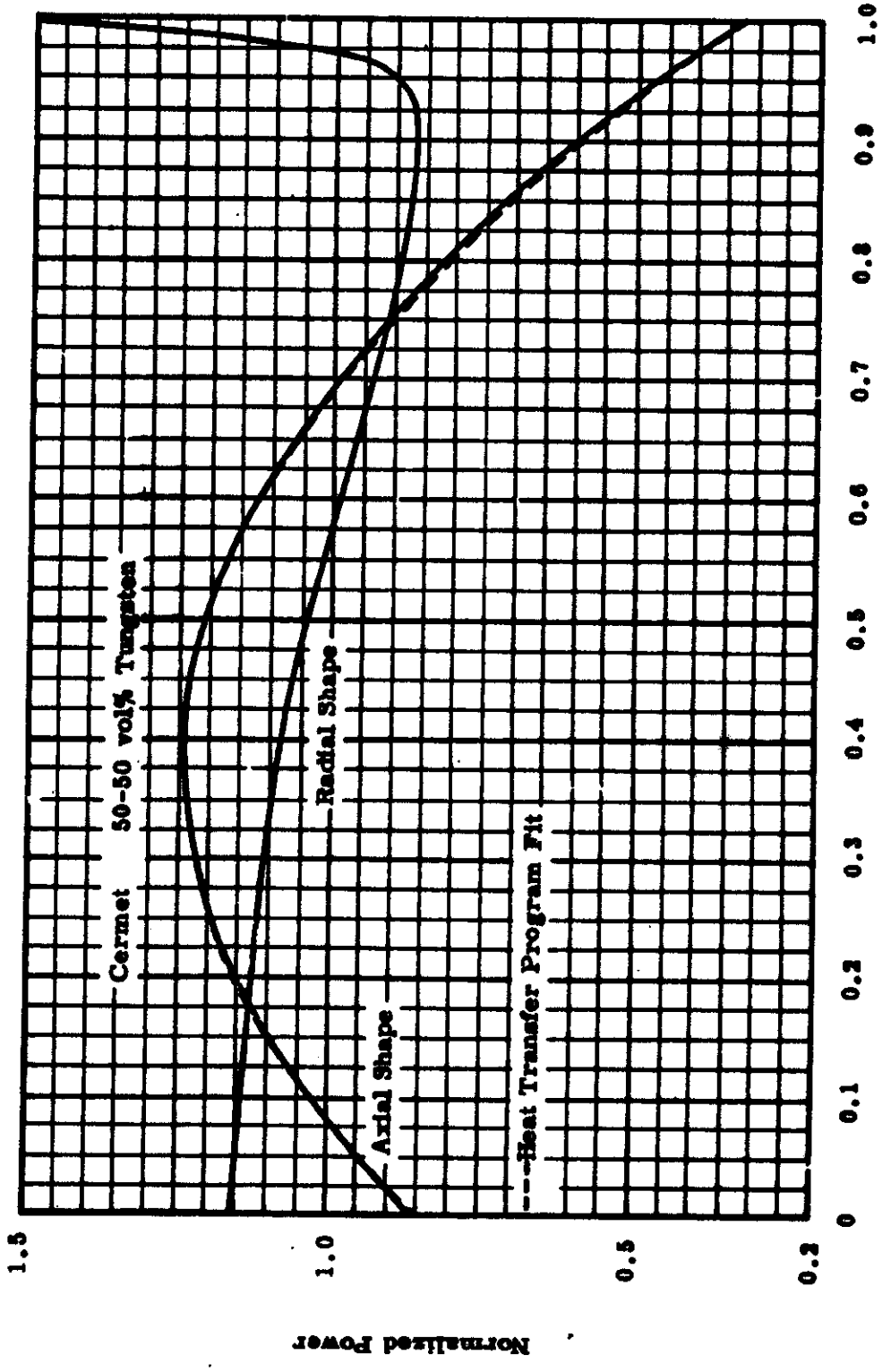

FIGURE 4.3

Uniform Core Power Shape $Pu^{239}N$

4.2 AXIAL TEMPERATURE DISTRIBUTION

Figures 4.4, 4.5, and 4.6 are the core coolant, wall, and cermet temperature profiles along the core lengths for the three uniform design point cores.

The maximum film temperature drop does not exceed 1300 °F in any of these cores while the tube-wall temperature limitation was successfully met within 10 to 20 °F. The calculations of the heat transfer coefficients is explained in Appendix B.

The wall and fuel temperatures plotted in Figures 4.4, 4.5, and 4.6, at the front and back face, are based on local coefficients utilizing entrance effects but neglecting heat transfer from the faces themselves and, hence, are conservative. It should also be noted that the profile hot spot temperature is a conservative value because the code used neglects heat conduction in the axial direction. The error is expected to be less than 10 to 30 °F.

The thermal conductivity used for the 50, 40, and 30 vol% cermets is shown in Figures 4.7 and 4.8. The method of calculation and sources of data are included in Appendix C. The conductivities for the two cermet fuel types are not much different; i.e., the conductivity of the tungsten matrix is so high as to predominate over the lower conductivity of the ceramic fuel particles, in the range of compositions considered. The calculated conductivities used are somewhat higher than some of the experimental data shown in Appendix C, but it can be seen from Figures 4.4 - 4.6 that this would result in only a small error in fuel temperature.

4.3 CORE CHARACTERISTICS 50 VOL%–TUNGSTEN AT 0.75 TO 1.0 TOTAL PRESSURE RATIO

The results of this parametric study compare, much as the design point cores, the thermal and physical aspects of the three fuels as a function of total pressure ratio across the core and fuel content in the cermet. The parameters investigated, over a range of total pressure ratio, are presented in Figures 4.9 through 4.15, for a fuel volume fraction in the cermet of 50%. Similar curves may be plotted from the calculations made for fuel volume fractions of 30% and 70%, but these are not included here.

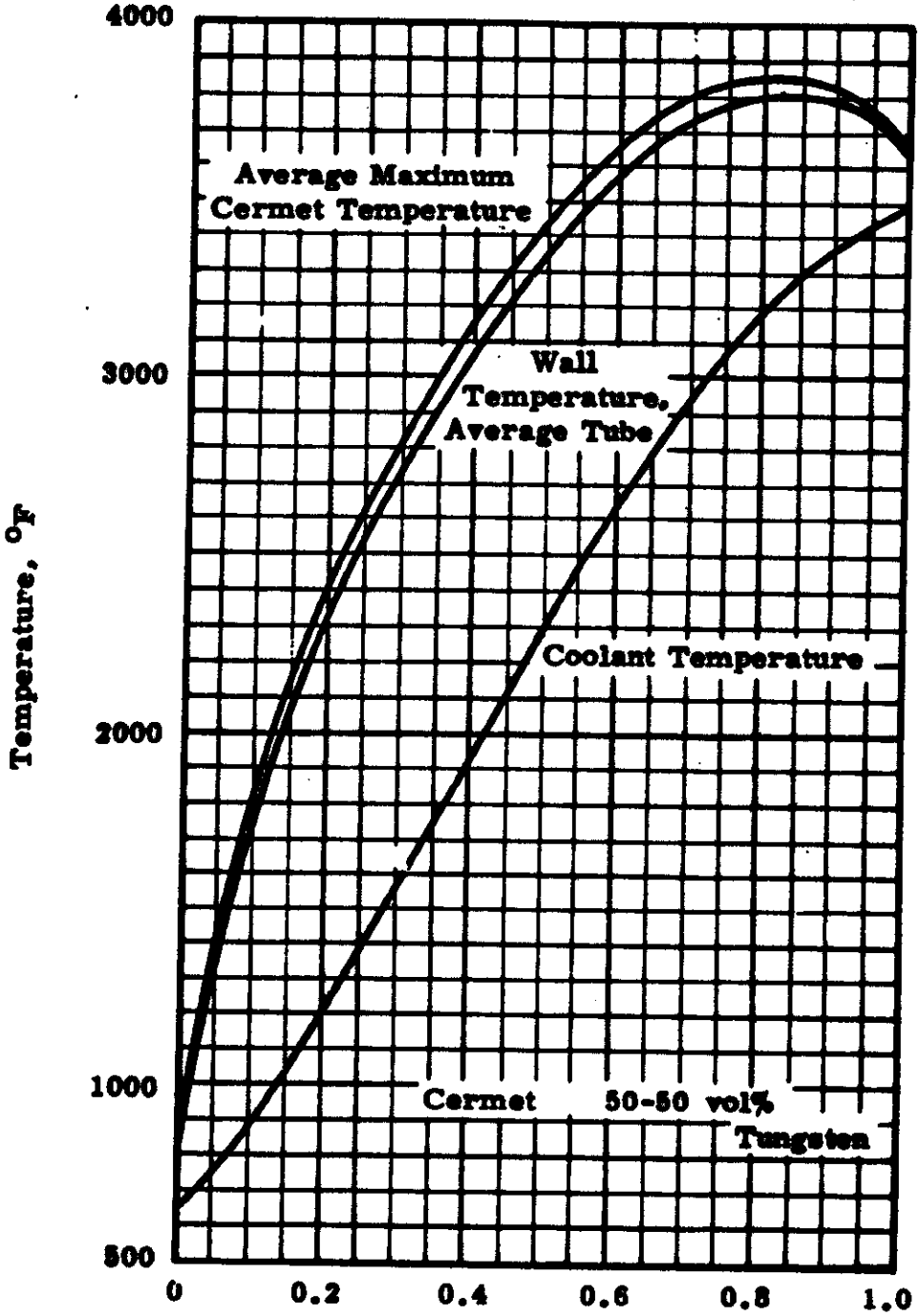

FIGURE 4.4

$U^{235}O_2$ Typical Axial Temperature Profiles; Design Point Uniform Core

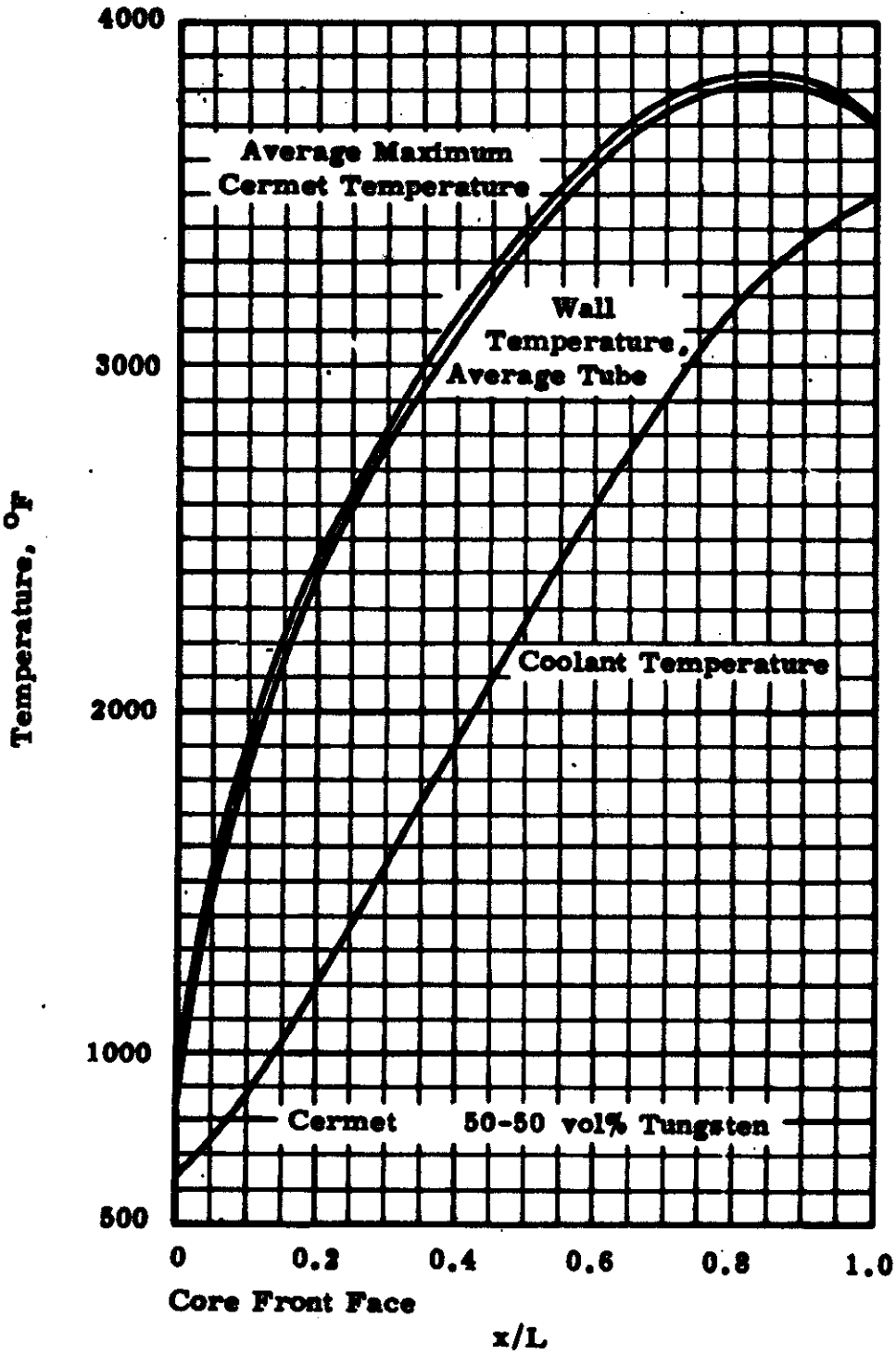

FIGURE 4.5

$U^{233}O_2$ Typical Axial Temperature Profiles; Design Point Uniform Core

[redacted]

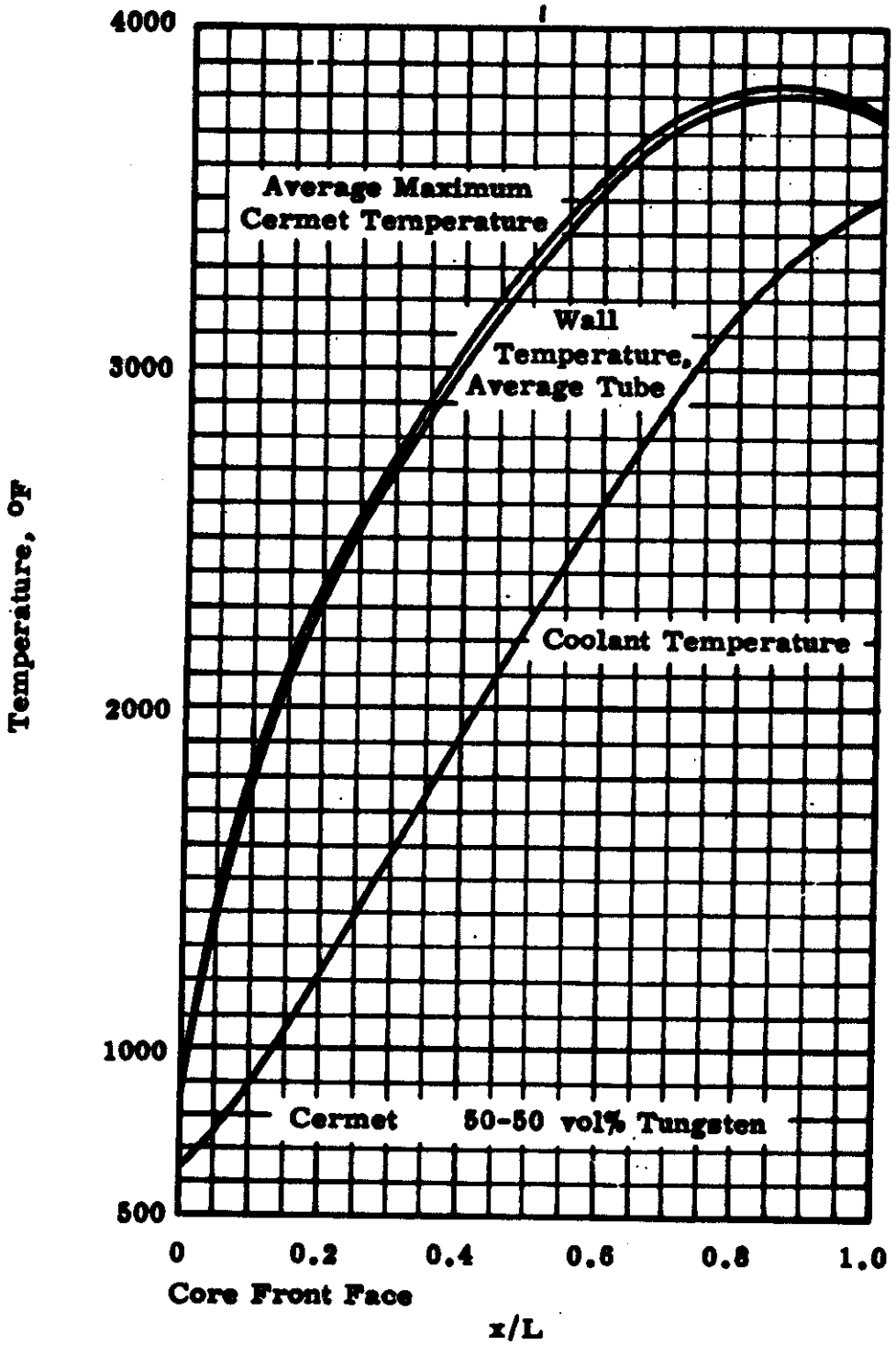

FIGURE 4.6

$Pu^{239}N$ Typical Axial Temperature Profiles; Design Point Uniform Core

[redacted]

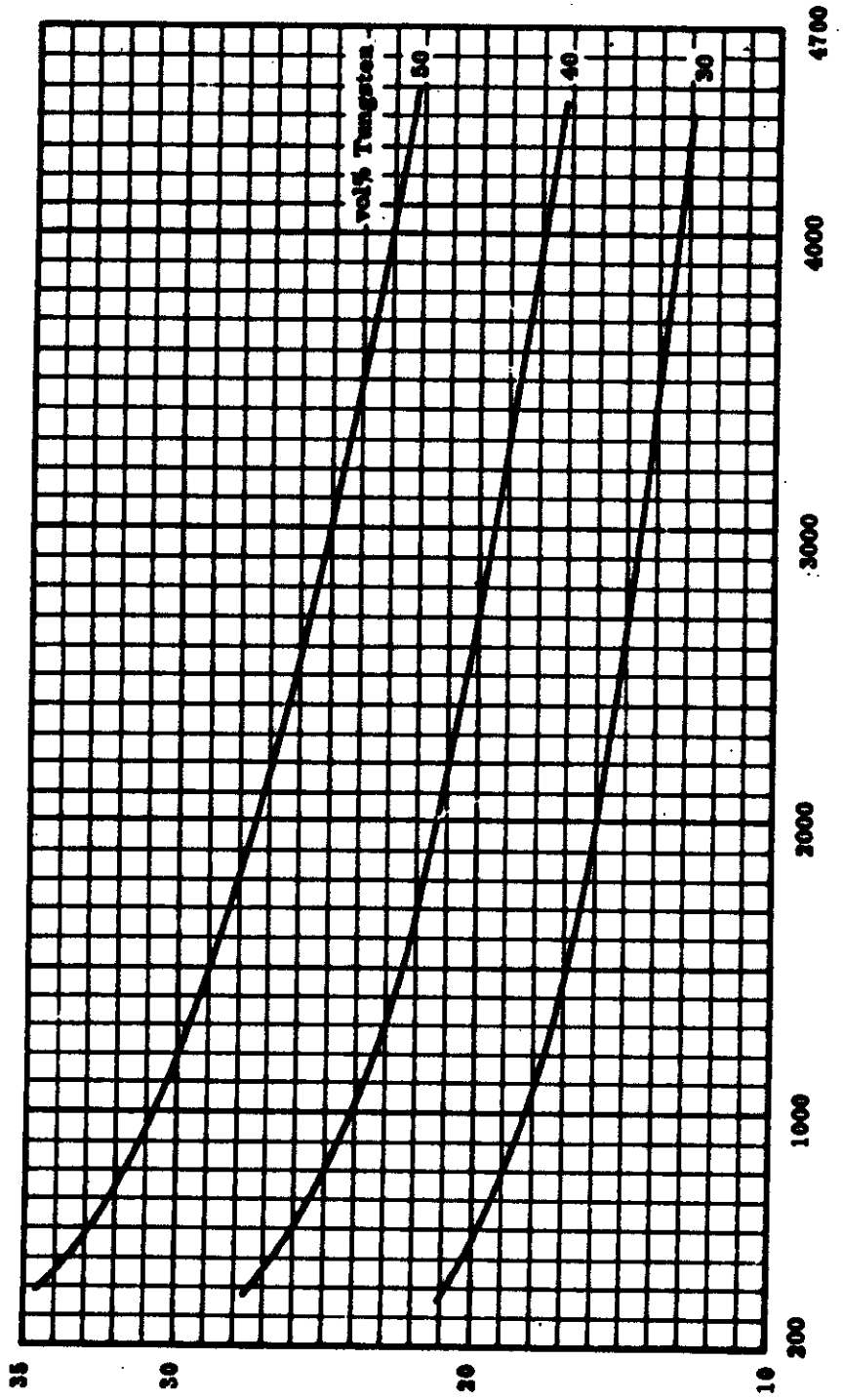

FIGURE 4.7
Thermal Conductivity of UO_2—W Cermets as Calculated from Appendix C

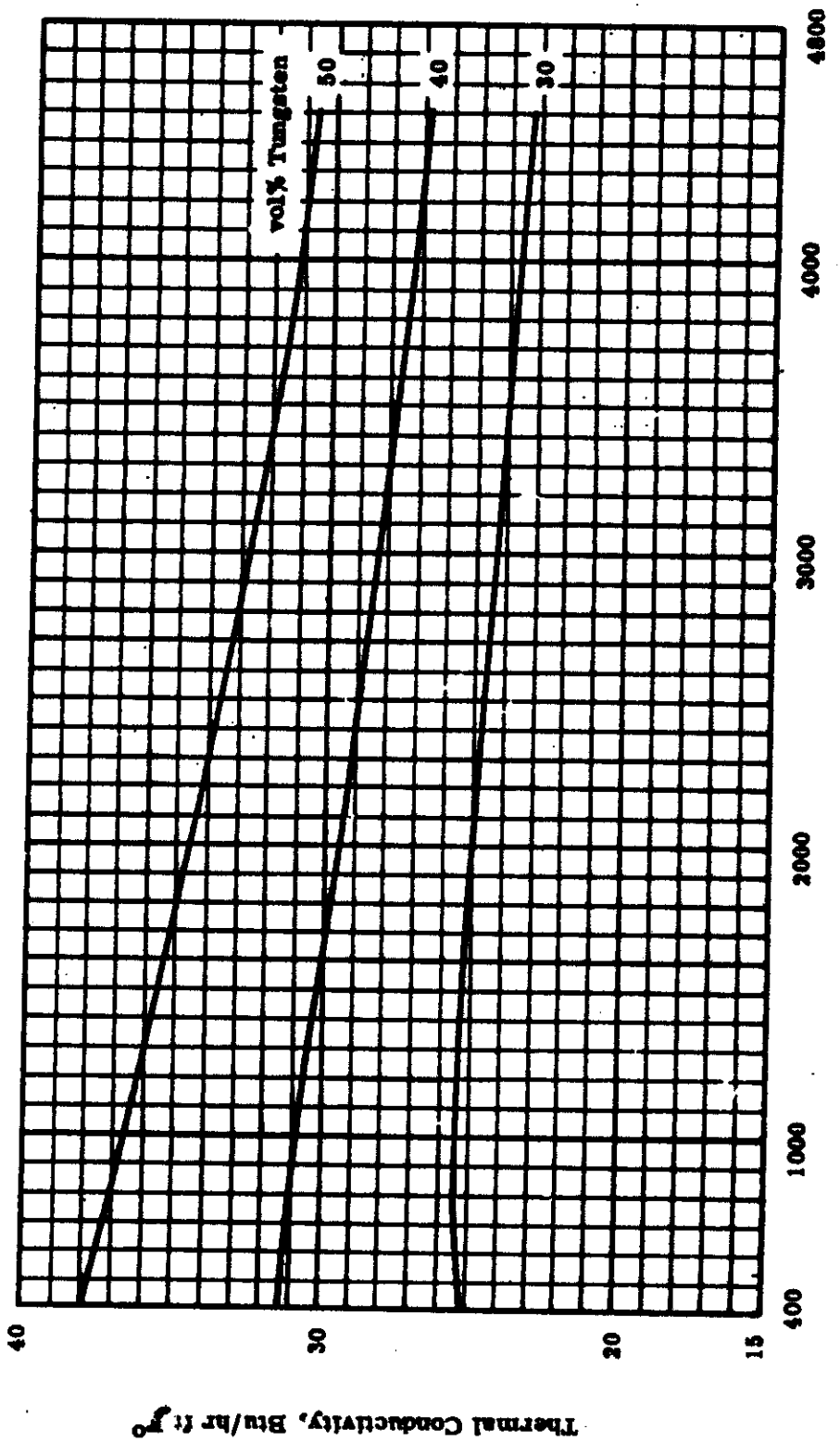

FIGURE 4.8
Thermal Conductivity of PuN (UN) Cermets as Calculated from Appendix C

FIGURE 4.9

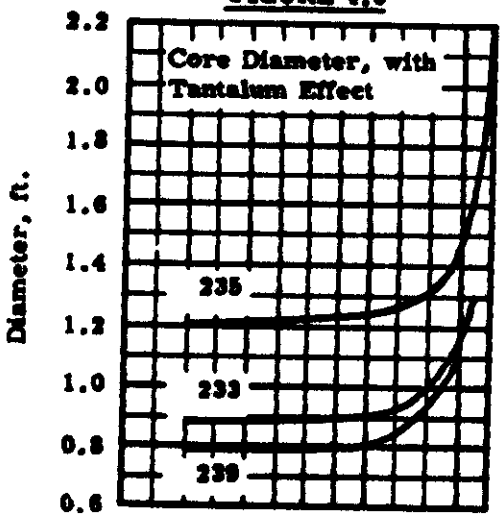

FIGURE 4.11

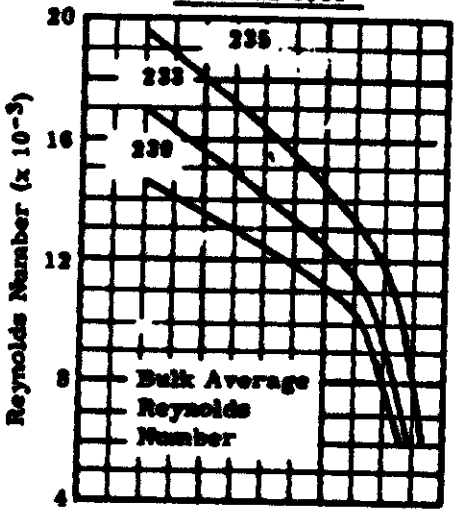

1 - Cermet Fraction: Cermet fraction 100% dense; the 5% cermet fraction voids are included with the gross "void" fraction

FIGURE 4.10

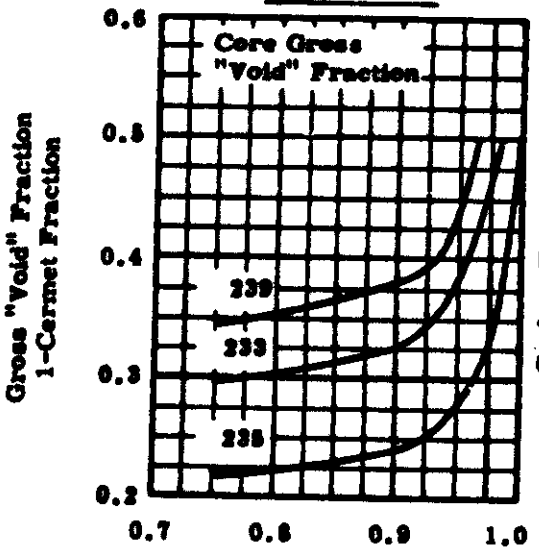

FIGURE 4.12

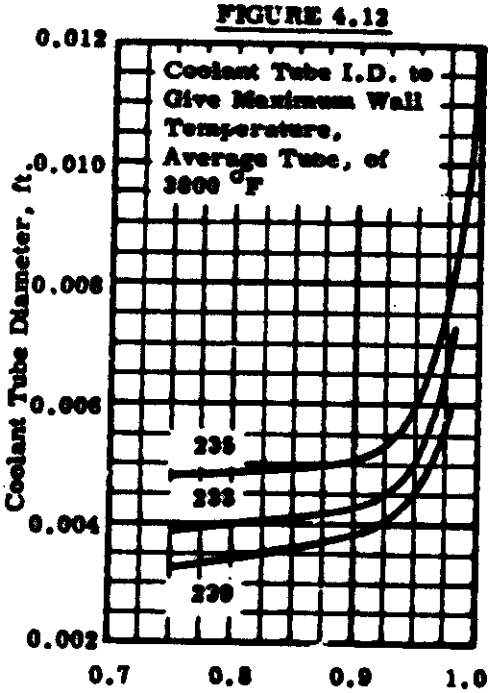

FIGURES 4.9 - 4.12

Core Diameter, 1 - Cermet Fraction, Coolant Bulk Average Reynolds Number and Tube ID 50-50 vol% Cermets

[redacted]

FIGURE 4.13

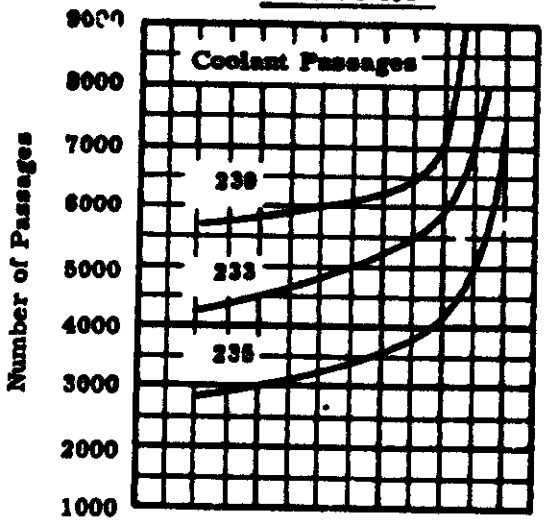

FIGURE 4.14

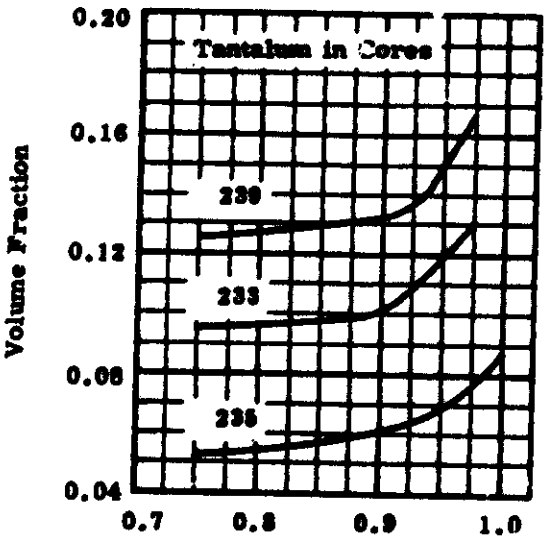

FIGURE 4.15

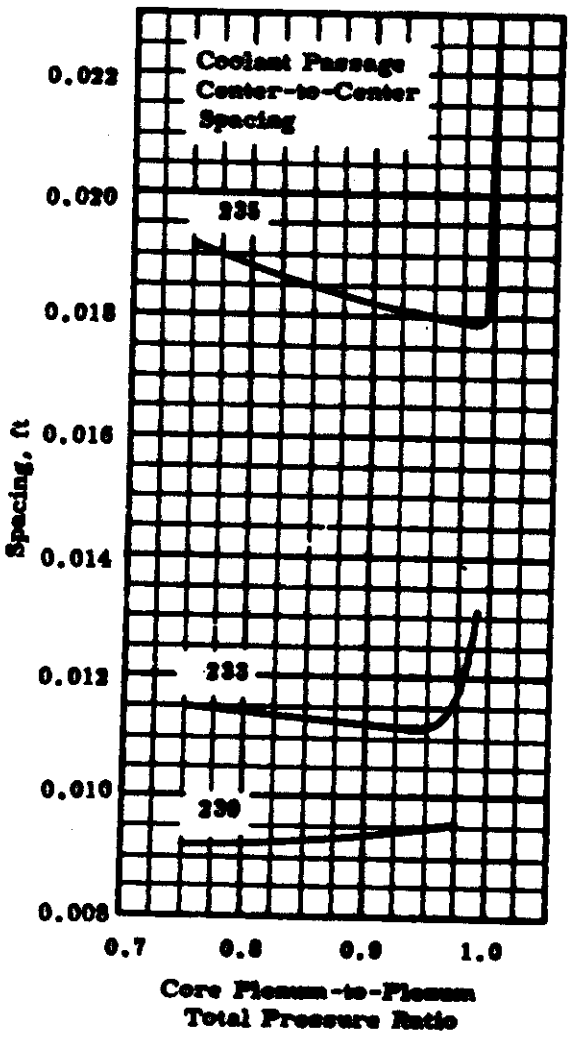

FIGURES 4.13 - 4.15

**Number of Coolant Passages,
Volume Fraction of Tantalum and Tube Center-to-Center Spacing
50-50 vol% Cermets**

For lower total pressure ratios the relative characteristics of reactors using the three fuels holds much as at design point pressure ratio of 0.95. However, the difference diminishes as the pumping losses decrease at higher pressure ratios. The core size, Figure 4.9, decreases rapidly down to about 10% total pressure loss and there remains almost constant. The variation in size with total pressure ratio, between the fuels and for a given fuel, will allow a rational engineering size selection when the core is placed in a power generating system.

If a total power plant system were optimized on the basis of kW/lb, the U^{235}, U^{233}, and Pu^{239} cores would be operated at different total pressure ratios, depending on the system thermodynamic partial derivatives, rather than at the same total pressure ratio.

Since the shield and pressure vessel sizes are a function of core size, additional indirect savings in system volume and weight, for example, could be realized. Such a system analysis, could be expected to result in a higher optimum total pressure drop, and the low Reynolds number problem would be alleviated as demonstrated in Figure 4.11.

Several additional plots of tube hydraulic diameter, volume fraction of tantalum, 1 - cermet fraction, and other core particulars, for the range of total pressure ratios investigated, are included in Figures 4.10, 4.12 through 4.15. Figure 4.10 shows the inactive core volume fraction (1 - C.F.) required to meet cooling conditions for various coolant total pressure ratios. The minimum tube ID, Figure 4.12, is about 0.045 in., about 1/64th in. smaller in diameter than used in the 710 Test Reactor reference design.

4.4 APPLICATION OF RESULTS, AN EXAMPLE:

An application of the total pressure ratio curves is helpful in interpreting the results. For example, assume it is desired to describe a 50-50 vol% PuN-W, 10 MW_t core with coolant exit of 3500 ^{o}F, entrance of 635 ^{o}F and total pressure ratio of 0.90. Table 4.1 is derived from Figures 4.9 through 4.15.

[redacted]

TABLE 4.1

0.90 TOTAL PRESSURE RATIO 50-50 vol% PuN-W
10 MW_t CORE CHARACTERISTICS

Core Diameter, ft	0.62
Bulk Average Reynolds Number	11,200
Coolant Tube ID, ft	0.0038
Number of Coolant Tubes	6,300
Coolant Tube Center-to-Center Spacing, ft	0.0094
Volume Fraction of Ta, Including Rod Clad	0.133
Cermet Fraction (100% Dense)	0.62

The approximate volume fraction devoted to element spacing and clad is 10%. The voids in the cermet are 5% of the cermet fraction or about 3.1%. Hence, 1.0 - 0.62 - 0.031 - 0.1 - 0.133 = 0.116, or 11.6% of the core volume is devoted to coolant. The coolant volume fraction can be found in another manner from Table 4.1 and Appendix B.

$$\alpha_c = \frac{N_t \pi D_H^2}{\pi D_{eq}^2} = \frac{6.3\ 10^3 \quad (3.8)^2\ 10^{-6}}{(8.2)^2 \quad 10^{-2}} = 0.135.$$

This figure is within the plotting accuracy of the curves; since the cermet-fraction could easily be low or high by two percentage points. The curves in the SUMMARY OF MAJOR RESULTS were derived in this manner with the design point homogeneous cores verified on the computer.

4.5 CORE CHARACTERISTICS AT 0.95 TOTAL PRESSURE RATIO FOR CERMET FUEL FRACTIONS FROM 70 to 30%

Additional savings in weight, volume, and size are available by decreasing the volume fraction of tungsten in the cermets. This is shown, for a constant total pressure ratio of 0.95, in Figures 4.16 through 4.18. The minimum core weight is at the lowest tungsten content of 30 vol%. At this point the core weights are 280, 320, and 630 lb for plutonium, U^{233},

FIGURE 4.16

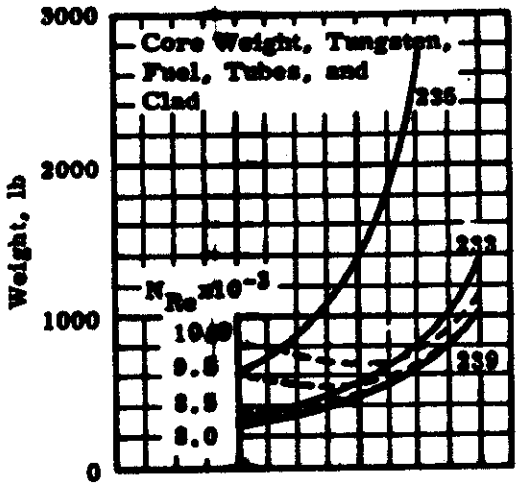

FIGURE 4.17

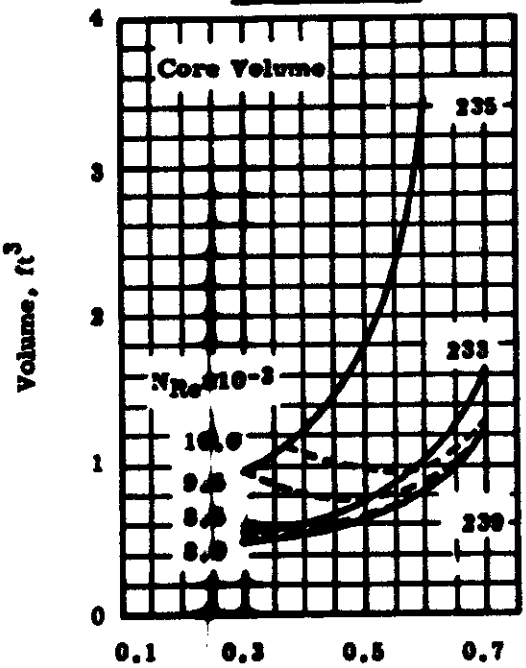

FIGURE 4.18

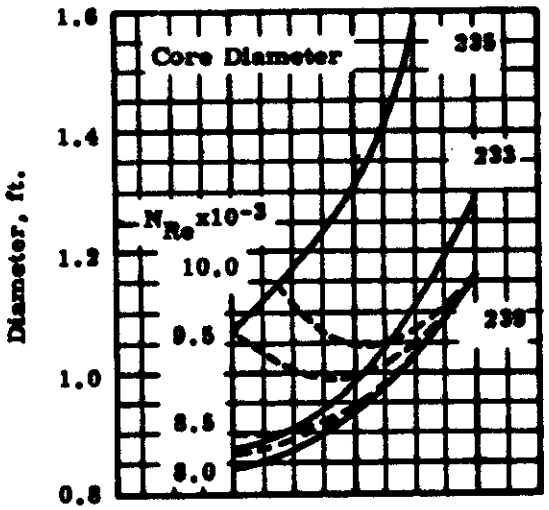

FIGURE 4.19

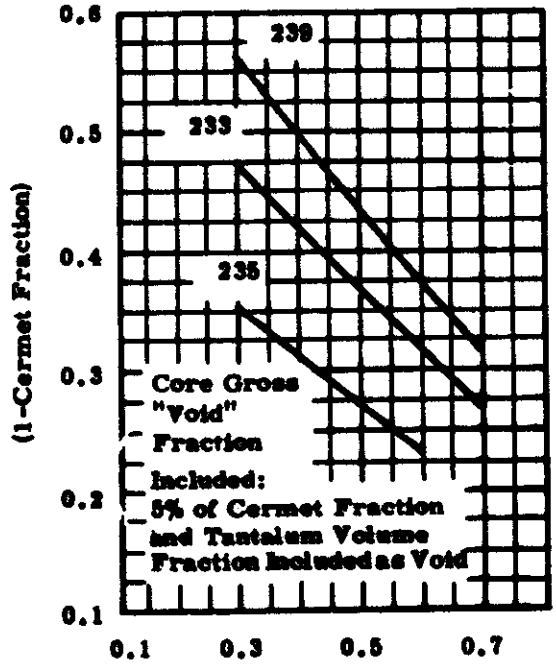

Volume Fraction of Tungsten in Cermets, 100% Dense
0.95 Total Pressure Ratio

FIGURES 4.16 - 4.19

Core Weight, Volume, Diameter and Gross Void Fraction

and U^{235}, respectively; compared with 471, 533, and 1370 lb at the design point. Other pertinent core characteristics are shown in Figures 4.19 through 4.24. From the thermal standpoint there is no impediment and even a small advantage in going to higher fissile fractions. Figures 4.25 and 4.26 show the temperature profiles in the smaller U^{233} and U^{235} cores. The difference between the wall temperatures and maximum fuel temperatures is seen to be even less than the higher thermal conductivity design point cores. This somewhat anomalous situation is brought about because the smaller cores require more tubes, as shown in Figure 4.21 and, therefore, have closer tube spacing, as shown in Figure 4.20. The feasibility of increasing the fuel content of the cermets would depend principally on metallurgical behavior, performance under irradiation, and thermal expansion characteristics.

Aside from the metallurgical and structural problems associated with these considerations, a difficulty may be the fabrication tolerances needed for the close tube spacing required in these small cores. Alternatively, if it should become desirable for metallurgical reasons to use a more dilute cermet, this can be accomplished without penalty and even with a savings in size and weight by changing the fissile material from U^{235} to U^{233} or plutonium. This is illustrated in Figures 4.16 through 4.18. Referring to Figure 4.16, it can be seen that a U^{235} fueled core with 50 vol% tungsten in the cermet weighs 1400 lb, whereas U^{233} and plutonium fueled cores with 70 vol% tungsten weigh < 1400 lb and 1000 lb, respectively.

Figure 4.23 illustrates the quantity of tantalum required in these cores. The maximum is about 19% for 30 vol% W cermet cores having a cermet - fraction of 44%.

An important parameter not investigated in this study is variation of core power. Though not examined specifically, it is evident that the U^{233} and Pu^{239} cores should be even more favorable than U^{235} in size and weight at lower powers. As shown in Figures 3.1, 3.2, and 3.3,

FIGURE 4.20

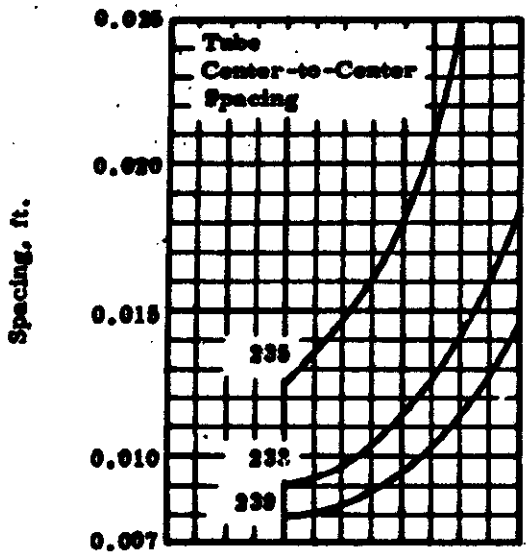

FIGURE 4.21

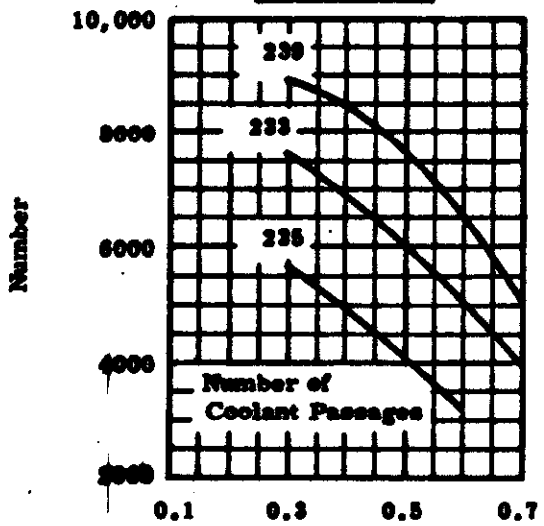

FIGURE 4.22

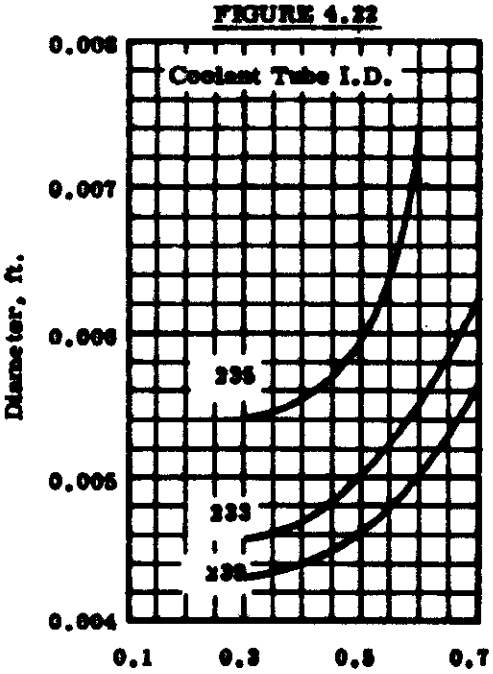

Volume Fraction of Tungsten in Cermets, 100% Dense
0.95 Total Pressure Ratio

FIGURES 4.20 - 4.22

Coolant Tube Spacing, Number and Diameter

FIGURE 4.23

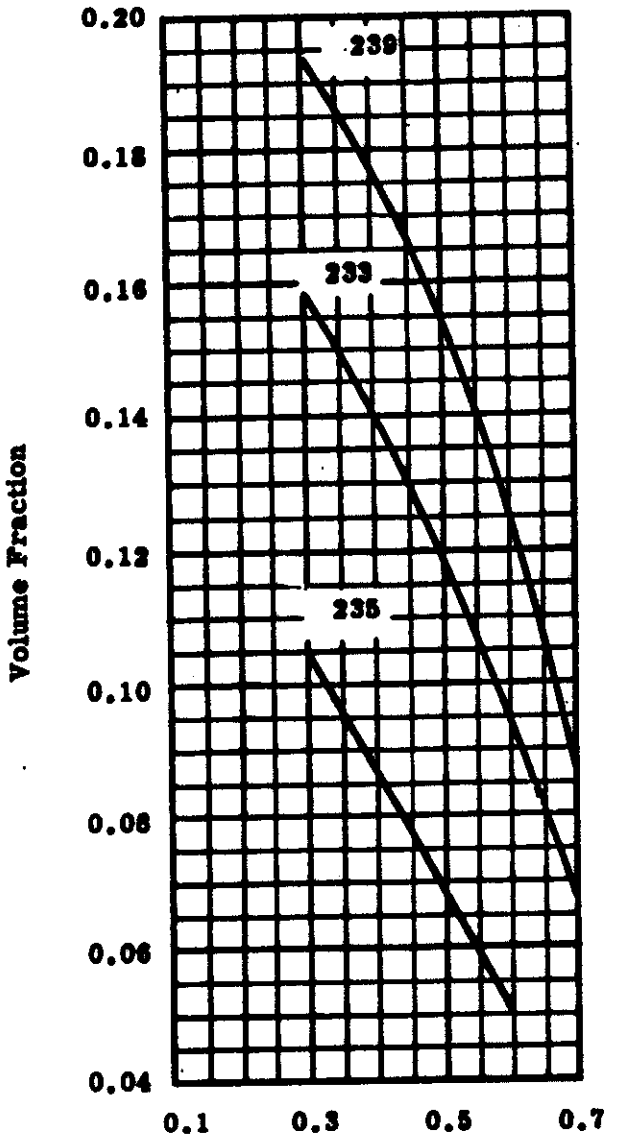

FIGURE 4.24

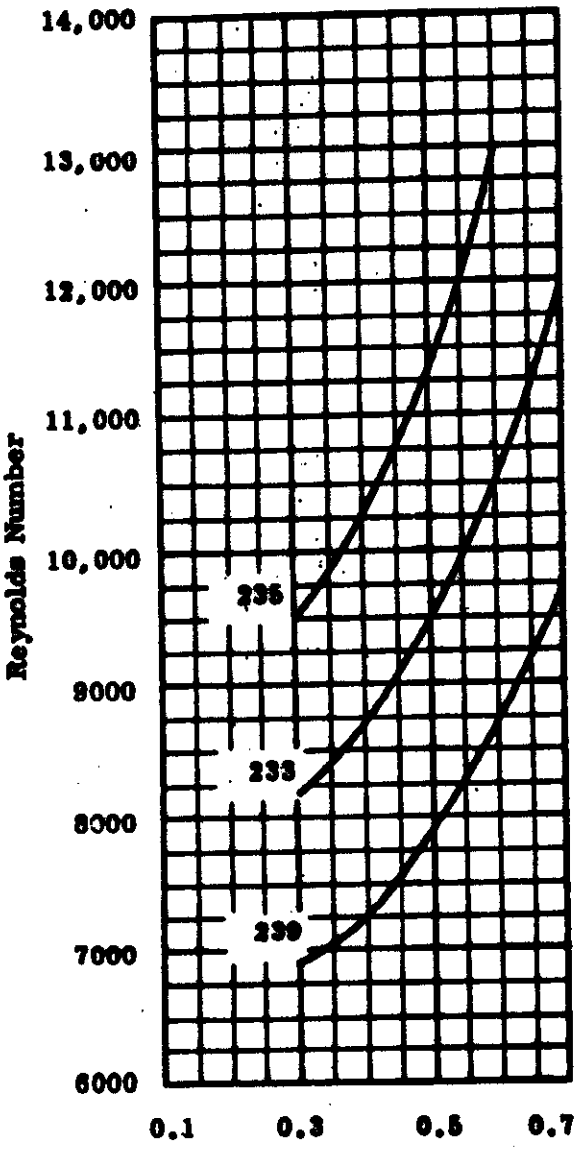

Volume Fraction of Tungsten in Cermets, 100% Dense
0.95 Total Pressure Ratio

FIGURE 4.23 - 4.24

Volume Fraction of Tantalum in Core and Bulk Average Reynolds Number

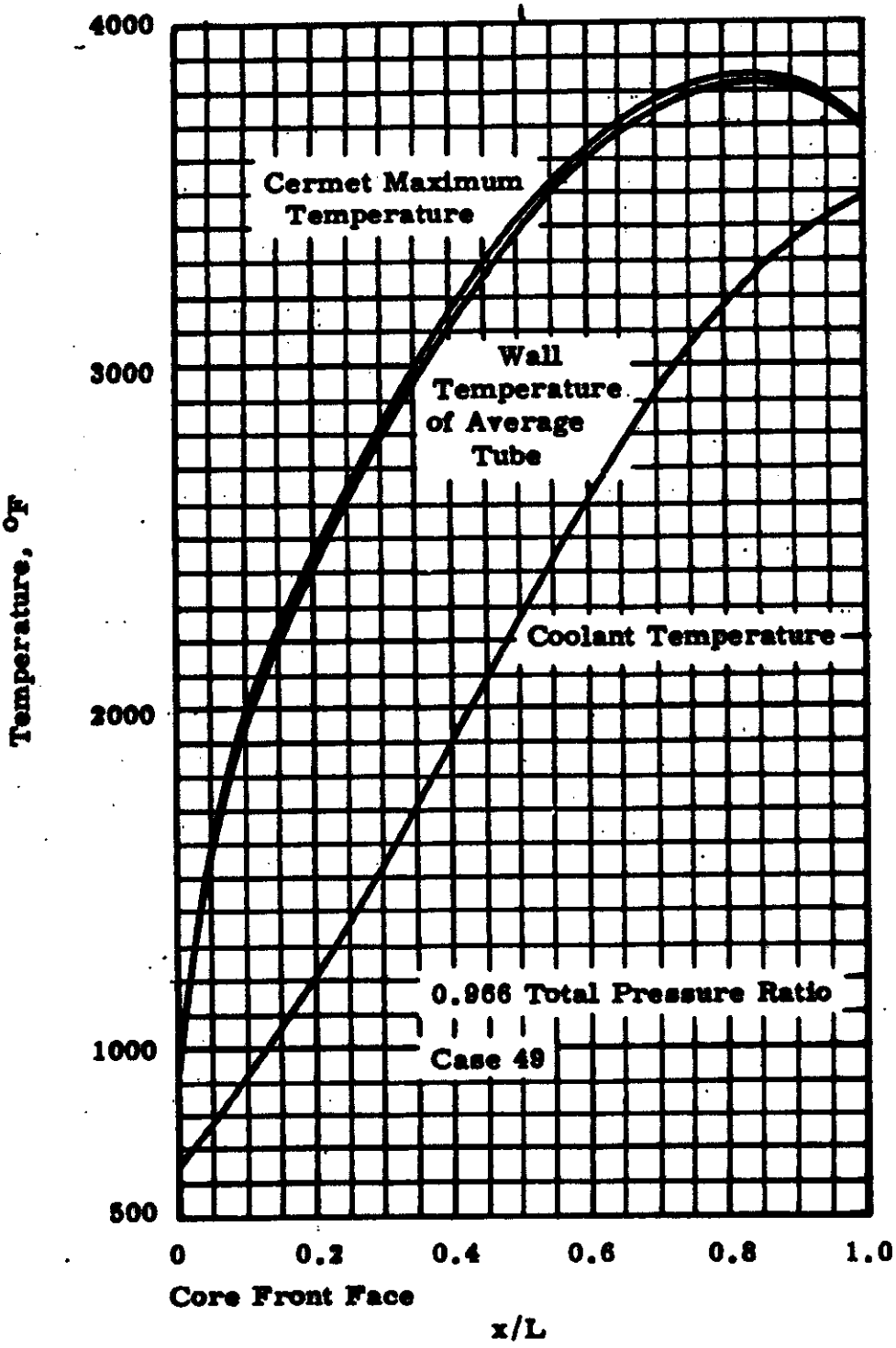

FIGURE 4.25

$U^{233}O_2$ Typical Core Temperatures for 30 vol% Tungsten in Cermets

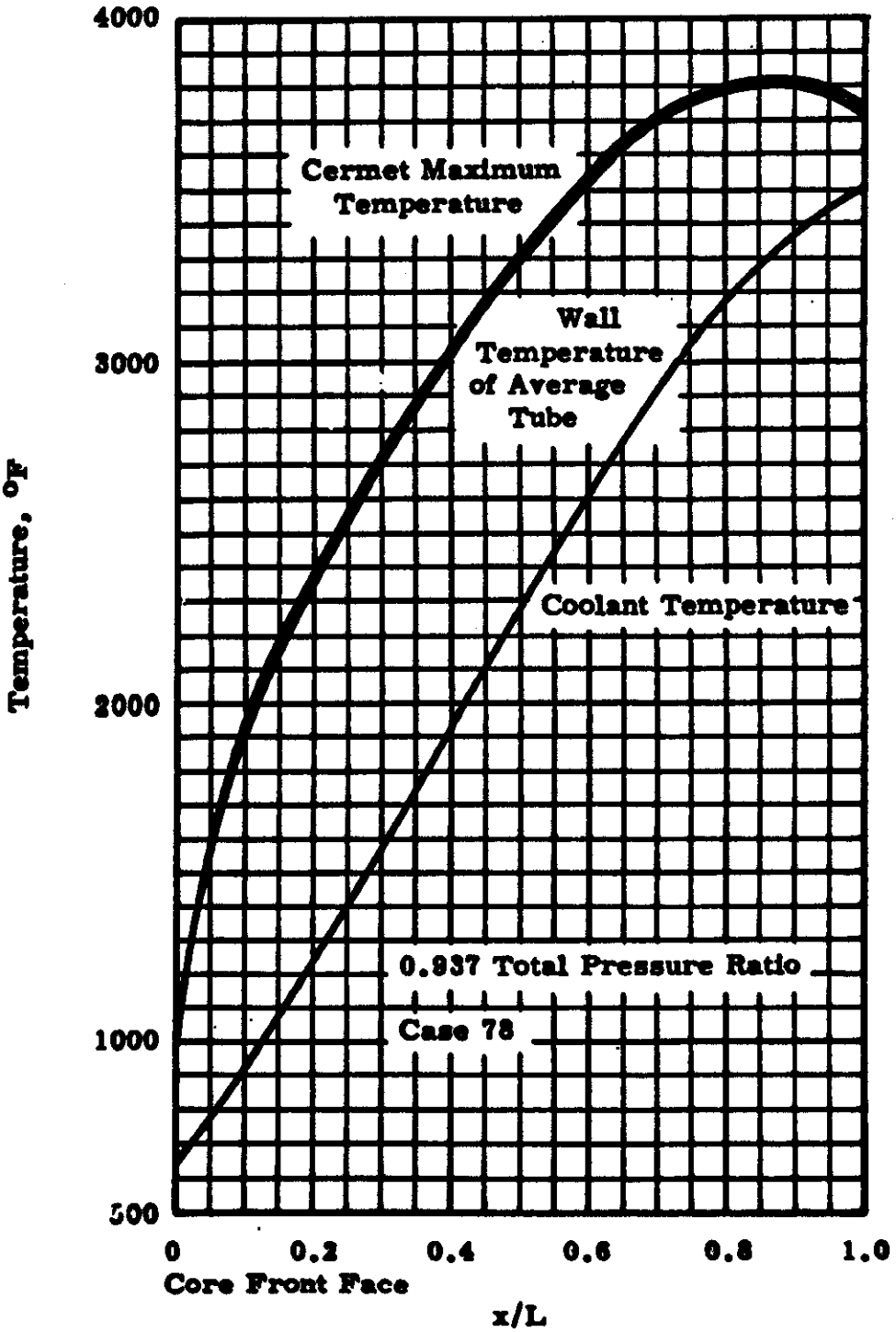

FIGURE 4.26

$Pu^{239}N$ Typical Core Temperatures for 30 vol% Tungsten in Cermets

the required void fraction at a power of 10 MW for U^{233} and Pu^{239} cores increases by almost 100% over U^{235} because the coolant area must be about the same for all equal power design points, but the U^{233} and Pu^{239} core diameters are still less than U^{235}. Lower power applications will enable a decrease in coolant area, core void, and diameter allowing an increase in the practability of the small cores at lower powers. This can be qualitatively visualized by imagining the 0.94, 0.95, and 0.96 total pressure ratio lines on Figures 3.1, 3.2, and 3.3 to be constant power lines at one total pressure ratio.

4.6 EFFECT OF LOW REYNOLDS NUMBER

For plutonium fueled cores with high total pressure ratio (near 1), the exact design point cannot be met: the coolant bulk average Reynolds number is about 7700 at a pressure ratio of 0.95. The transition region, between laminar and turbulent pipe flow, usually occurs at Reynolds numbers between 2000 to 3000. The design point Reynolds number of 8000 is chosen in consideration of the following three factors: (1) laminar to turbulent transition has been observed to be delayed, in carefully controlled experiments, up to Reynolds numbers of 8 to 10 thousand; (2) there is a great deal of difference between laminar and turbulent pressure drop; and (3) the flow is either wholly laminar or turbulent.

The last two statements infer that, if a channel is operated near this region of flow, the passage may be alternately "starved" and "flooded" with consequent pressure fluctuations and hot spots. An additional consideration concerns the confidence we can place in the classical compressible flow equations which are based on high Reynolds number flow but used for laminar flow.

As the viscosity of gases increase with temperature, the entrance Reynolds number is, at design point, about 130% of the average Reynolds number while the exit is about 70% of the average. Thus, even at an average 8000 the exit is about 5600. On the other hand, the flow being initially turbulent, (Reynolds number = 10,500) gives some confidence that even at 5600 transition is remote because the flow is already turbulent.

The point under discussion lies not with the fuel itself but is inherent because of the small cores with consequent higher volumetric heat generation rates. Approximately the same flow area is required for all cores at equal total pressure ratios; hence, the heat flux is higher in smaller cores with the tubes smaller and of greater number to achieve the same wall temperature. The smaller but more numerous tubes reduce the Reynolds number.

5.0 REACTOR SIZES AND FUEL INVENTORIES

5.1 BASIS FOR NEUTRONIC ANALYSES

The three fuels under consideration were PuN-W, $U^{233}O_2$-W, and $U^{235}O_2$-W. The isotopic composition of Pu was assumed to be 95 wt% Pu^{239} and 5 wt% Pu^{240}. The isotopic composition of U^{235} was taken to be 93 wt% U^{235} and 7 wt% U^{238}. For the $U^{233}O_2$ cermet, the U^{233} content was assumed to be 100%.

For the purposes of the criticality calculations, all reactors were represented as radially reflected cylinders with a core L/D of unity. A total axial reflector savings of 12 cm was used for all cores. The radial reflector was assumed to be beryllium at 0.9 TD. A summary of the material densities is given in Table 5.1.

Most of the criticality calculations were carried out by means of a one-dimensional (radial) diffusion theory code. Nuclear Cross section data were taken from the 16 group Hansen-Roach compilation.[5]

Diffusion theory overestimates the critical size of small reactors. As a consequence, the critical size estimates for the smaller PuN and $U^{233}O_2$ fueled reactors are expected to be more pessimistic than the estimates for the $U^{235}O_2$ cores. Nevertheless, the use of diffusion calculations was judged adequate for comparative studies.

TABLE 5.1

MATERIAL DENSITIES

Material	ρ(g/cc)	N nuclei/b-cm
Beryllium	1.85	0.1236385
Tungsten	19.3	0.06322757
Tantalum	16.6	0.0552544
PuN (95 wt% Pu^{239}, 5 wt% Pu^{240})	14.2	
		N^{239} = 0.03210077
		N^{240} = 0.00168951
		N^{N} = 0.03379028
$U^{233}O_2$	10.97	
		N^{233} = 0.02492937
		N^{O} = 0.04985874
$U^{235}O_2$ (93 wt % U^{235}, 7 wt % U^{238})	10.97	
		N^{235} = 0.0229924
		N^{238} = 0.0017306
		N^{O} = 0.0494461

5.2 RESULTS OF CRITICALITY CALCULATIONS

Figures 5.1 through 5.6 show the required critical core size for PuN, $U^{233}O_2$, and $U^{235}O_2$ fueled reactors for various core void fractions and cermet compositions. In all calculations, a 15 cm radial Be reflector has been assumed.

Figures 5.1 through 5.3 show the critical core diameter as a function of core void fraction for 30, 50, and 70 vol% tungsten in the fuel matrix. Figures 5.4 through 5.6 give cross plots of the first three graphs—that is, diameter versus vol% tungsten in the fuel for core void fractions of 0.2, 0.35, and 0.5.

5.3 EFFECT OF TANTALUM CLADDING

To test the effect of tantalum (a possible cladding material) on critical size and fuel inventory, the previous calculations were repeated

FIGURE 5.1

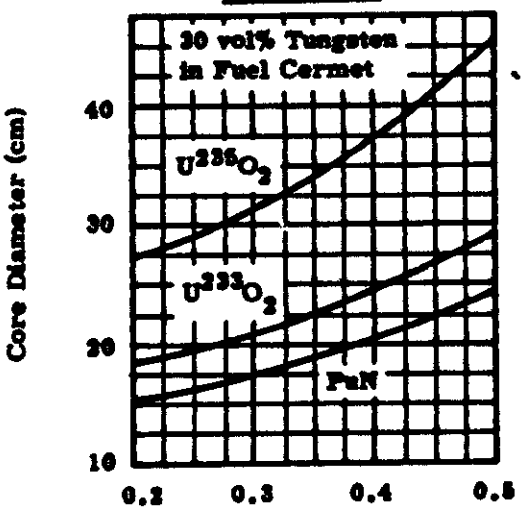

$\frac{\text{Ta vol\%}}{\text{void vol\%}} = 1/3$

16 cm Be Radial Reflector
L/D = 1, 12 cm Axial
Reflector Savings

FIGURE 5.2

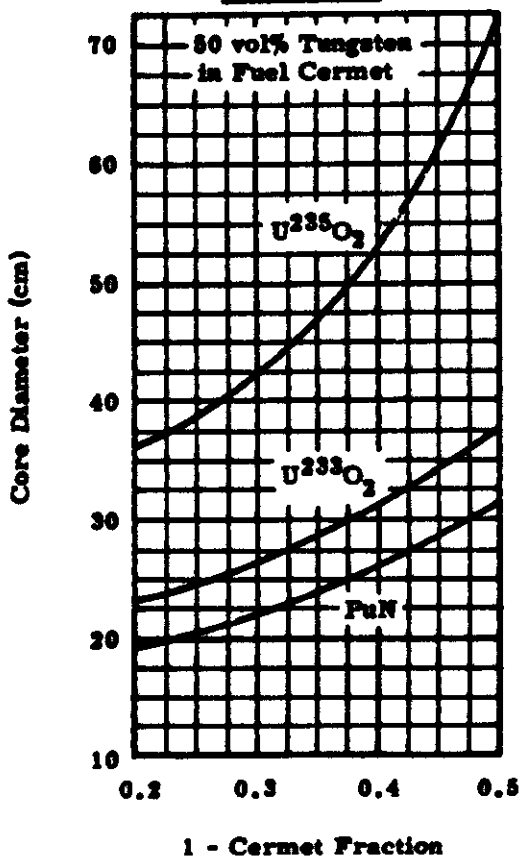

FIGURE 5.3

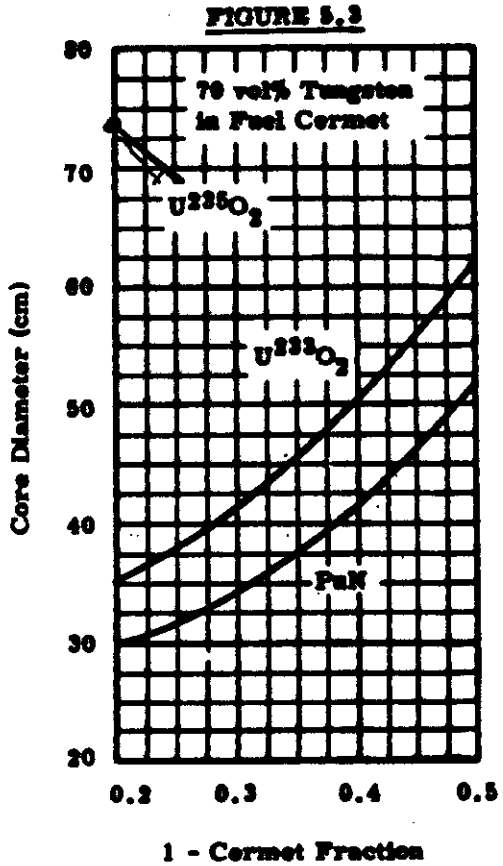

FIGURES 5.1 - 5.3

Critical Core Size Versus 1 - Cermet Fraction

FIGURE 5.4

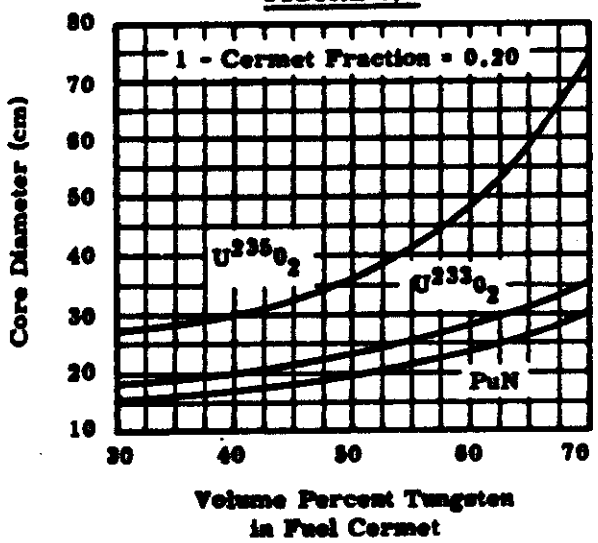

$\frac{\text{Ta vol\%}}{\text{void vol\%}} = 1/3$

15 cm Be Radial Reflector
L/D = 1, 12 cm Axial Reflector
Savings

FIGURE 5.5

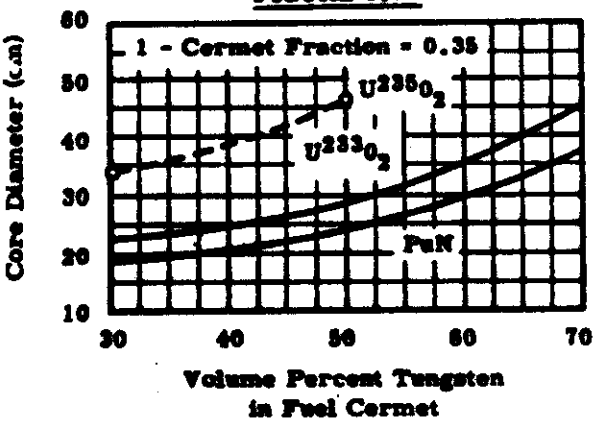

FIGURE 5.6

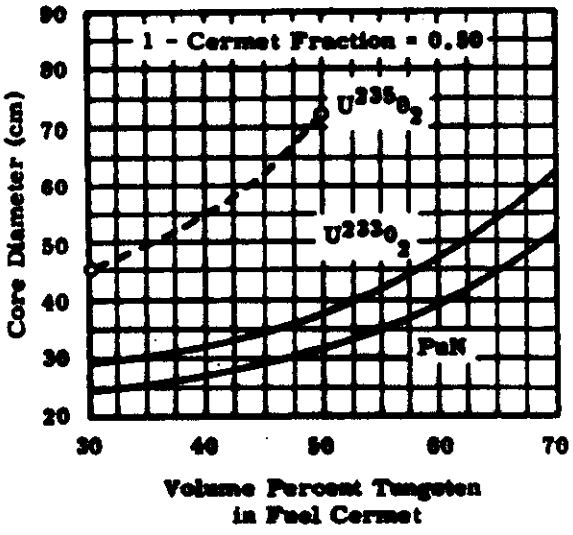

FIGURES 5.4 - 5.6

Critical Core Size Versus Vol% Tungsten in Fuel Cermet

[redacted]

with 1/4 of the original void filled with tantalum. The results are given in Figures 5.7 through 5.12. To make Figures 5.7 through 5.12 comparable to Figures 5.1 through 5.6, the independent variable has been changed to one minus the cermet (fuel + W) fraction, (1 - CF), rather than the void fraction. If no tantalum is present, one minus the cermet fraction is equivalent to the void fraction.

By comparing Figures 5.1 through 5.6 with Figures 5.7 through 5.12, it can be seen that the effect of tantalum is rather small. This small net effect is due to two compensating tendencies. On one hand, the absorption cross section of tantalum tends to decrease reactivity. This effect, however, is partially or totally balanced by the decrease in leakage caused by the scattering cross section. The effect of absorption predominates in the larger reactors; whereas the effect of scattering predominates in the smaller, high leakage reactors.

6.0 REFLECTOR CONTROL

6.1 REACTOR MODEL AND METHODS OF CALCULATION

Important interactions exist between core composition and the effectiveness of reactor control. In practice, rotating control drums containing poison are used to furnish the required reactivity changes. The analysis of this type of geometry, however, is rather difficult. For the purpose of comparing the effectiveness of different absorber locations and reflector materials, much simpler geometric models are adequate. Most of the calculations described in this section were carried out by means of one-dimensional(radial) transport calculations with 16 energy groups. The effect of drum rotation was simulated by changing the radial position of a B_4C (natural boron) annulus.

If more quantitative information regarding reflector control is required, one must resort to 2-D calculations. A series of 2-D (r, θ) calculations were carried out for some selected reactor configurations. These are discussed at the end of this section.

FIGURE 5.7

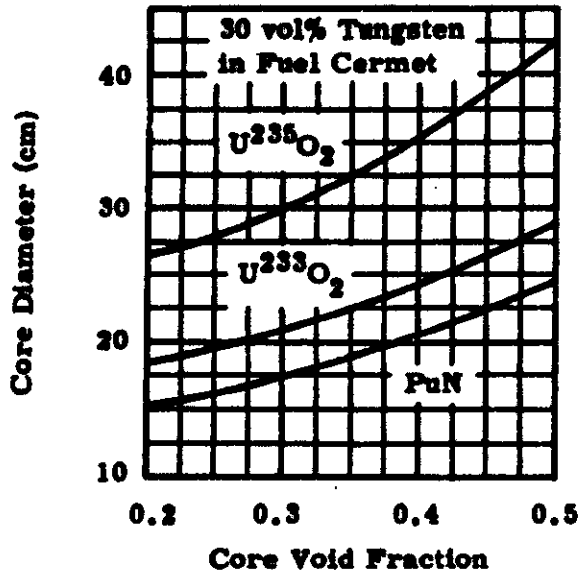

15 cm Be Radial Reflector
L/D = 1, 12 cm Axial
Reflector Savings

FIGURE 5.8

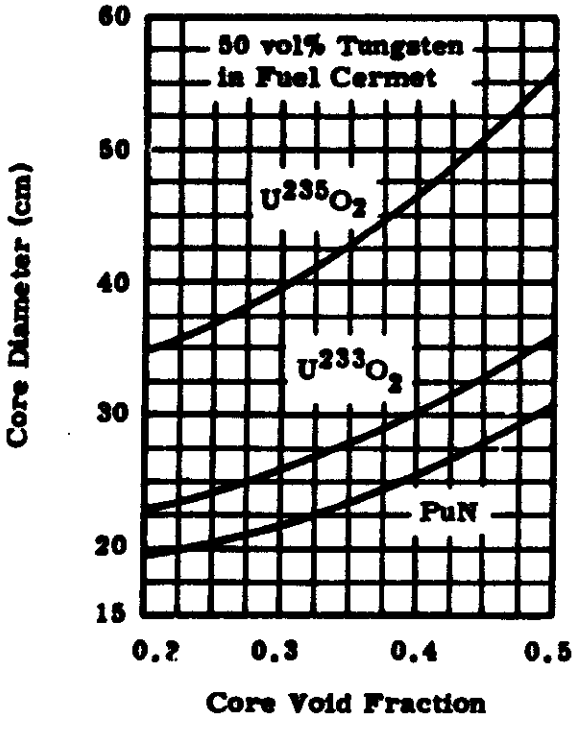

FIGURE 5.9

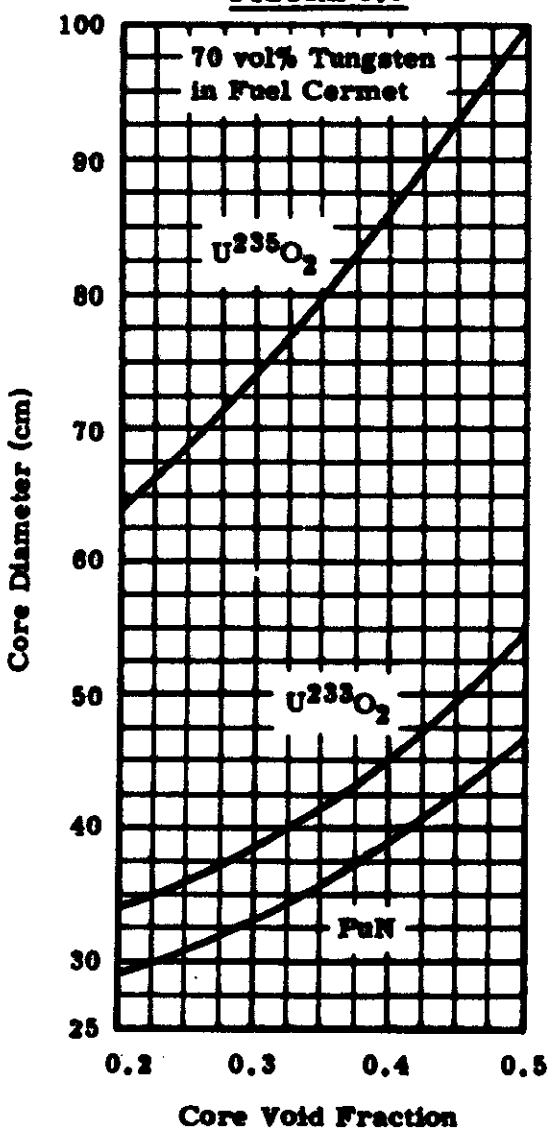

FIGURES 5.7 - 5.9

Critical Core Size Versus Core Void Fraction

FIGURE 5.10

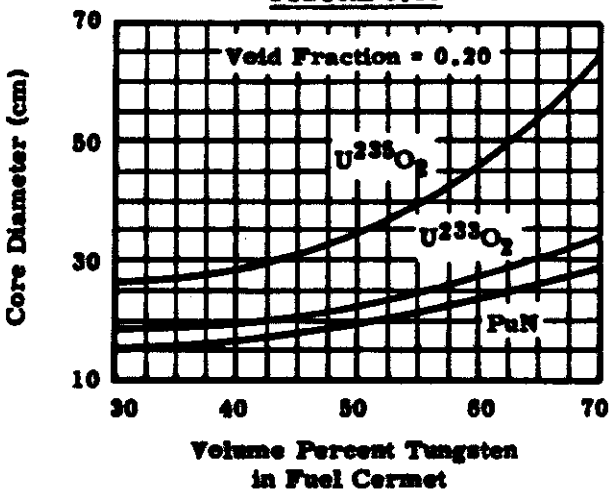

15 cm Be Radial Reflector
L/D = 1, 12 cm on Axial Reflector Savings

FIGURE 5.11

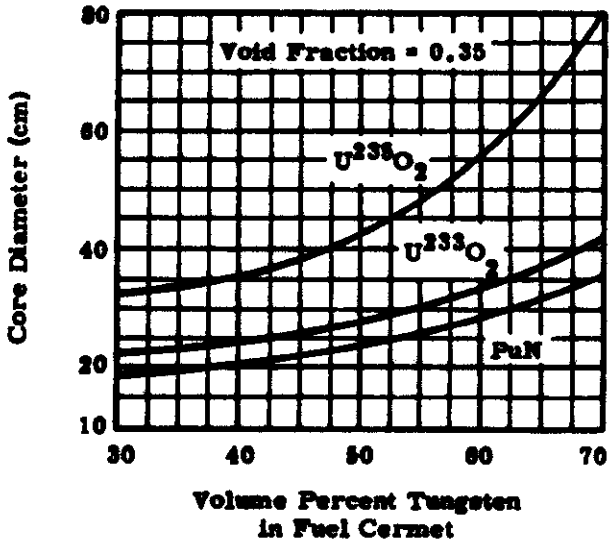

FIGURE 5.12

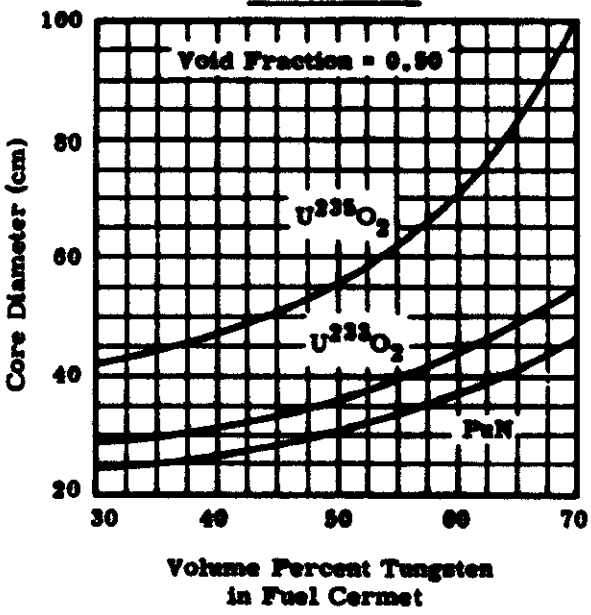

FIGURES 5.10 - 5.12

Critical Core Size Versus Vol% Tungsten in Fuel Cermet

6.2 REFLECTOR MATERIAL AND TOTAL REFLECTOR WORTH

In principle, either a light or a heavy material could be used as a radial reflector. A light material, such as beryllium, is usually preferable from a neutronics viewpoint. There are two reasons for this choice. First, the reflector savings per unit mass of reflector is greater for a light reflector than for a heavy reflector. This argument is demonstrated in Figure 6.1 for the archetypal elements beryllium and nickel. Second, a light reflector will enhance the worth of a control drum by moderating the spectrum. The marked contrast between the poison worth in a beryllium and a nickel reflector is shown in Figure 6.2.

6.3 CORE SIZE AND TOTAL REFLECTOR WORTH

Owing to the high leakage rate in the compact reactors under consideration, the total reactivity tied-up in the reflector is appreciable. As the core size is decreased and the core leakage fraction increased, the total reflector worth is also increased. This point is demonstrated in Figure 6.3 for a reactor fueled with $U^{235}O_2$-W.

If reflector control is accomplished by the physical removal of reflector sections, the smaller cores would have a control advantage. It does not follow, however, that reflector poison control also increases with decreasing core size. The reasons for this behavior will be discussed in the following paragraphs.

6.4 EFFECT OF CORE SIZE AND COMPOSITION ON CONTROL SWING

To investigate the characteristics of reflector poison control, the multiplication constant was computed as a function of the position of a 1 cm B_4C annulus for various core sizes and compositions. In all calculations, a 15 cm Be(0.9 ρ_o) reflector was assumed.

Figure 6.4 shows the reflector poison worth in PuN, $U^{233}O_2$, and $U^{235}O_2$ fueled reactors of equal size. Different fuel compositions are used to keep the multiplication constant in the vicinity of unity. Similar plots are given in Figures 6.5 and 6.6 for cores with equal void fractions and equal power capabilities, respectively. From these graphs, it is clear that the

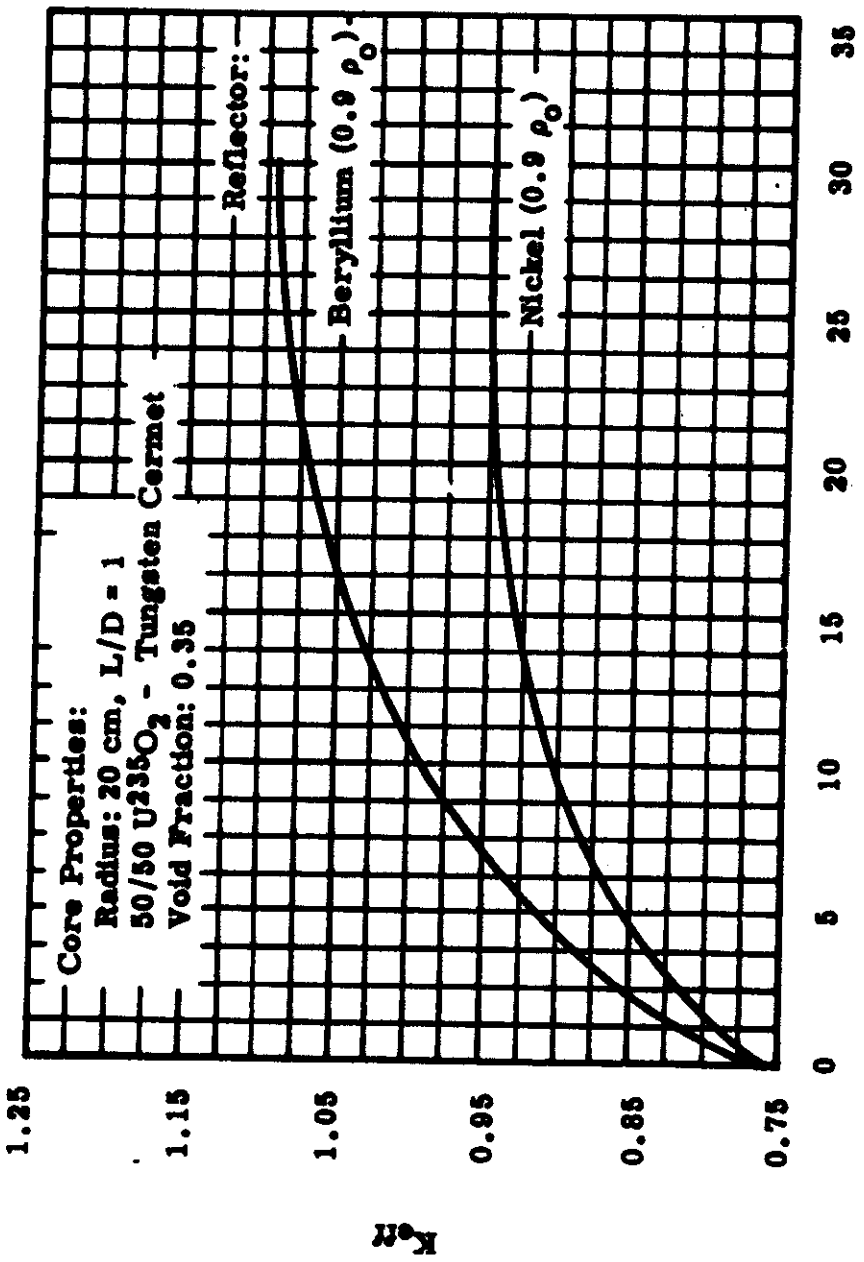

FIGURE 6.1
Reflector Reactivity Worth

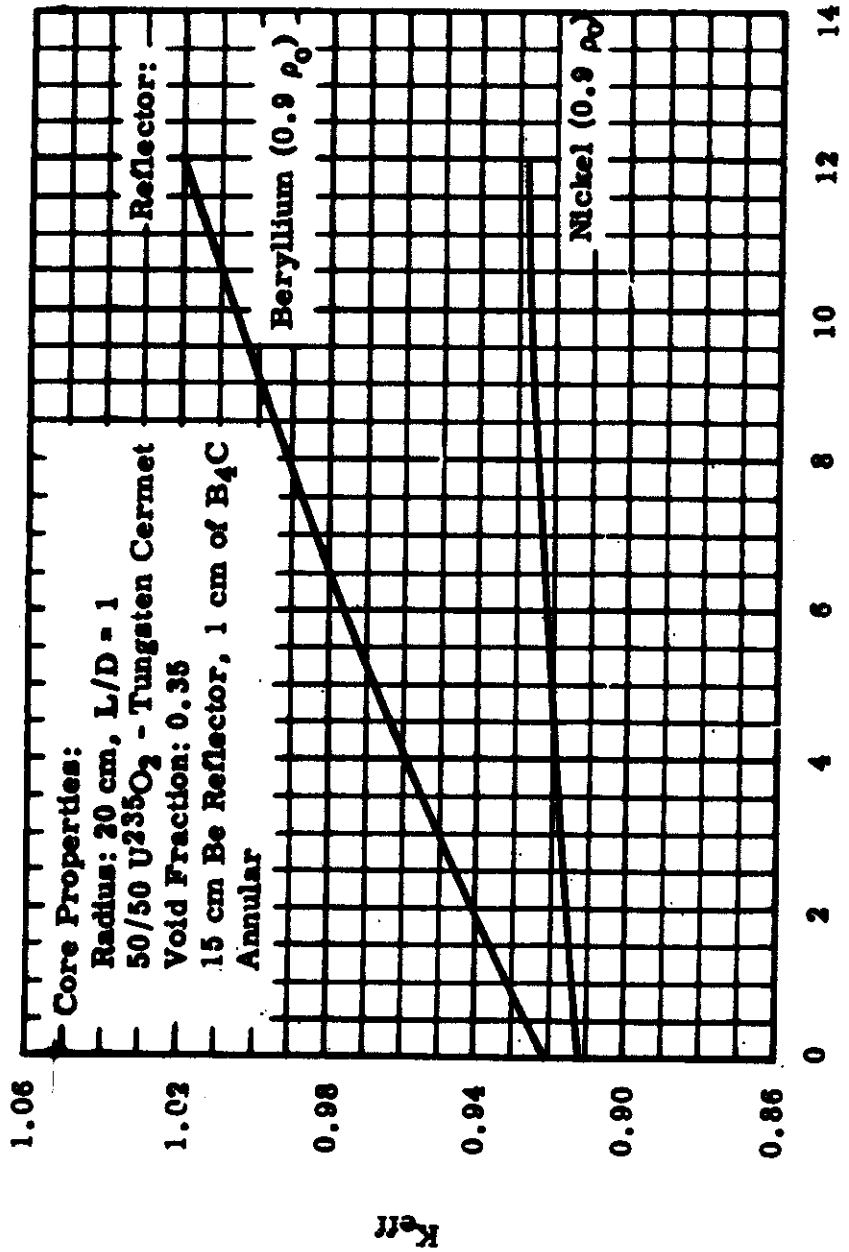

FIGURE 6.2
Reactivity Worth of B_4C Annulus

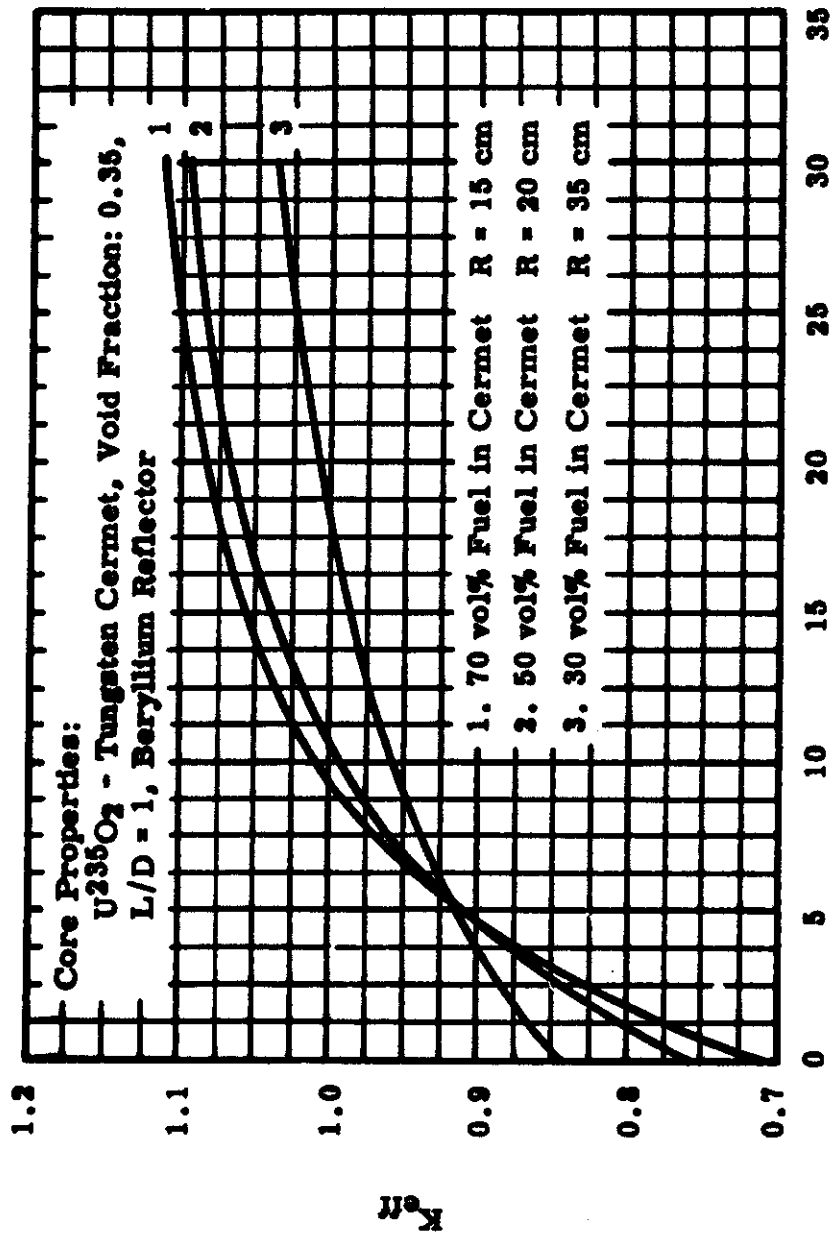

FIGURE 6.3

Effect of Core Size on Total Reflector Worth

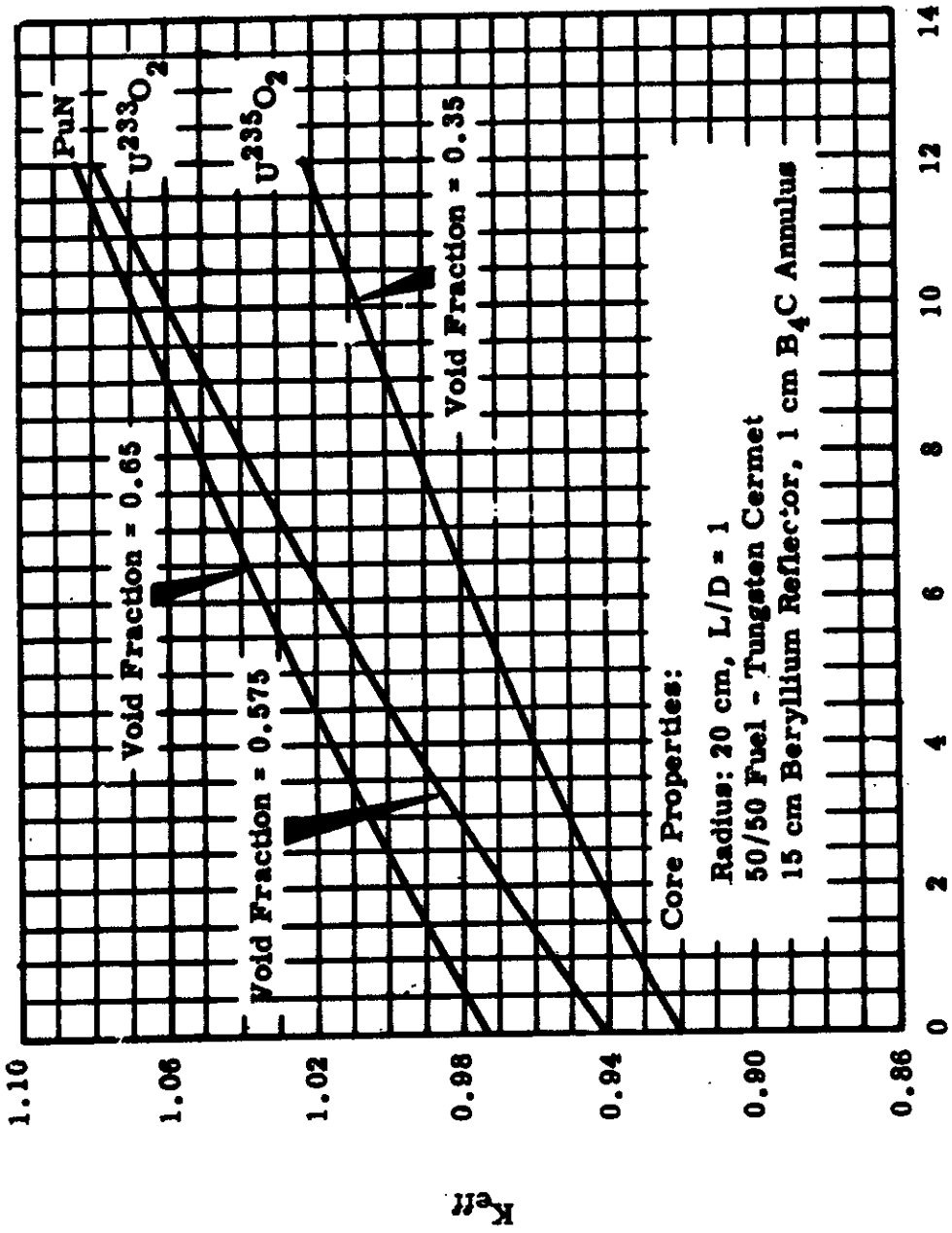

FIGURE 6.4

Reactivity Worth of B_4C Annulus for Equal Size Cores

[redacted]

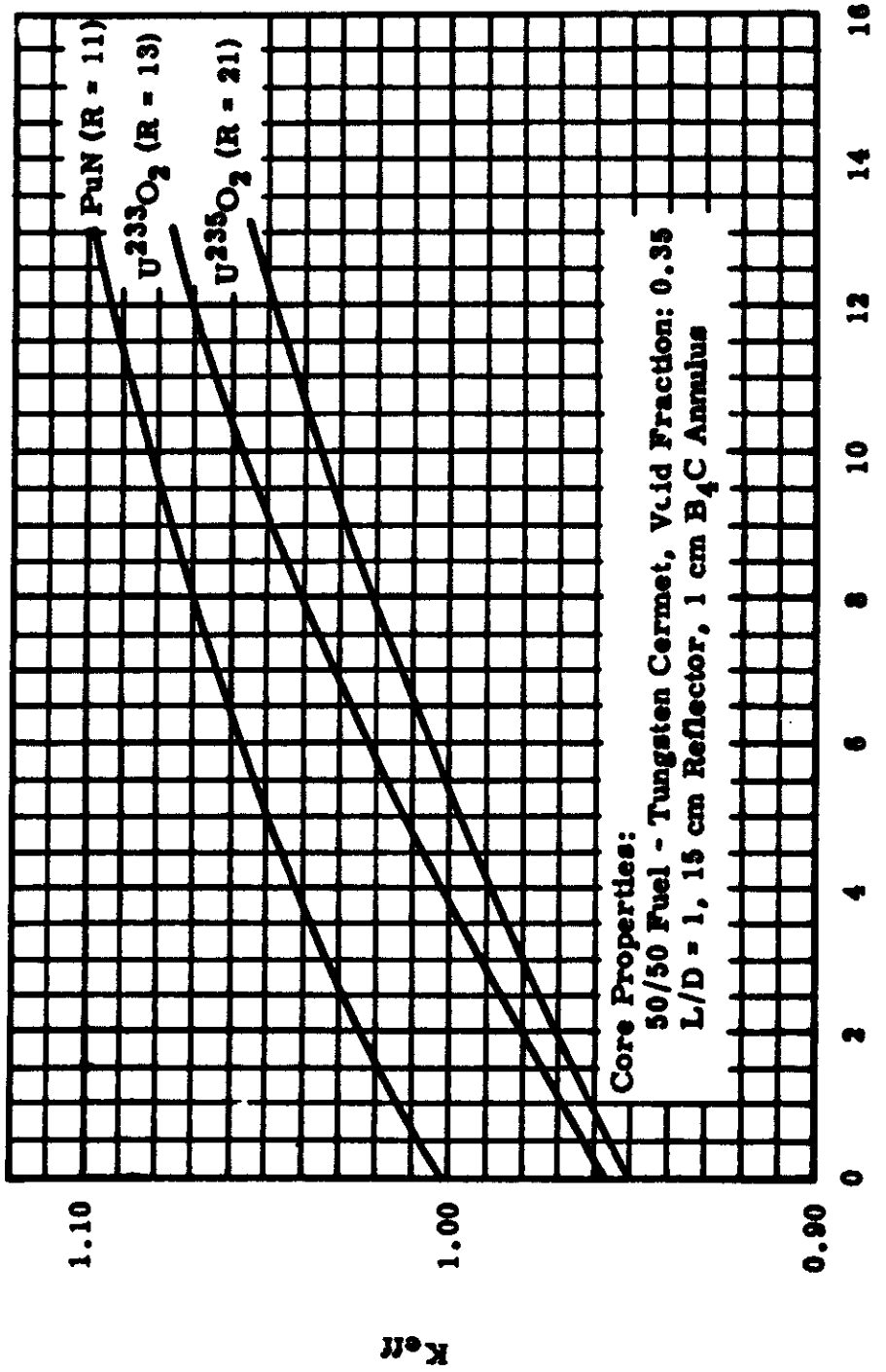

FIGURE 6.5

Reactivity Worth of B_4C Annulus for Equal Composition Cores

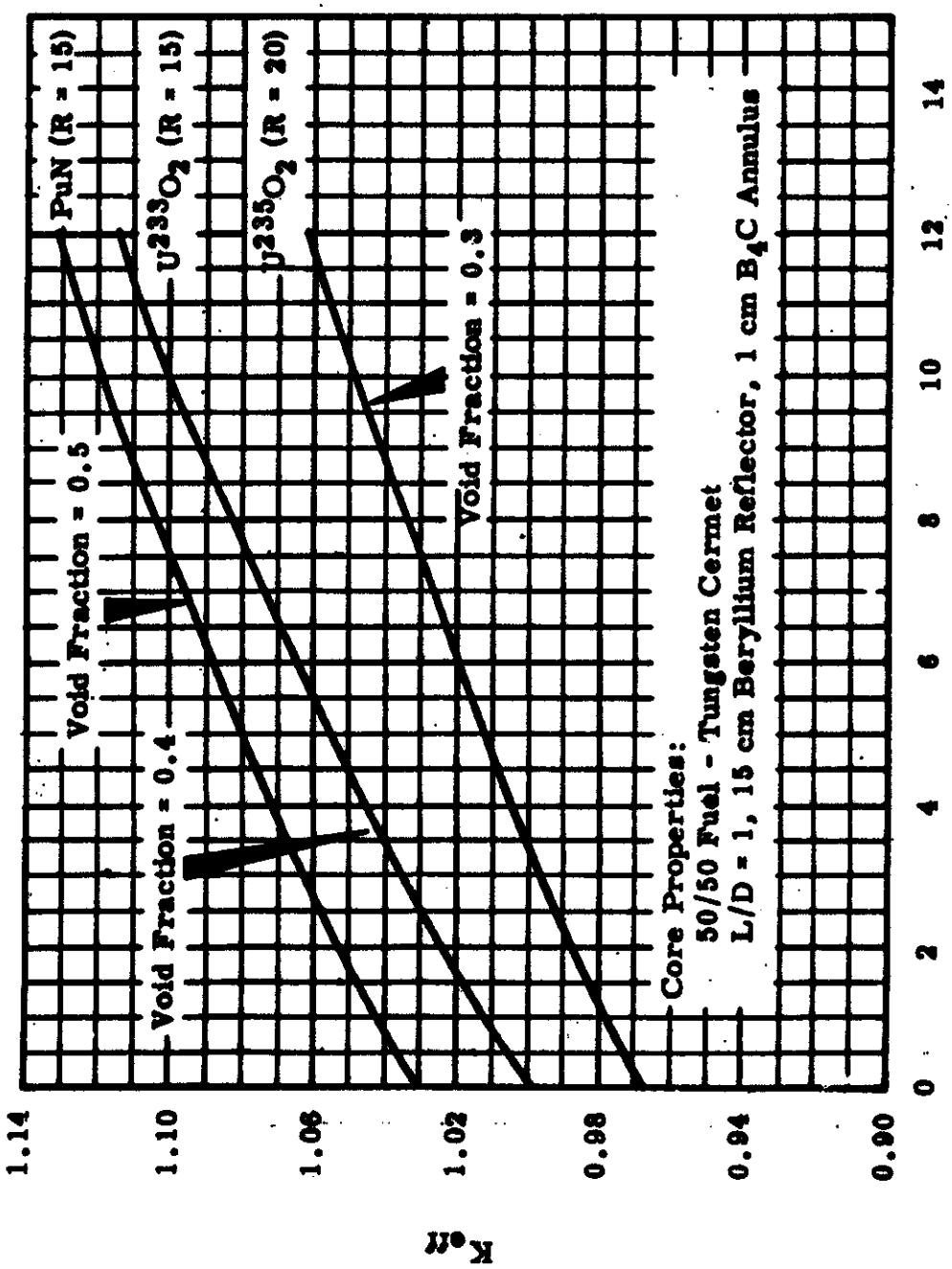

FIGURE 6.6

Reactivity Worth of B_4C Annulus for "Equal Power" Cores

reflector poison reactivity worth is rather insensitive to the core size and fuel material. This behavior can be understood, in part, by noting that the fast neutrons can easily pass through 1 cm of B_4C. Thus, even though the fast neutron leakage is increased as the core size is decreased, the effect of the B_4C annulus does not appreciably change. As a result, the small cores do not appear to have a major control advantage compared to the larger cores if reflector poison control elements are used.

6.5 EFFECT OF POISON ANNULUS THICKNESS

As stated previously, a B_4C ring appears quite porous to fast neutrons, yet almost black to the thermal tail of the spectrum. One would therefore surmise that a thin poison annulus would be almost as efficient as a thick annulus. Figure 6.7 demonstrates that this is indeed the case. It should be noted, however, that the poison saturation may not be nearly as rapid if discrete reflector drums are used in place of the homogeneous annulus.

6.6 COMPARISON OF DISCRETE REFLECTOR POISON ELEMENTS AND POISON ANNULI

In the previous discussion, the reflector control was simulated by the radial displacement of homogeneous poison annuli. To compare this geometry with a discrete poison element geometry, the multiplication constant was computed as a function of the fraction of the total sector subtended by discrete poison arcs. This model is obviously more suitable than homogeneous annuli for the analysis of rotating poison drums located in the reflector. Furthermore, it is directly applicable to systems using translating reflector poison elements.

The results are shown in Figure 6.8 for poison sectors of 30 and 90 degrees. All computations were performed using a two-dimensional (R-θ) transport theory model with 16 energy groups. From this graph, it is clear that a homogeneous poison annulus gives a good simulation of a set of closely spaced poison arcs. This indicates that an annulus should give a reasonable approximation to a set of closely spaced reflector drums.

[redacted]

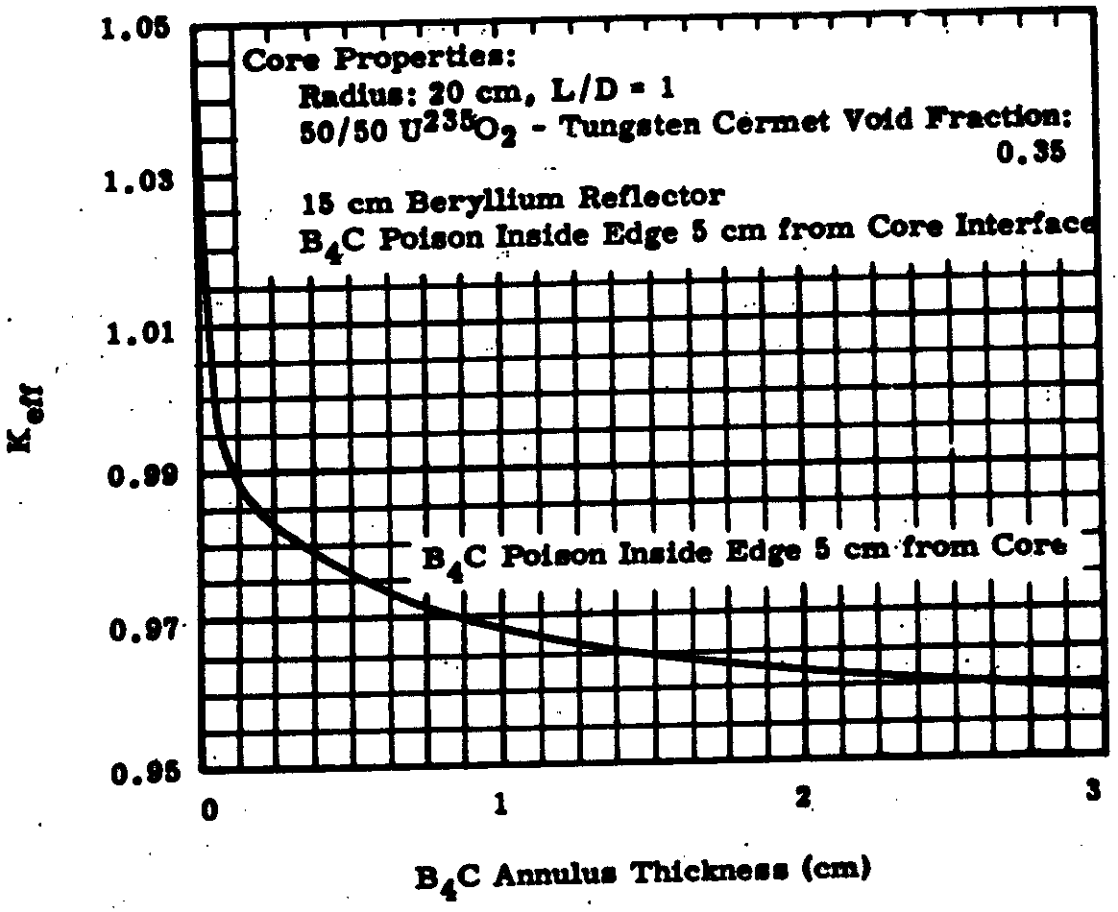

FIGURE 6.7

Effect of Poison Annulus Thickness on Reactivity

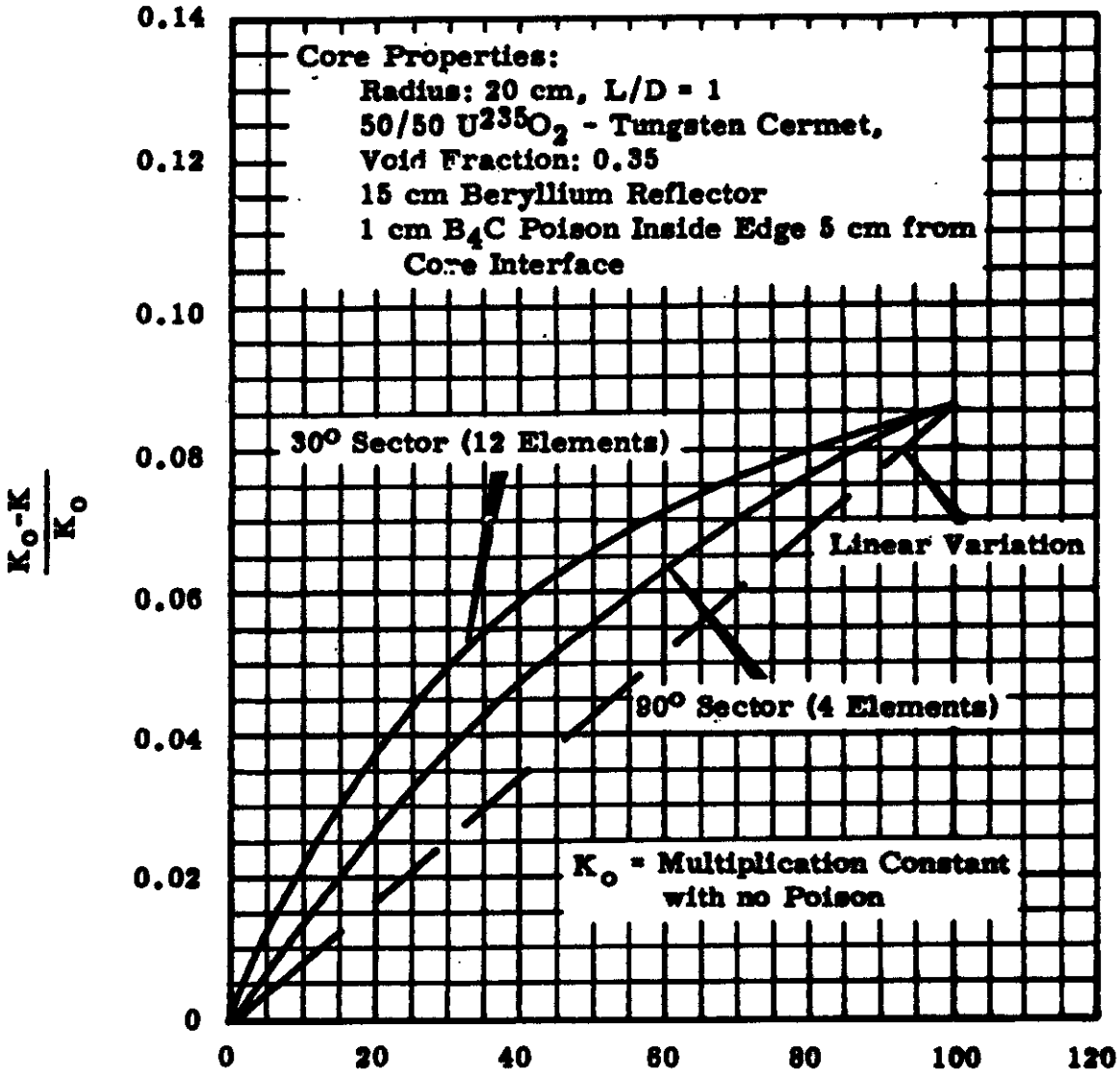

FIGURE 6.8

Reactivity Worth of Discrete Poison Arcs

7.0 ESTIMATES OF REACTOR LIFE AND SHIM CONTROL REQUIREMENTS

7.1 APPROXIMATE FORMULAS FOR REACTOR ENDURANCE

For long-lived gas-cooled compact reactors, a major portion of the control requirements is shim control. It is relatively simple to obtain a good estimate of the reactivity life and corresponding shim control requirement for the small fast reactors considered in this report. These reactors have essentially zero fuel conversion; and the fission products have a negligible effect on reactivity.

If we consider only burnup of fissile fuel, it can be shown that:

$$\delta k \sim \left(\frac{\eta-1}{\eta}\right) \frac{\delta M}{M_o}, \qquad (7.1)$$

where:

δk = reactivity variation, (shim control)

η = effective eta of fuel $(\nu\sigma_f/\sigma_a)$,

M_o = fuel mass,

δM = change in fuel mass.

Converting fuel mass to equivalent fission energy, Equation (7.1) becomes

$$\delta k \sim -\ 0.39 \left(\frac{\eta-1}{\eta}\right) \frac{P(MW)}{M_o\ (kg)}\ T\ (days), \qquad (7.2)$$

or

$$T(d) = -\ C\ \frac{M_o\ (kg)}{P(MW)}\ \delta k, \qquad (7.3)$$

where

$$C = \frac{\eta}{0.39\ (\eta-1)}\ . \qquad (7.4)$$

Approximate values of η, $\frac{\eta-1}{\eta}$, and C are listed in Table 7.1 for the three fuels of interest.

TABLE 7.1

PARAMETERS FOR BURNUP EQUATIONS

Fuel	η_{eff}	$\left(\frac{\eta-1}{\eta}\right)_{eff}$	C
Pu^{239}	3.1	0.68	3.8
U^{233}	2.4	0.58	4.4
U^{235}	2.08	0.52	4.9

7.2 NUMERICAL RESULTS OF BURNUP CALCULATIONS

In order to check the validity of Equations (7.1) and (7.2), the fuel burnup at 10 MW power level was computed using a 16 energy group diffusion theory model with four radial burnup zones. Production and burnup of Pu^{240} were taken into account, although the fission products were not.

Figures 7.1 through 7.3 give the multiplication constant as a function of time for reactors fueled with U^{235}, U^{233}, and Pu^{239}. Two void fractions are considered for each fuel. Note that in all cases the multiplication constant is almost exactly a linear function of time. Furthermore, the slope is quite close to that predicted by Equation (7.2).

A few observations should be made on the above results. For a given reactivity control span, it is clear from Equation (7.3) that the reactor life is roughly proportional to the critical fuel mass. This indicates that for a given reactivity control span, the smaller PuN and $U^{233}O_2$ fueled reactors will have a shorter reactivity life than $U^{235}O_2$ reactors for a given total power. Moreover, a given $\delta M/M$ causes a larger reactivity change in Pu and U^{233} fueled reactors since these fuels have a relatively high value of eta.

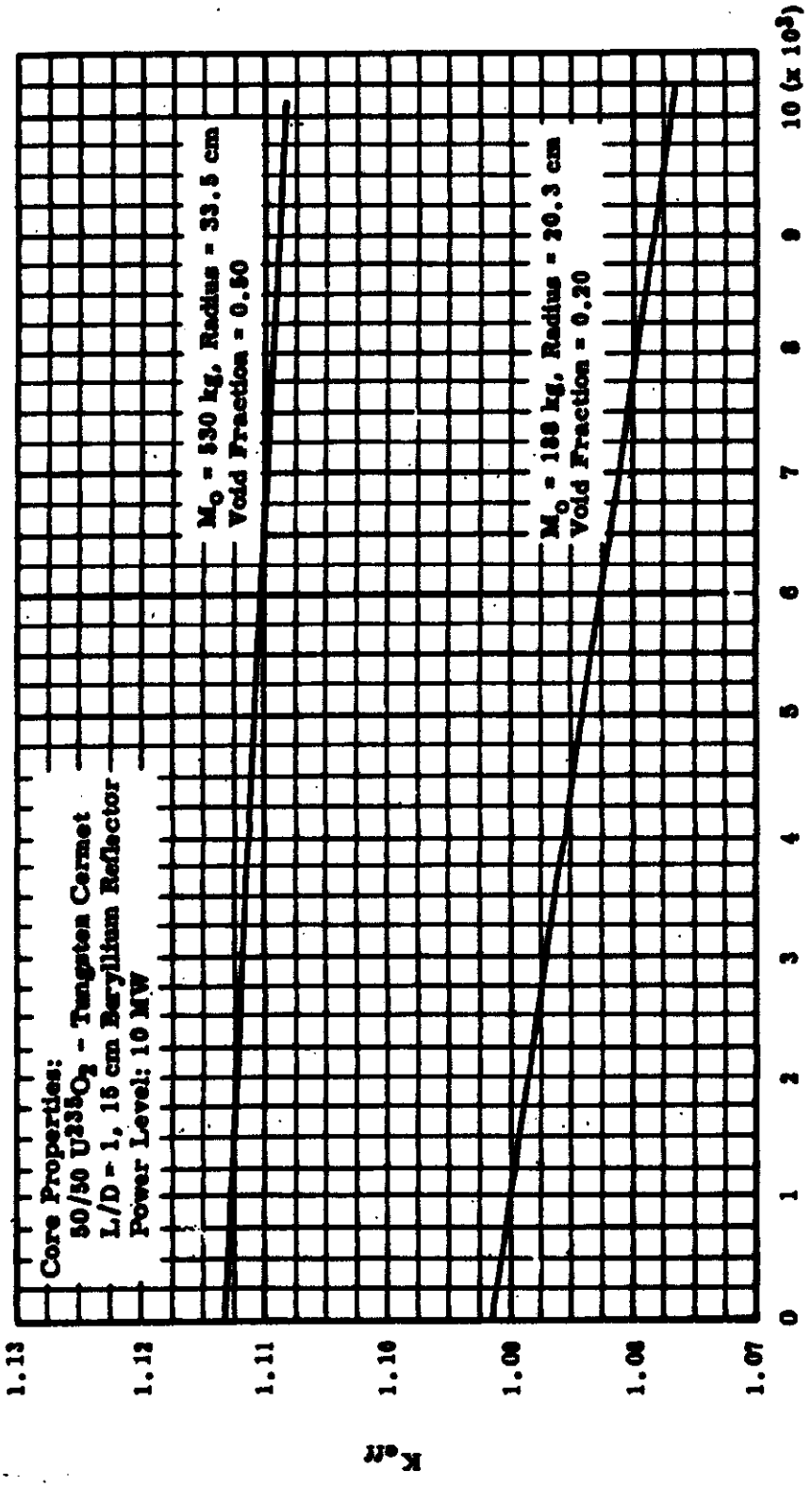

FIGURE 7.1

Reactivity Lifetime Characteristics: $U^{235}O_2$ - Tungsten Cores

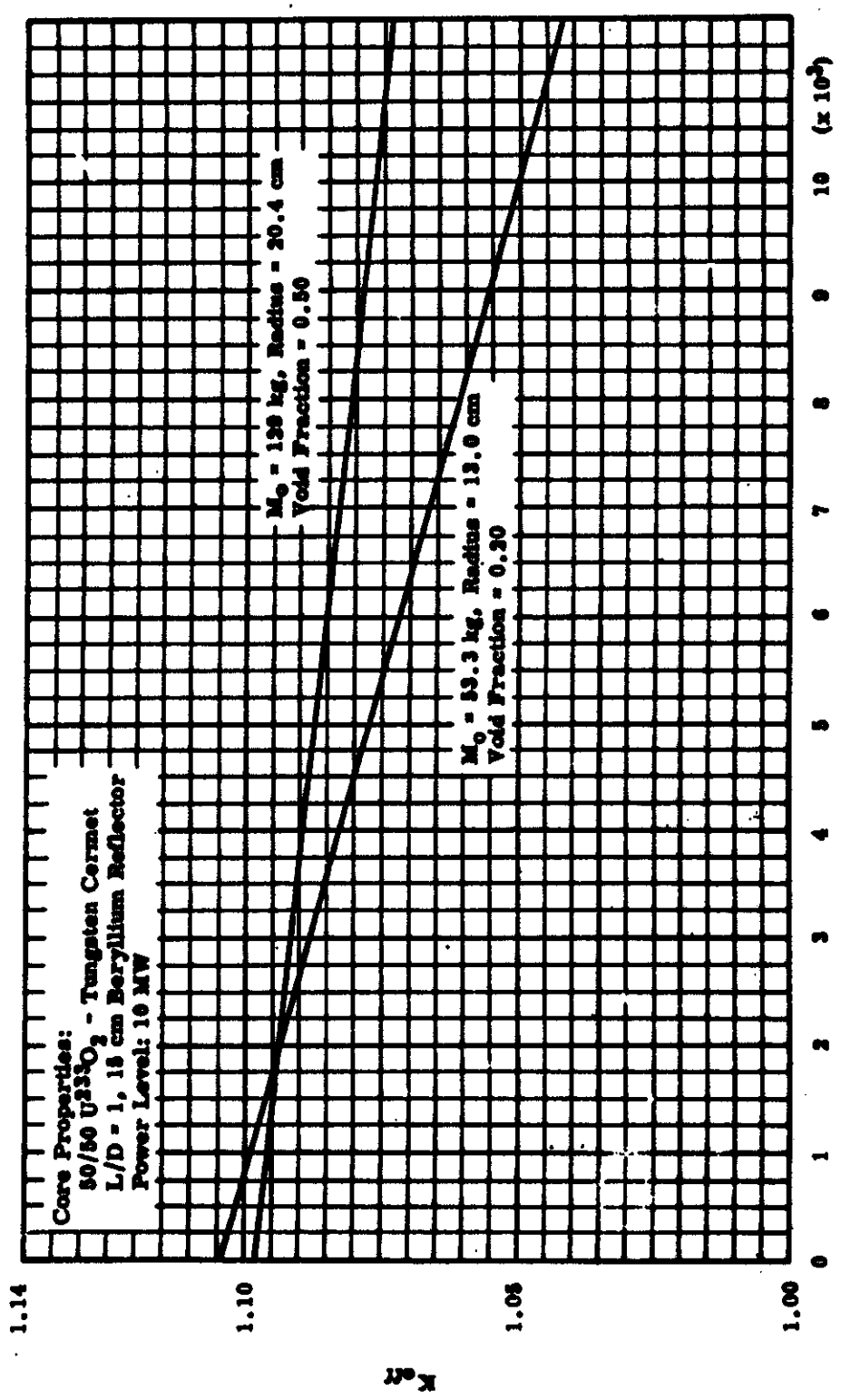

FIGURE 7.2

Reactivity Lifetime Characteristics: $U^{233}O_2$ - Tungsten Cores

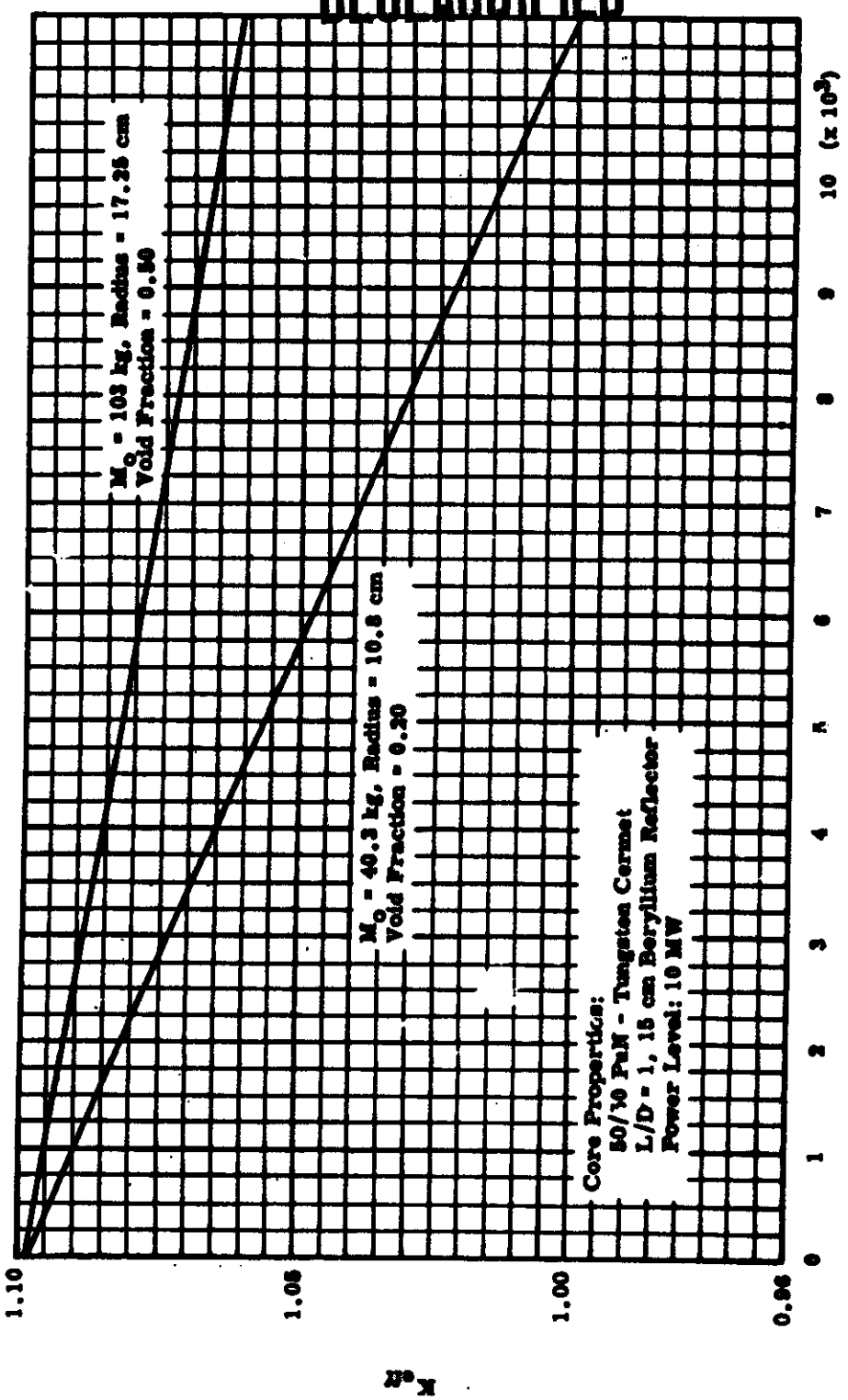

FIGURE 7.3

Reactivity Lifetime Characteristics: PuN - Tungsten Cores

8.0 REACTIVITY COEFFICIENTS

8.1 EFFECT OF REACTOR COOLANT ON REACTIVITY

The common closed cycle gas coolants, such as neon and helium, have a negligible effect on reactivity. The presence of an appreciable amount of hydrogen, however, does cause a pronounced change in spectrum and reactivity. Hydrogen moderates neutrons into a higher cross section region, which consequently increases reactivity by increasing the capture rate in the fuel.

Figure 8.1 shows the effect of a uniform hydrogen addition to PuN, $U^{233}O_2$, and $U^{235}O_2$ fueled reactors. These results were obtained using a one-dimensional transport model with 16 energy groups. For this analysis, the microscopic cross sections were assumed to be independent of hydrogen density.

Although these results are, at best, only rough approximations, they do indicate that the use of hydrogen in compact fast reactors can pose serious control problems. The PuN core appears least affected by the hydrogen addition.

8.2 FUEL EXPANSION COEFFICIENT

Another important reactivity coefficient is associated with the expansion of fuel. The axial fuel expansion coefficient was computed by calculating the multiplication constant as a function of the core length. The fuel inventory was conserved by uniformly decreasing the fuel density while increasing the core length.

Table 8.1 gives the expansion coefficient data for reactors fueled with PuN, $U^{233}O_2$, and $U^{235}O_2$. As one would expect, all fuels have approximately the same expansion coefficient in terms of $\delta k/(\delta L/L)$. In terms of dollars, of course, the expansion coefficients in Pu^{239} and U^{233} fueled reactors are about three times larger than those in U^{235} fueled reactors.

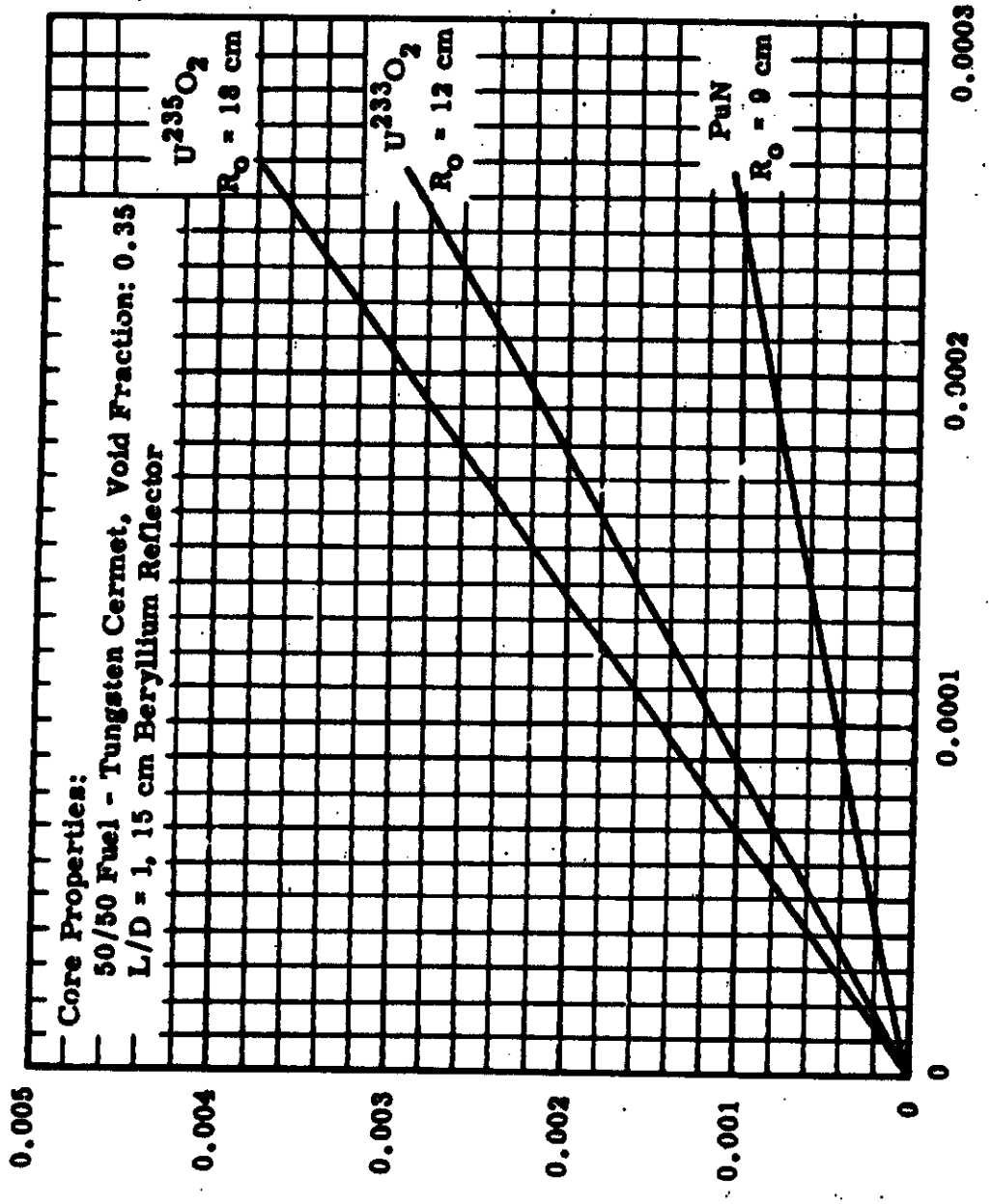

FIGURE 8.1

Effect of Hydrogen on Reactivity

TABLE 8.1

FUEL EXPANSION DATA*

Parameter	$U^{235}O_2$	$U^{233}O_2$	PuN
Delay Fraction, β	0.0064	0.0026	0.0021
Core Length, cm	36	24	19
$\delta k/(1\% \frac{\delta L}{L})$	-0.00401	-0.00464	-0.00429
$\delta k (\$)/(1\% \frac{\delta L}{L})$	-0.627	-1.78	-2.04

* Void Fraction = 0.35
50 vol% fuel in cermet.

APPENDIX A

EVALUATION OF FLUID-DYNAMIC CALCULATIONS IN COMPARISON WITH THE 710 TEST REACTOR REFERENCE DESIGN

Though the analytical method used for this study was developed independently, verification of the design calculations was achieved by frequently comparing with the 710 Test Reactor design as described in reports published by the General Electric Nuclear Materials and Propulsion Operation (NMPO). This helped assure comparable results or identify differences in the results arising from the methods used.

Sufficient information is available in Tables 3. 1, 3. 3, and Figures 3. 13 and 3. 14 of document GEMP-310[6] to define a model. Two methods of comparison are possible: one on the basis of the overall size of a U^{235} fueled reactor as calculated in this study and by NMPO, and the second on the basis of comparing the results of fluid flow and heat transfer analyses for a reactor core with a set of consistent design assumptions. The first comparison includes the influence of any differences in nuclear analysis in addition to those in the heat transfer model, but also serves to illustrate the effect on the reactor design of any differences observed using the second basis of comparison.

The overall results are shown, as core diameter, in Figure 3. 3. It is seen that these are in reasonably favorable agreement. The smaller core size, calculated from the BNW physics model, results in a larger void fraction than that utilized in the 710 design; but the coolant flow areas are essentially the same.

The heat transfer and fluid-flow calculations were also compared on a common basis using the geometry and heat generation profiles given in document GEMP-310. The design parameters held constant for this comparison were the number of coolant tubes and the core pressure drop. Calculations were made for two tube wall temperature limits: 3800 and 3838 °F. Results for zoned cores are shown in Table A-1.

TABLE A-I

ZONED CORES

Zone	Outer Radius Zone, in.	Cermet Fraction in Zone, Vol %	Hydraulic Diameter of Coolant Tubes in Zone, in.	Total Pressure Ratio	Maximum Average Tube Wall Temperature, °F	Core Power, MW	Number of Passages	Cool Flow Rate, lb/sec	Average Exit Temperature, °F
710 Reference Design (NMPO)									
1	0.79	76.0	0.065		3838				
2	3.45	75.9	0.065		3838				
3	4.81	76.0	0.065		3838				
4	6.18	76.4	0.065		3838				
5	7.40	76.0	0.065		3838		3241		
6	7.69	74.3	0.072		3794		258		
7	7.97	72.7	0.078		3771		264		
8	8.26	69.3	0.090		3792		270		
				0.958		10.242	4033	12.67	3500
710 Reference Design (BNW)									
1	0.79	73.2	0.078		3799				
2	3.45	73.2	0.078		3801				
3	4.81	73.2	0.078		3791				
4	6.18	73.2	0.078		3799				
5	7.40	73.6	0.077		3802		3248		
6	7.69	73.8	0.077		3801		252		
7	7.97	72.4	0.082		3791		248		
8	8.26	68.0	0.094		3799		287		
				0.958		10.062	4036	13.84	3253

The results are comparable within the accuracy of the model except for the coolant flow and exit temperature. To determine if this was brought about, in part, by close adherence to a maximum tube wall temperature of 3800 °F, calculations were made for a limit of 3838 °F. Relaxation of this criterion to higher wall temperatures would allow a decrease in coolant flow, resulting in a higher coolant exit temperature. Results are shown in Table A-2. With the relaxation in tube wall temperature, only a 25 °F increase in exit temperature is realized.

Another difference between the calculations is the use of a different set of isothermal friction coefficients. The disparity between the designs apparently is due to the difference in computing frictional losses. For this comparison, the number of tubes, pressure drop, and wall temperature are fixed. Hence, with the given friction coefficient and pressure ratio, there is one tube diameter, heat transfer coefficient, and exit temperature available.[7] The net result of reduction in the value of friction coefficient used or increase in number of tubes (decrease tube diameter) increases the heat transfer coefficient allowing an increase in coolant temperature while keeping the tube wall temperature, flow and pressure drop constant. This results in the desired increase in exit temperature. It is seen that the major discrepancy between the two thermal analyses results in a more conservative estimate of core pressure drop or tube wall temperatures by the BNW method. Based on the foregoing discussion, this arises from a difference in friction coefficient. The appropriate references are discussed in Appendix B.

TABLE A-II

DUPLICATING, USING BNW ANALYSIS,
THE TUBE TEMPERATURE PROFILE IN GEMP-310

Zone	Outer Radius Zone, in.	Cermet Fraction in Zone, Vol %	Hydraulic Diameter of Coolant Tubes in Zone, in.	Total Pressure Ratio	Maximum Average Tube Wall Temperature, °F	Core Power, MW	Number of Passages	Cool Flow Rate, lb/sec	Average Exit Temperature, °F
1	0.79	73.4	0.078		3839				
2	3.46	73.4	0.078		3839				
3	4.81	73.4	0.078		3839				
4	6.18	73.4	0.078		3839		3246		
5	7.40	73.8	0.077		3836		252		
6	7.68	73.8	0.077		3801		248		
7	7.97	72.4	0.083		3791		267		
8	8.26	69.0	0.094		3799		4033		
				0.958		10.07		13.52	3276

APPENDIX B

THERMAL AND FLUID-FLOW ANALYSIS OF CORE

B-1 INTRODUCTION

This appendix will deal with the following items:

A. Definition of thermal-hydraulic model
B. The breakdown of this model into its constituent volume fractions
C. A brief analysis and explanation of the methods used to handle the heat transfer and fluid flow. *

B-2 MODEL

B-2. 1 General Description

The heat transfer and fluid-flow model considers only those surfaces and volumes where a significant portion of the reactor's heat is generated or transported. These portions are:

A. The cermet ("fuel")**
B. The coolant tube wall
C. The toolant passages.

The portion of the core excluded consists of:

A. Void fraction in cermet (cermet not 100% of theoretical density)
B. Spacing between elements
C. "Fuel" rod cladding.

The "fuel" rods are hexagonal and consist of finely divided fissile material immersed in a continuous matrix of tungsten. The coolant passages are circular and uniformly spaced on a triangular lattice within the

---

* A 7090 Fortran IV program was written to do this work. A detailed analysis covering this is included in Reference (3).

** That portion of the core components where the major amount of heat is generated. Gamma heating rate of the clad, etc., was estimated to have a negligible effect on this study.

"fuel" rod. Only certain integral numbers of rods are permitted, according to the flats dimension, as shown in Table B-I.

TABLE B-I

Number of Rods	Equivalent Radius of Core, cm	Equivalent Radius of Core, in.	Dimension Across Flats
7	5	1.97	1.362
31	10	3.94	1.295
55	15	5.90	1.460
85	20	7.87	1.560
211	30	11.81	1.490
265	35	13.78	1.550

A smooth variation between radius, number of rods and tubes can be achieved by changing the flats dimension.

The differences between the actual core, physics model, and heat transfer model is illustrated in Figure B-1. The physics model is a right circular cylinder whose diameter and sectional area corresponds to the sectioned area of the core. The physics model includes the cermet void, spacing of elements and clad as well as the "fuel" and coolant tubes all distributed in a homogeneous manner.

B-2.2 Constituent Volume Fractions

To determine whether a critical core of given size, void fraction, and power has sufficient coolant voids available to meet thermal design conditions the voids must be alloted, according to geometry, to tube walls, tubes, element spacing, clad and void fraction in cermet. The allotment is based upon the following development.

By definition, for the actual core

$$\alpha_F + \alpha_f + \alpha_s + \alpha_c + \alpha_{oc} + \alpha_{tc} = 1.0 \qquad (1)$$

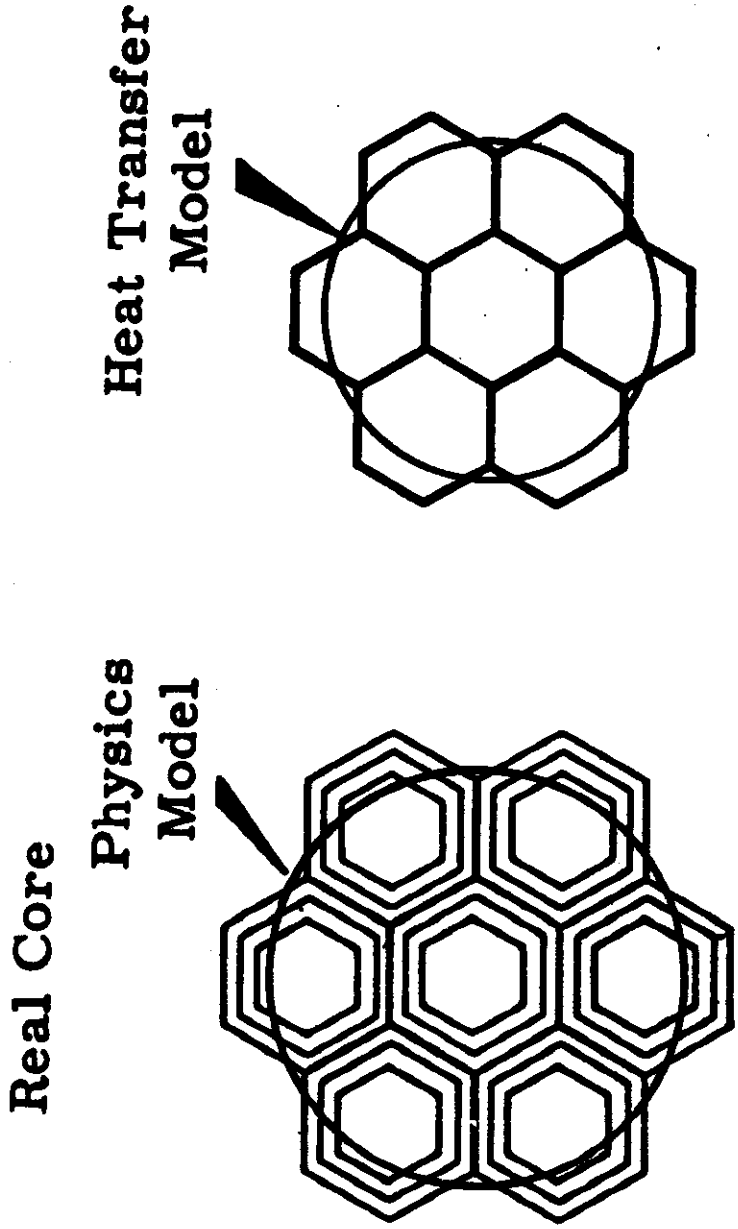

FIGURE B-1

Comparison of Real Core, Physics and Heat Transfer Models

where

α_{fr} = volume fraction of 100% dense cermet
α_v = volume fraction of cermet voids
α_s = volume fraction of element spacing
α_c = volume fraction of coolant voids
α_{oc} = volume fraction of fuel element clad
α_{tc} = volume fraction of coolant passage clad.

For a given fractional spacing, P, and flats dimension, ℓ, the area of each element, including spacing is

$$A_E = .867\ \ell^2\ (1 + P)^2 \quad . \tag{2}$$

With N fuel elements in the core, the total reactor area normal to its axis is

$$A_T \cong N\ A_E = .867\ N\ \ell^2\ (1 + P)^2 \quad . \tag{3}$$

This equation also includes the spacing area on the periphery of the core and introduces a negligible but conservative error and will be retained because of its simplicity.

The spacing area, A_s, is

$$\begin{aligned} A_s &= \text{total area minus the area of elements} \\ &= N\ [.867\ \ell^2\ (1 + P)^2 - .867\ \ell^2] \\ &= .867\ N\ \ell^2\ (2P + P^2) \quad . \end{aligned} \tag{4}$$

If t_{oc} is the clad thickness then the outer clad area, A_{oc}, is

$$\begin{aligned} A_{oc} &= .867\ N\ [\ell^2 - (\ell\ \ 2t_{oc})^2] \\ &= 3.46\ N\ t_{oc}\ (\ell - t_{oc}) \quad . \end{aligned} \tag{5}$$

For N_t tubes of inner diameter, D_{it}, in the core the coolant area, A_c, is

$$A_c = N_t\ D_{it}^2\ \pi/4 \quad . \tag{6}$$

For a tube wall thickness, t, and corresponding equivalent tube thickness, t_e, the area associated with the tube wall is

$$A_{tc} = N_t \; D_{it} \; \pi \; t_e \tag{7}$$

where

$$t_e = t + \frac{t^2}{D_{it}} \; .$$

From Equation (1) the average void area in the cermet, A_f, is

$$A_f = (A_T - A_s - A_{oc} - A_c - A_{tc}) \cdot (1 - \frac{\rho}{\rho_t}) \tag{8}$$

where

$\frac{\rho}{\rho_t}$ is the fraction of theoretical density of the cermet.

The actual cermet area at 100% of theoretical density is

$$A_F = (A_T - A_s - A_{oc} - A_c - A_{tc}) \; \frac{\rho}{\rho_t} \; . \tag{9}$$

The core is symmetric and of uniform area so the volume fractions are the ratio of the area in question to the total core cross-sectional area. Doing this obtains

$$\alpha_s = \frac{A_s}{A_T} = \frac{.867 \; N \; \ell^2 \cdot (2P + P^2)}{.867 \; N \; \ell^2 \; (1 + P)^2} = \frac{(2P + P^2)}{(1 + P)^2} \tag{10}$$

$$\alpha_{oc} = \frac{4t_{oc} \; (\ell - t_{oc})}{\ell^2 \; (1 + P)^2} \tag{11}$$

$$\alpha_c = \frac{N_t \; D_{it}^{\,2} \; \pi}{3.46 \; \ell^2 \; (1 + P)^2 \; N} \tag{12}$$

$$\alpha_{tc} = \frac{N_t \; D_{it} \; \pi \; t_e}{.867 \; \ell^2 \; (1 + P^2) \; N} \tag{13}$$

$$\alpha_f = \left(1 - \frac{\rho}{\rho_t}\right)\left(1 - \frac{A_s}{A_T} - \frac{A_{oc}}{A_T} - \frac{A_c}{A_T} - \frac{A_{tc}}{A_T}\right)$$

$$= \left(1 - \frac{\rho}{\rho_t}\right)\left(1 - \alpha_s - \alpha_{oc} - \alpha_c - \alpha_{tc}\right) \quad (14)$$

Similarly,

$$\alpha_F = \frac{\rho}{\rho_t}(1 - \alpha_s - \alpha_{oc} - \alpha_c - \alpha_{tc}) \quad . \quad (15)$$

In the physics model the neutronics are assumed to be the same for a smooth cylinder of area equal to that of a roughly cylindrical core made from hexagonal rods of length identical to the cylinder. Based on this presumption we can define a core of equivalent area (volume) to that of the actual core

$$\pi r_{eq}^2 = A_T = .867\ N\ \ell^2\ (1 + P)^2 \quad . \quad (16)$$

where r_{eq} is the radius described in Figure B-1 Physics Model. The denominators in Equations (12) and (13) can be replaced by πr_{eq}^2 and a constant.

B-2.3 Summary, Core Geometry

It is now convenient to group the volume fractions into a gross void fraction, α_G, and coolant tube and tube wall volume fraction, α_V.

$$\alpha_G = \alpha_s + \alpha_{oc} + \alpha_f + \alpha_c + \alpha_{tc} \quad (17)$$

$$\alpha_V = \alpha_c + \alpha_{tc} \quad . \quad (18)$$

For a given size reactor and associated void fraction, α_s, α_{oc}, and α_f are constant, (fixed spacing, "fuel density", and clad thickness); consequently, α_V is constant. If, however, it is desirable to design to a fixed wall or fuel temperature, α_c and α_{tc} are not constant by virtue of our ability to change tube diameter (and consequently number of tubes) to arrive at the appropriate temperature. The important thing to note is that α_V is constant during this process.

We can now mathematically define a new reactor (the heat transfer model) with 100% theoretical density "fuel," and without element clad or spacing. In this reactor

$$\alpha'_F + \alpha'_V = 1 \quad . \tag{19}$$

(Prime denotes heat transfer model.).

As a consequence of this definition

$$\alpha'_F = \frac{\alpha_F}{\alpha_F + \alpha_V} \tag{20}$$

and

$$\alpha'_V = \frac{\alpha_V}{\alpha_F + \alpha_V} \quad . \tag{21}$$

The area of the heat transfer core may now be found by requiring that the area for coolant flow be the same in the physics and heat transfer cores, i. e.,

$$\alpha_V \pi r_{eq}^2 = \alpha'_V \pi r'^2_{eq} \tag{22}$$

so that

$$r'_{eq} = r_{eq} \sqrt{\frac{\alpha_V}{\alpha'_V}} \tag{23}$$

where r'_{eq} is the radius described in Figure B-1 heat transfer model.

The physics criticality survey was first done neglecting clad material effects and assuming the clad to be void. α_G or α_F are independent but constrained so that

$$\alpha_F + \alpha_G = 1 \quad . \tag{24}$$

[redacted]

Once $\frac{\rho}{\rho_t}$, ℓ, α_G, r_{eq}, t_{oc}, t, and P are named the allotment of the remaining quantities (except α_c and α_{tc}) may be found as follows:

$$\alpha_s = \frac{2P + P^2}{(1 + P)^2} \tag{10}$$

$$\alpha_{oc} = \frac{4t_{oc} \quad (\ell - t_{oc})}{\ell^2 \quad (1 + P)^2} \tag{11}$$

From Equations (15) and (17)

$$\alpha_V = 1 - \frac{\rho_t}{\rho} \alpha_F - \alpha_s - \alpha_{oc} \tag{25}$$

α_V is broken into its constituents after determining the number and diameter of tubes by using Equations (12), (13), and (16) and consequently a trial and error process.

Finally,

$$\alpha_f = \left(1 - \frac{\rho}{\rho_t}\right)\left(1 - \alpha_s - \alpha_{oc} - \alpha_V\right) \tag{14}$$

B-3 Method Used to Handle the Core Heat Balance and Pressure Drop

We will first consider a core with uniform distribution of cooling passages of a single size, with cognizance taken of the axial power shape. Axial conduction in the cermet and tube walls is considered to be negligible in comparison with the axial heat rate in the coolant passages. Finally, the radial power profile is brought into account by zoning the core into annular volumes separated by adiabatic rings and varying the void ratio while holding the number of tubes constant and changing their diameter. * The previous and following analysis holds, except for criticality criteria, in each zone.

* This work was also performed using the computer code described in Reference (3).

B-3. 1 Heat-Transfer Equations

The axial power profile is accounted for by fitting a four-term polynomial to a normalized shape. The normalization factor is the average volumetric heat generation arrived at by taking the reactor power and dividing by the volume of "fuel." With this approach the expression for the coolant total temperature is

$$\frac{T_o}{T_{o_1}} = 1 + \frac{L\bar{q}'''}{G\xi C_p T_{o_1}}\left[A\zeta + B\frac{\zeta^2}{2} + C\frac{\zeta^3}{3} + D\frac{\zeta^4}{4}\right] \qquad (26)$$

where

L = core length
G = mass velocity
ξ = fluid flow area/fuel area
C_p = specific heat of coolant
A, B, C, D = constants in polynomial fit
ζ = dimensionless axial distance, $\frac{x}{L}$
$\bar{q}'''$ = core averaged volumetric heat generation rate
T_o = total temperature
T_{o_1} = total temperature at core inlet.

The expression developed for wall temperature is

$$\frac{T_w}{T_{o_1}} = \frac{A_{fu}\bar{q}'''}{hpT_{o_1}}\left[A + B\zeta + C\zeta^2 + D\zeta^3\right] + \frac{T_o}{T_{o_1}} \qquad (27)$$

where

A_{fu} = fuel area
h = local heat transfer coefficient
p = perimeter of tubes.

B-3. 2 System Pressure Drop

Selecting a one-dimensional compressible flow with friction and heat addition model obtains the following differential statement for total pressure:

$$\frac{d\frac{P_o}{P_{o_1}}}{\frac{P_o}{P_{o_1}}} = -\frac{\gamma M^2}{2}\left[\frac{dT_o}{T_o} + \frac{4fL}{D_{it}}\,d\zeta\right] \tag{28}$$

where

P_o = total pressure
γ = ratio of specific heats
M = mach number.

Shapiro[8] suggests the following method as valid for $M < .3$:
Mach number at any point along the passage is

$$M^2 = \left(\frac{P_{o_1}}{P_o}\right)\frac{T_o}{T_{o_1}}\left(\frac{1+\frac{\gamma-1}{2}M^2}{1+\frac{\gamma-1}{2}M_1^2}\right)^{\frac{\gamma+1}{\gamma-1}} M_1^2 \tag{29}$$

Inserting Equation (29) into Equation (28) yields

$$\left(\frac{P_o}{P_{o_1}}\right)d\left(\frac{P_o}{P_{o_1}}\right) = -\frac{\gamma}{2}M_1^2\left(\frac{1+\frac{\gamma-1}{2}M^2}{1+\frac{\gamma-1}{2}M_1^2}\right)^{\frac{\gamma+1}{\gamma-1}}\frac{T_o}{T_{o_1}}\left[d\frac{\left(\frac{T_o}{T_{o_1}}\right)}{\left(\frac{T_o}{T_{o_1}}\right)} + \frac{4fL}{D_{it}}\,d\zeta\right] \tag{30}$$

For low mach numbers the first bracketed term on the right-hand side of Equation (30) remains nearly constant. He suggests, therefore, using the mean value of

$$\left(\frac{1+\frac{\gamma-1}{2}M^2}{1+\frac{\gamma-1}{2}M_1^2}\right)^{\frac{\gamma+1}{\gamma-1}}$$

which is

$$\overline{[f(M^2)]} = \frac{1}{2}\left[1 + \left(\frac{1 + \frac{\gamma - 1}{2}M^2}{1 + \frac{\gamma - 1}{2}M_1^2}\right)^{\frac{\gamma + 1}{\gamma - 1}}\right] \tag{31}$$

Inserting the appropriate portion of Equation (29) into Equation (31) yields

$$\overline{[f(M^2)]} = \frac{1}{2}\left[1 + \left(\frac{P_o}{P_{o_1}}\right)^2\left(\frac{T_{o_1}}{T_o}\right)\frac{M^2}{M_1^2}\right] \tag{32}$$

Proceeding to find the exit total pressure using the developed equations yields

$$\left(\frac{P_{o_2}}{P_{o_1}}\right)^2 = 1 - \frac{\gamma M_1^2}{2}\left[1 + \left(\frac{P_{o_2}}{P_{o_1}}\right)^2\left(\frac{T_{o_1}}{T_{o_2}}\right)\frac{M_2^2}{M_1^2}\right]\left\{\frac{T_{o_2}}{T_{o_1}} - 1 + \frac{4fL}{D_{it}}\left[1 - \frac{L\bar{q}'''}{G\xi C_p T_{o_1}}\left(\frac{A}{2} + \frac{B}{6} + \frac{C}{12} + \frac{D}{20}\right)\right]\right\} \tag{33}$$

Solving Equation (33) for the total pressure ratio

$$\left(\frac{P_{o_2}}{P_{o_1}}\right)^2 = \frac{1 - \frac{\gamma M_1^2}{2}\left\{\frac{T_{o_2}}{T_{o_1}} - 1 + \frac{4fL}{D_{it}}\left[1 + \frac{L\bar{q}'''}{2G\xi C_p T_{o_1}}\left(A + \frac{B}{3} + \frac{C}{6} + \frac{D}{10}\right)\right]\right\}}{1 + \frac{M_1^2}{2}\left(\frac{T_{o_1}}{T_{o_2}}\right)\left(\frac{M_2}{M_1}\right)^2\left\{\frac{T_{o_2}}{T_{o_1}} - 1 + \frac{4fL}{D_{it}}\left[1 + \frac{L\bar{q}'''}{2G\xi C_p T_{o_1}}\left(A + \frac{B}{3} + \frac{C}{6} + \frac{D}{10}\right)\right]\right\}} \tag{34}$$

Inspection of Equation (34) reveals two unknowns: M_2 and P_{o_2}. An additional relationship is

$$\frac{P_{o_2}}{P_{o_1}}\sqrt{\frac{T_{o_1}}{T_{o_2}}} = \frac{\left[\frac{A}{A^*}\right]_{s, M_2}}{\left[\frac{A}{A^*}\right]_{s, M_1}} \tag{35}$$

$\left[\frac{A}{A^*}\right]$ = ratio of area at M to sonic area in an isentropic expansion. (See Reference 9 for tabulation of functions.)

B-3.3 Solution of the Heat-Transfer and Fluid Flow Equations

The system of equations is solved by assuming the quantity of fluid flow to be known and calculating, in the following order:

1. The coolant total temperature:

$$\frac{T_o}{T_{o_1}} = 1 + \frac{L\bar{q}'''}{G\xi C_p T_{o_1}}\left[A\zeta + B\frac{\zeta^2}{2} + C\frac{\zeta^3}{3} + D\frac{\zeta^4}{4}\right]$$

2. The coolant passage wall temperature:

$$\frac{T_w}{T_{o_1}} = \frac{A_{fu}\bar{q}'''}{hpT_{o_1}}\left[A + B\zeta + C\zeta^2 + D\zeta^3\right] + \frac{T_o}{T_{o_1}}$$

3. The system total pressure loss:

$$\left(\frac{P_{o_2}}{P_{o_1}}\right)^2 = \frac{1 - \frac{\gamma M_1^2}{2}\left\{\frac{T_{o_2}}{T_{o_1}} - 1 + \frac{4fL}{D_{it}}\left[1 + \frac{L\bar{q}'''}{2G\xi C_p T_{o_1}}\left(A + \frac{B}{3} + \frac{C}{6} + \frac{D}{10}\right)\right]\right\}}{1 + \frac{\gamma M_1^2}{2}\left(\frac{T_{o_1}}{T_{o_2}}\right)\left(\frac{M_2}{M_1}\right)^2\left\{\frac{T_{o_2}}{T_{o_1}} - 1 + \frac{4fL}{D_{it}}\left[1 + \frac{L\bar{q}'''}{2G\xi C_p T_{o_1}}\left(A + \frac{B}{3} + \frac{C}{6} + \frac{D}{10}\right)\right]\right\}}$$

The last is a trial-and-error solution accomplished by guessing, M_2 and calculating $\frac{P_{o_2}}{P_{o_1}}$, thence $\left[\frac{A}{A^*}\right]_{s, M_2}$ from

$$\left[\frac{A}{A^*}\right]_{s, M_2} = \left[\frac{A}{A^*}\right]_{s, M_1} \frac{P_{o_2}}{P_{o_1}} \sqrt{\frac{T_{o_1}}{T_{o_2}}}$$

calculating M_2 from standard tables, and finally reinserting M_2 to calculate a new total pressure ratio while comparing the latest value of M_2 to its previous to determine convergence. This method enables an analysis of arbitrary axial power profiles well suited to machine computation with minimal input information required.

B-4 FILM COEFFICIENTS

The correlation used in this report for determining local heat transfer coefficients is based on the bulk fluid temperature with correction for property changes by a bulk-to-wall temperature ratio proposed by Davenport, et al.[10]

$$N_{Nu} = .021 \quad N_{Re}^{.8} N_{Pr}^{.4} \left(\frac{T_w}{T_b}\right)^{-m} \left[1 + \left(\frac{x}{D}\right)^{-.7}\right] \qquad (36)$$

Barnes and Jackson[11] suggested the same form and claim m is different for different gases while Davenport's results indicate (within experimental accuracy) m = .5 for air, nitrogen, and helium. Petukhov and Popov[12] find that a single factor of the following form may be used with 5 to 7% accuracy.

$$\frac{N_{Nu_b}}{N_{Nu_{ob}}} = \left(\frac{T_w}{T_b}\right)^{-m} \qquad (37)$$

where

N_{Nu_c} = adiabatic Nusselt number.

For hydrogen and air (the two gases investigated) Petukhov and Popov find m = 0.47 and 0.5, respectively, which seems to confirm Davenport's proposition. A value of m = 0.5 was used in this investigation.

B-5 FRICTION FACTOR

The friction coefficient used and shown in Figure B-2 was 135% of the bulk average coefficient based on the bulk average Reynolds number found by Taylor and Kirchgessner[13] and confirmed by Davenport, et al.[10]

B-6 CERMET TEMPERATURES

The cermet temperatures were calculated using a truncated series equation derived in Schneider's[14] text. He solves the problem of uniform tube spacing, thermal conductivity, and heat generation with homogeneous boundary conditions. The present investigation neglects the difference in thermal conductivity of the tube, clad and contact and it assumes the thermal conductivity is that of the cermet. This was estimated to not introduce more than a 10 °F error. The thermal conductivity used is illustrated in Figures 4.7 and 4.8. Their derivation is covered in Appendix C.

B-7 CORE HEAT LOSS BY THERMAL RADIATION

The maximum core heat loss by thermal radiation from its surface was estimated to determine if loss of heat in this manner could be neglected. The core surface was assumed to be an isothermal right-circular cylinder. The two ends and cylindrical surface were considered to be at 3800 °F and made of tantalum radiating to black surroundings at zero degrees absolute. The value of emissivity was taken from Reference (15). This data was recommended as the consequence of work done in Reference (16). Utilising the above assumptions the heat loss by thermal radiation is estimated at 0.04% of the net core power at a surface to volume ratio of 4.7 ft^2/ft^3 and was neglected.

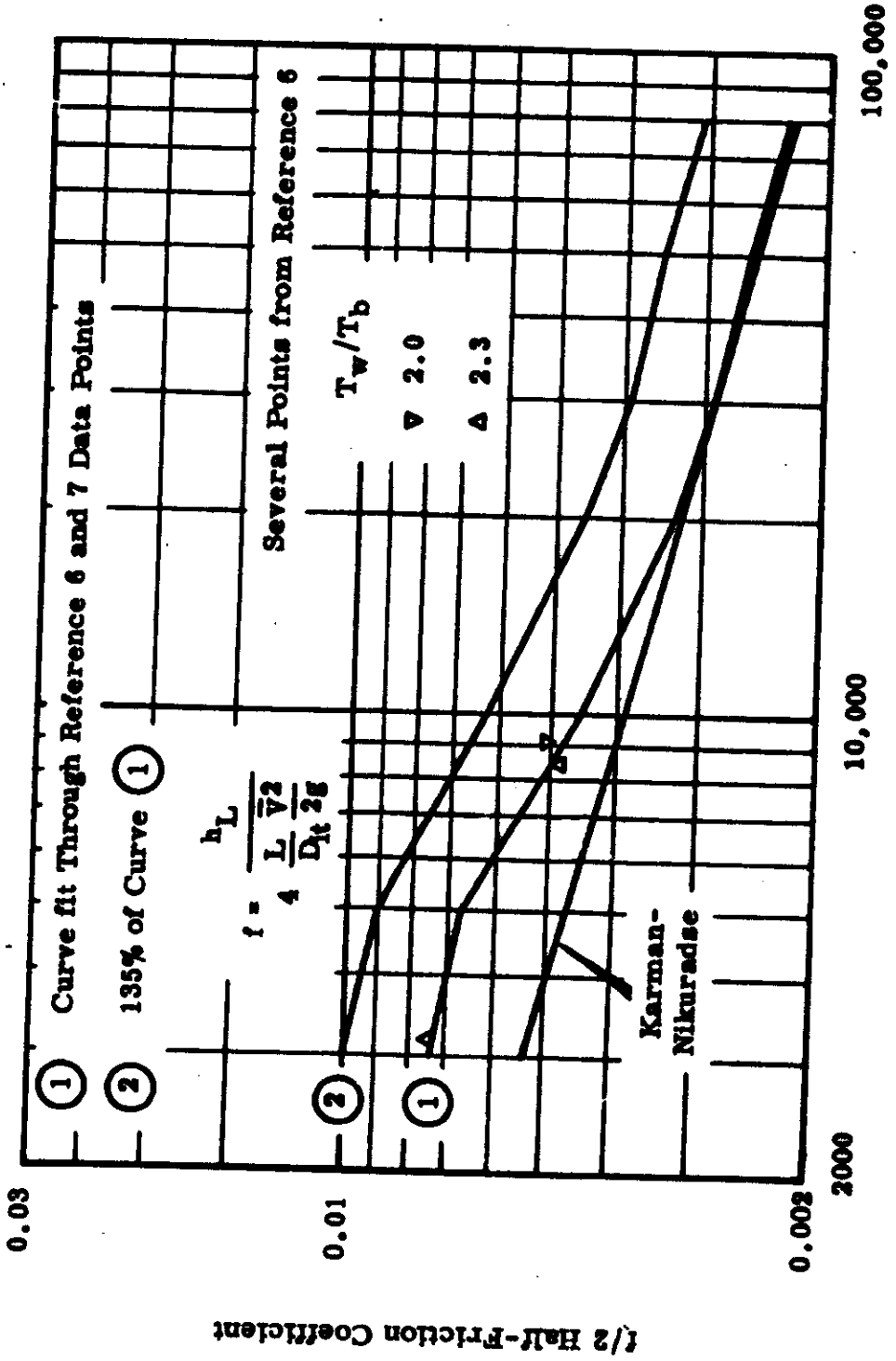

FIGURE B-2

Isothermal Bulk Average Half-Friction Coefficient

APPENDIX C

CORE MATERIALS AND COOLANT PROPERTIES

C-1 TRANSPORT PROPERTIES OF COOLANT*

The coolant used in this analysis is 10 vol% He–90 vol% Ne. Surprisingly, the experimental data available on neon's transport properties is nil. This is due, no doubt, to its relative scarcity and high cost. Because of the lack of information, the thermal conductivity and viscosity were found by two methods, depending on whether the temperature was above or below 900 °K. Below 900 °K these properties were calculated using the Lennard-Jones potential model which procedure is outlined by Bird, et al.[17] Above 900 °K, Amdur and Mason's[18] molecular beam scattering work was used. These properties were then combined according to the approximate formulae proposed by Wilke[19] and Mason and Saxena[20] for zero density gases. Their work was recently verified by Brokaw,[21] Saxena and Gandhi[22] by comparing with experimental and "exact" methods.

The results of this combination are shown on Figures C-1, C-2, and Table C-I. Satisfactory joining of the two methods is evidenced in the tables from which the curves were prepared. It is also apparent that the viscosity and thermal conductivity of the mix is very close to that of neon. Hence, fluid-dynamically, the mixture should behave much as neon.

As previously indicated all calculations of properties was done for zero pressure. Iwasa and Kestin,[23] among many other investigators, note that the behavior of transport properties of gas mixtures can be different from their pure components. In this light and since the operating pressure in this investigation is high; sufficient uncertainty was present to warrant an analysis of pressure effects on the transport properties of the mixture.

* Properties were combined using "MIX", an IBM 7090 FORTRAN IV program[4] for calculating transport properties of gases and their mixtures.

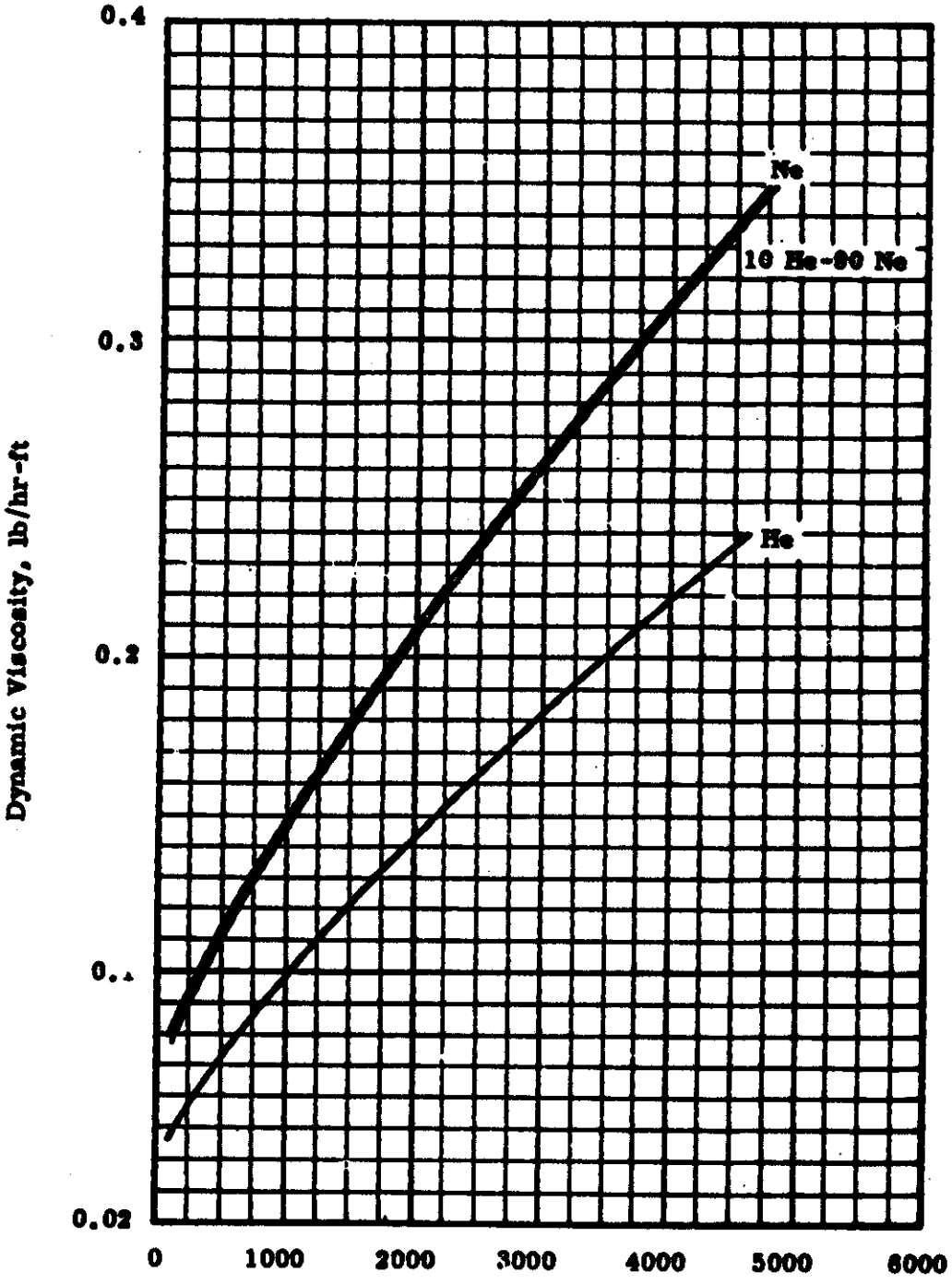

FIGURE C-1

Viscosity of He, Ne and 10 He-90 Ne Mix
Calculated with Reference (4)

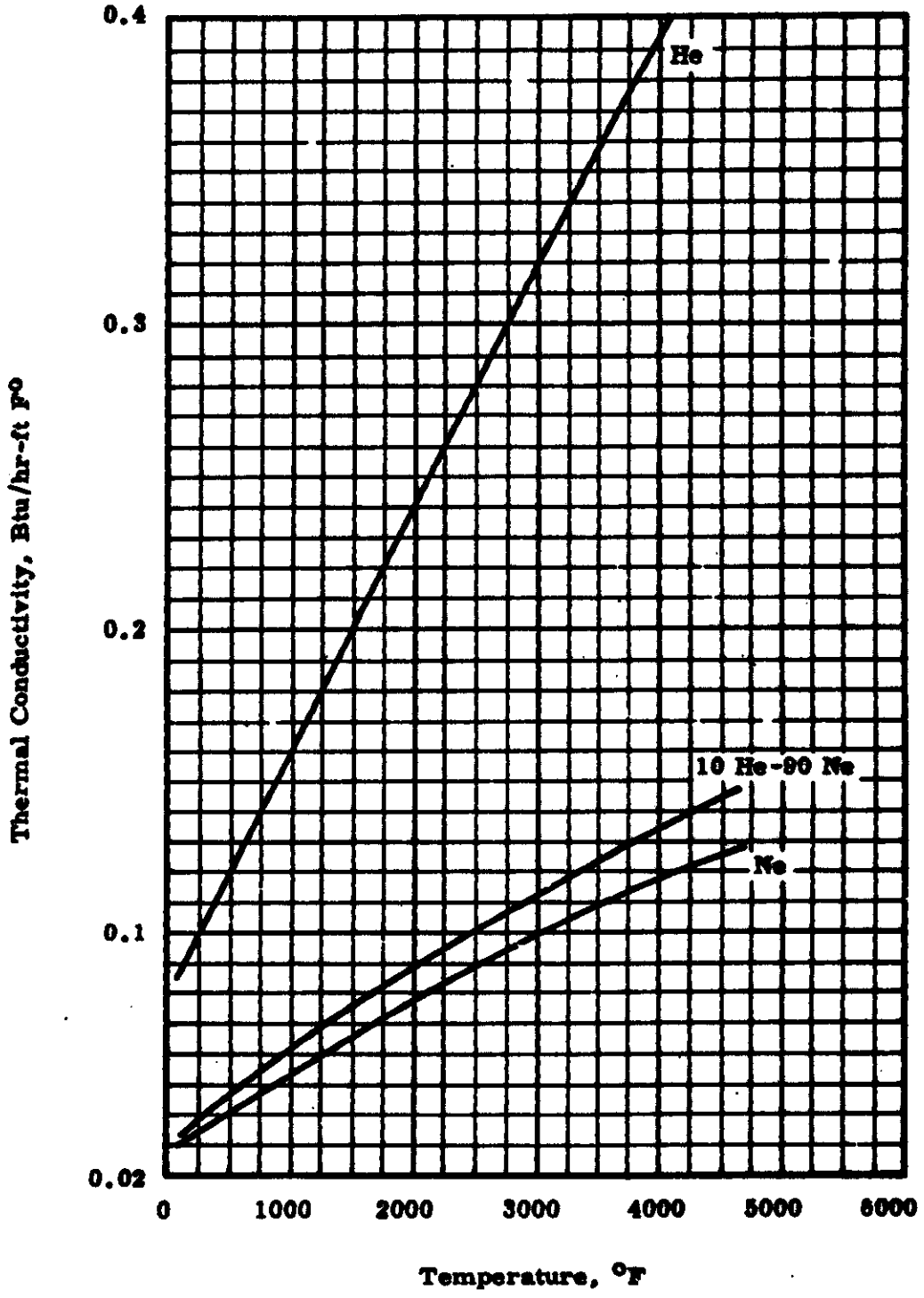

FIGURE C-2

Thermal Conductivity of He, Ne, 10 He-90 Ne Mix Calculated with Reference (4)

TABLE C-I

TABULATED TRANSPORT PROPERTIES

Temp., °F	Temp., °R	10% He–90% Ne Viscosity, lb/hr-ft	10% He–90% Ne Thermal Conductivity, Btu/hr-ft-F°	Viscosity Ne lb/hr-ft	Viscosity He lb/hr-ft	Thermal Conductivity Ne Btu/hr-ft-F°	Thermal Conductivity He Btu/hr-ft-F°
-60	400	0.0633	0.0267	0.0624	0.0396	0.0231	0.0738
140	600	0.0807	0.0344	0.0816	0.0506	0.0301	0.0942
340	800	0.0970	0.0415	0.0984	0.0621	0.0363	0.1155
540	1000	0.1126	0.0479	0.1137	0.0721	0.0419	0.1341
740	1200	0.1233	0.0537	0.1281	0.0811	0.0473	0.1508
940	1400	0.1408	0.0595	0.1421	0.0923	0.0524	0.1661
1140	1600	0.1541	0.0653	0.1556	0.0968	0.0574	0.1801
1340	1800	0.1665	0.0708	0.1675	0.114	0.0621	0.188
1540	2000	0.1795	0.0762	0.1805	0.123	0.0668	0.204
1740	2200	0.1917	0.0816	0.1927	0.133	0.0714	0.220
1940	2400	0.2034	0.0865	0.2045	0.141	0.0757	0.235
2140	2600	0.2151	0.0915	0.2163	0.149	0.0800	0.249
2340	2800	0.2265	0.0963	0.2278	0.156	0.0841	0.266
2540	3000	0.2376	0.1010	0.2390	0.163	0.0881	0.282
2740	3200	0.2487	0.1056	0.2500	0.172	0.0920	0.297
2940	3400	0.2596	0.1102	0.2610	0.179	0.0959	0.312
3140	3600	0.2700	0.1147	0.2715	0.187	0.0998	0.326
3340	3800	0.2804	0.1193	0.2820	0.193	0.1036	0.343
3540	4000	0.2910	0.1237	0.2925	0.202	0.1073	0.360
3740	4200	0.3014	0.1280	0.3030	0.209	0.1110	0.373
3940	4400	0.3105	0.1323	0.3120	0.217	0.1146	0.391
4140	4600	0.3186	0.1355	0.3200	0.225	0.1171	0.406
4340	4800	0.3280	0.1407	0.3295	0.231	0.1217	0.421
4540	5000	0.3375	0.1448	0.3390	0.238	0.1252	0.433

It is well known that aside from empirical methods (reduced properties), which are poorly documented for this system, enthalpy and internal energy departures, due to pressure, may be calculated from basic thermodynamic principles given an equation of state.[24] Amdur and Mason[18] calculated the first four virial coefficients of the virial equations of state for the pure gases from their molecular beam scattering measurements. In this paper they give methods for combining these virial coefficients to determine the equation of state for an arbitrary mixture of pure gases.

After combining, the first and second coefficients were found to be the major contributors, so the third and fourth were dropped. The investigation was conducted with this simplified equation as outlined by Lee and Sears.[24] The analysis showed the enthalpy departure to be less than 0.1% in the temperature range considered. In absence of further information this result was taken to be indicative of the effect of pressure on the remaining properties and was neglected.

C-2 THERMAL CONDUCTIVITY OF CERMETS

The thermal conductivity of sintered mixtures containing refractory materials is open to a good deal of question. Figure C-3 illustrates this proposal. One might expect a regular decrease in conductivity with increasing UO_2 content rather than the irrascible behavior portrayed in the figure. Some of the anomolies are probably due to method of specimen preparation. The controversy exists not only here but extends to the conductivity of tungsten as well; as illustrated in Figure C-4.

To resolve this situation and to extend our results to intermediate fissile contents and higher temperatures, a search of the available literature on the subject was conducted. Richter[25] and others[26] have reported on the subject in recent years. The authors consider numerous mathematical models and experiments that characterize insulating materials with no consideration of the low conductivity material immersed in a continuous matrix of relatively high conductivity. In absence of later work an equation reported by Maxwell[27] in 1860 for calculating the thermal conductivity of

[redacted]

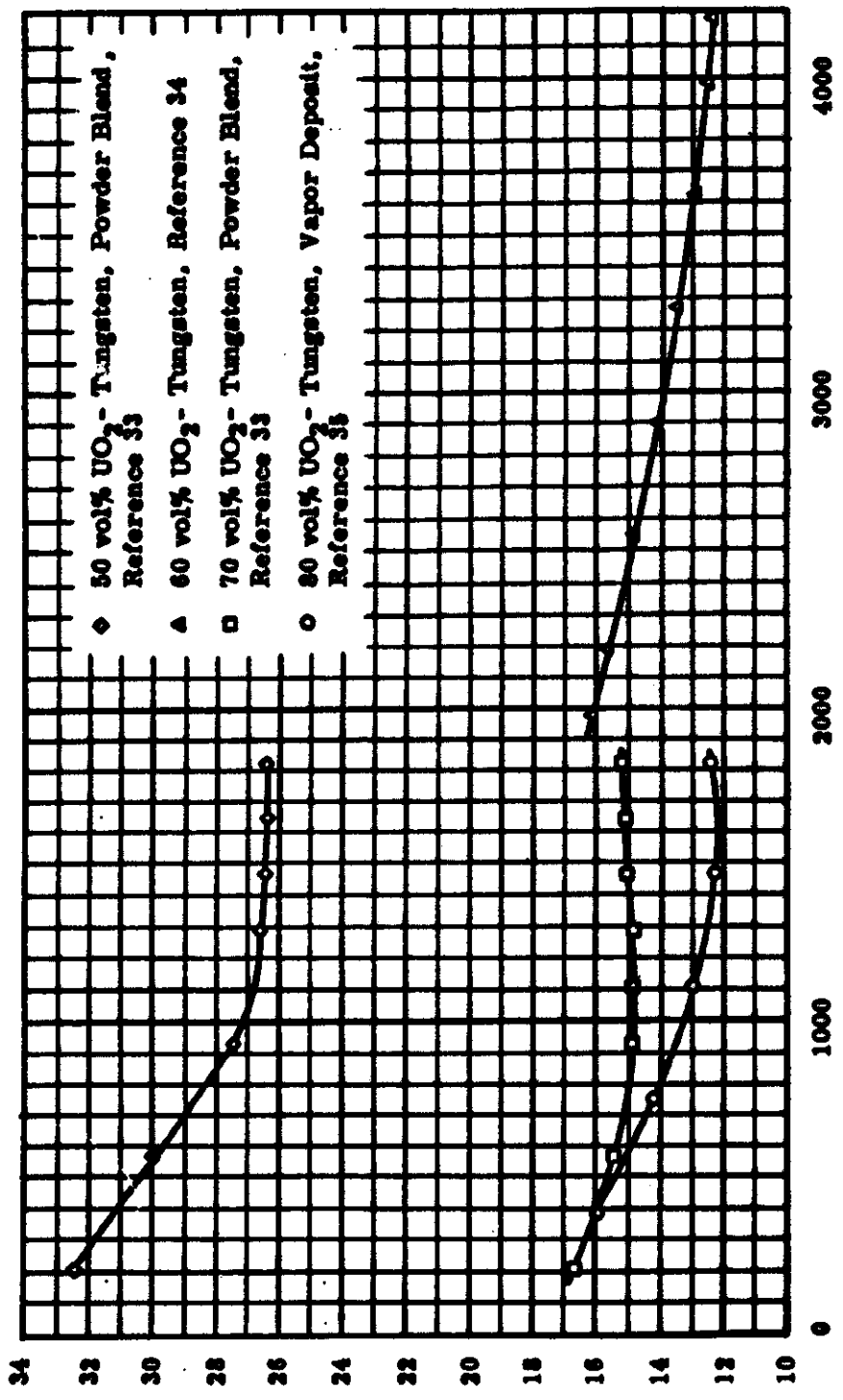

FIGURE C-3
Thermal Conductivity of UO_2-Tungsten Cermets

[redacted]

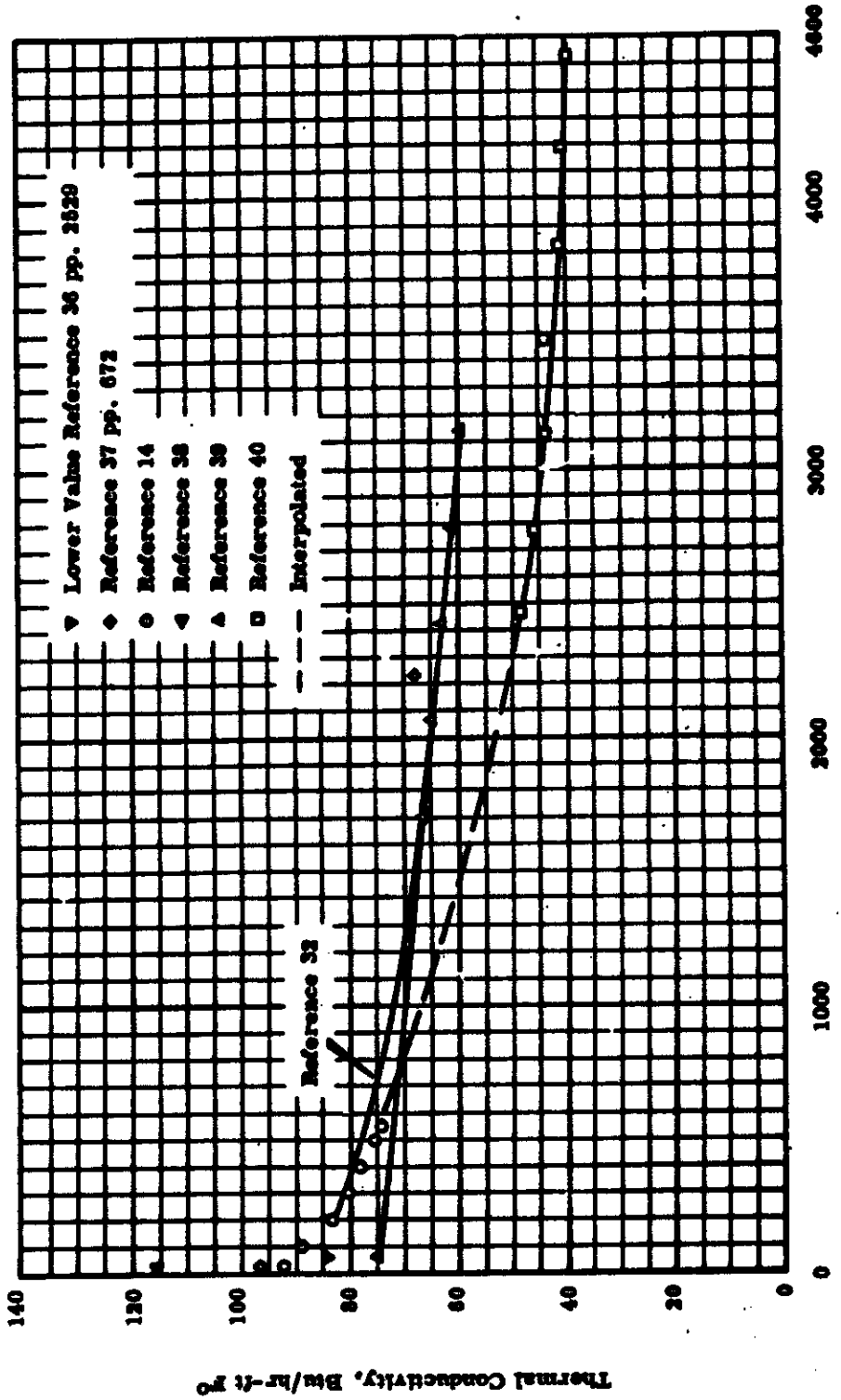

FIGURE C-4

Thermal Conductivity of Tungsten from Various Sources

gases was used. This work and the work of others along this vein is reviewed by Jakob[28] and Kulcinski.[29] Maxwell's equation is adapted by Euken (see Jakob, page 85) for the purpose at hand. The final result is:

$$\frac{K_a}{K_s} = \frac{1 - \left(1 - a\frac{K_p}{K_s}\right)b}{1 + (a - 1)\,b} \qquad (1)$$

where

K_a = apparent thermal conductivity of "mixture"
K_p = thermal conductivity of particulate matter (fissile material)
K_s = thermal conductivity of material in the matrix (tungsten)

and,

$$a = \frac{3K_s}{2K_s + K_p}$$

$$b = \frac{V_p}{V_s + V_p} \quad \text{(volume fraction of particulate matter).}$$

The equation is derived for small values of b but Euken assumes $b \leq 0.5$. Kulcinski compares this work against more recently proposed models concluding that the difference is small (<2%). For the present purposes, this relationship was used for $b \leq 0.7$ (not without some substantiation as will be discussed now).

The properties used in this portion of the study were published in the following references and are presented in graphical form in Figures C-4, C-5, and C-6.

UO_2[30]
PuN[31]
W[32]

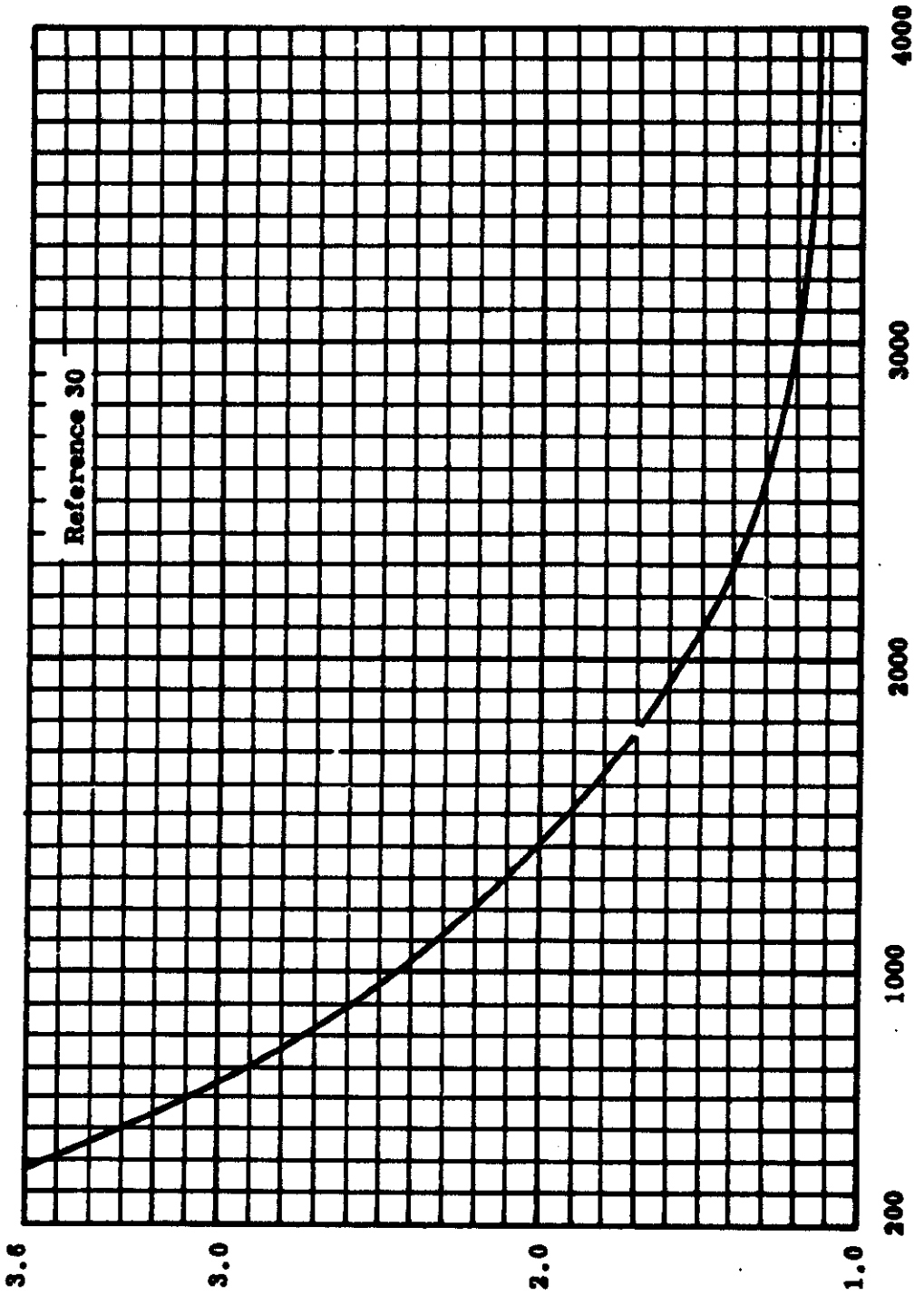

FIGURE C-5
Thermal Conductivity of UO_2

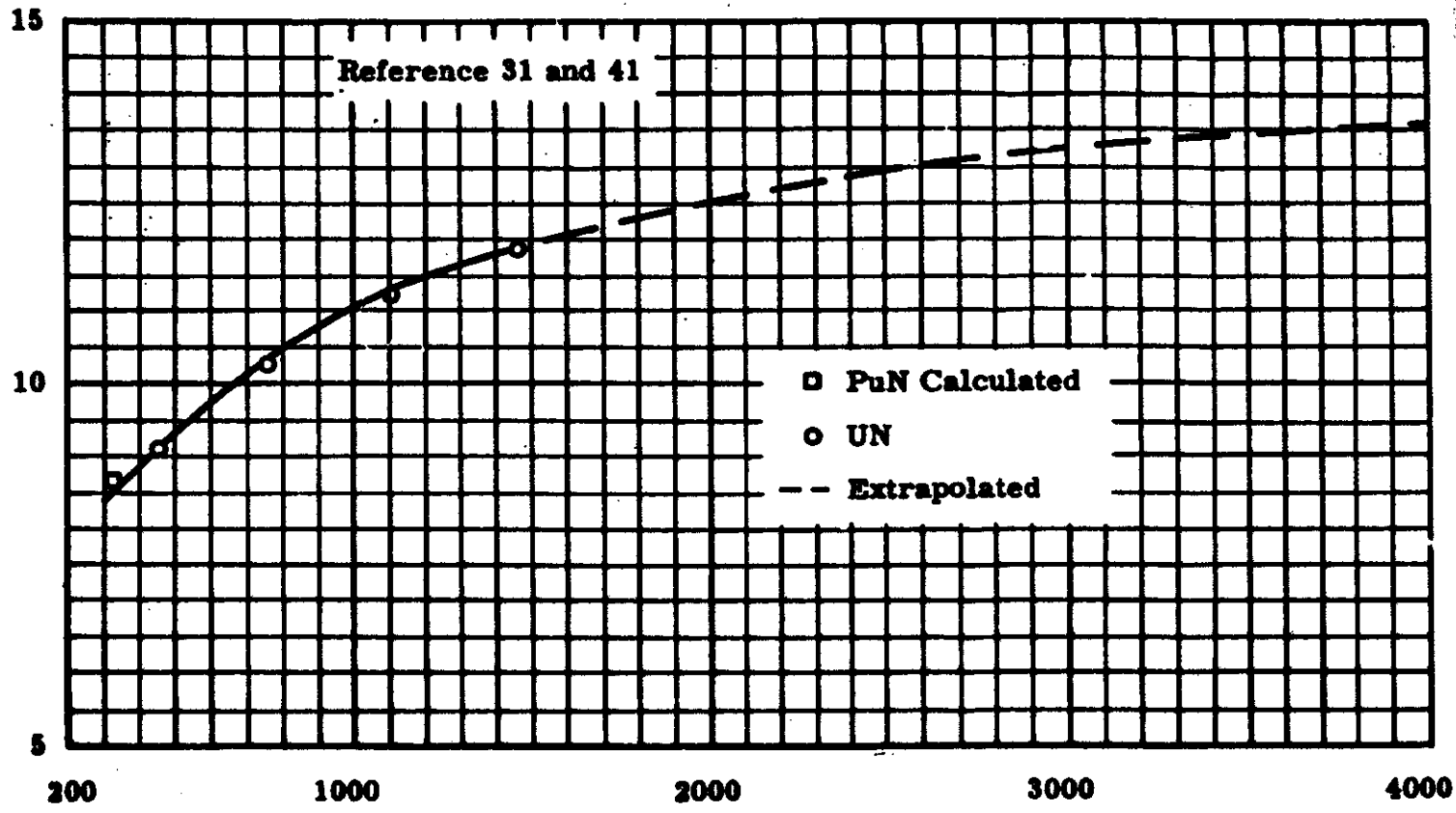

FIGURE C-6

Thermal Conductivity of UN and PuN

No experimental data are available for the thermal conductivity of PuN at elevated temperature, but the calculated value of PuN published in Reference (31) was so close to that for UN that the values used were for UN.

Rearranging "a" in Equation (1) yields:

$$a = \frac{3K_s}{2K_s + K_p} = \frac{3}{2 + \frac{K_p}{K_s}} \qquad (2)$$

Inspection of Equations (1) and (2) reveals that $\frac{K_a}{K_s}$ can be expressed as a function of $\frac{K_p}{K_s}$ for discrete values of b. The apparent thermal conductivity data in Figure C-3 was so expressed using the thermal conductivity of UO_2 given in Reference (30). This information is plotted in Figure C-7 for the values of tungsten conductivity reported in References (32), (39), and (40).

The selection of tungsten data was based on the following premise: as the thermal conductivity of UO_2 is rather small in comparison with tungsten, the ratio $\frac{K_a}{K_s}$ should not change much with temperature, $\frac{K_p}{K_s}$. The USNRDL data[40] is seen to not conform with this premise. As the dimensionless plots of $\frac{K_a}{K_s}$ versus $\frac{K_p}{K_s}$ of Reference (32) and (39) are not much different, the selection between the last two curves was based on the preponderance of data documenting the tail-up shown in Reference (32). Use of the USNRDL data would lead to a slightly higher predicted fuel temperature.

Also plotted in Figure C-7 is the prediction using Maxwell's equation and UO_2 and tungsten data as selected above. The agreement is surprisingly good being at worst about 25% at low temperatures reducing to several percent at 800 °C. The correspondence is also good for the vapor deposited material (80 vol% UO_2) where the poorest agreement might be expected due to the assumptions imposed by Maxwell's equation.

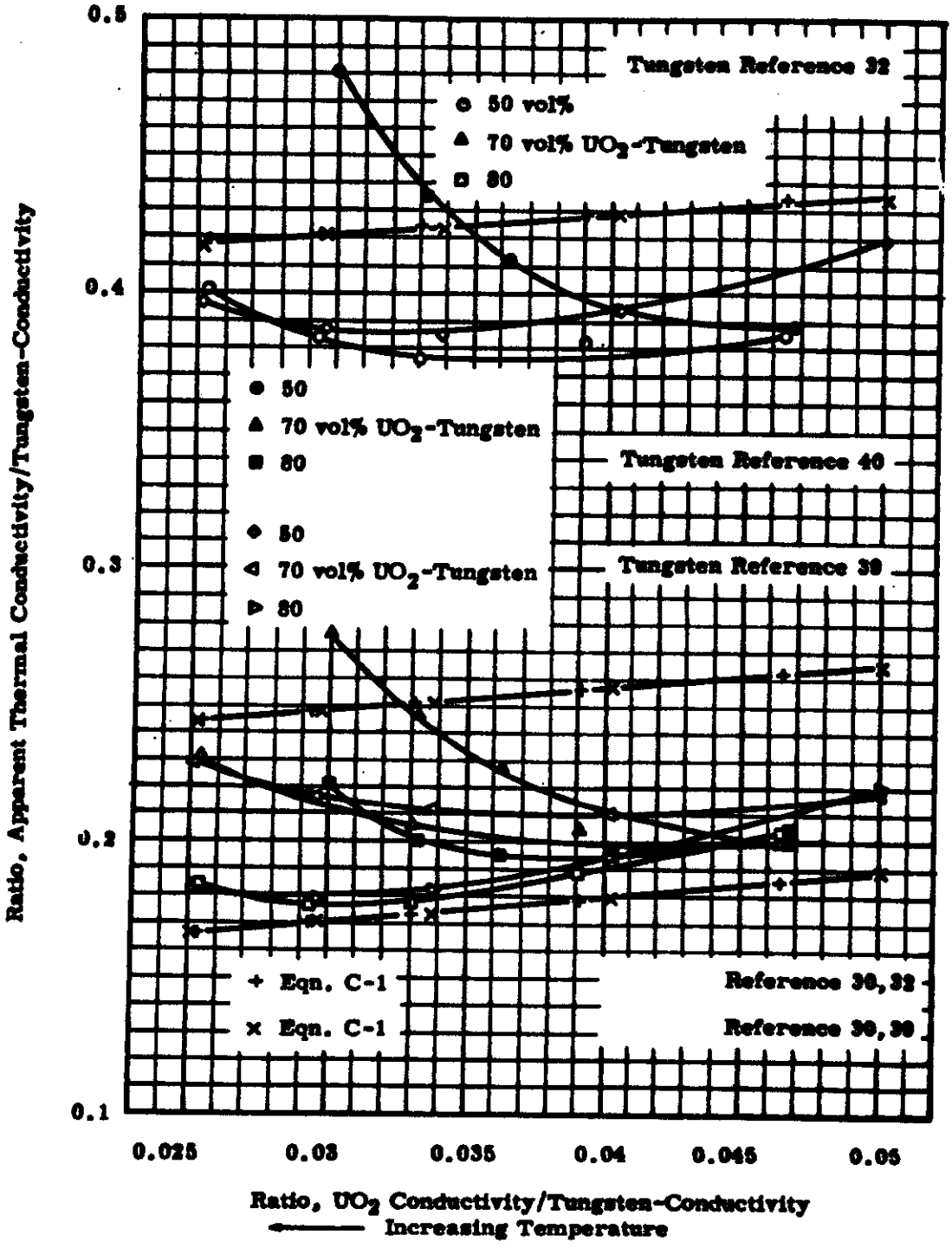

FIGURE C-7

Reduced, Calculated, and Reduced Experimental Thermal Conductivity of UO_2 Cermets Utilizing Equations C-1 and 2 and UO_2 Conductivity from Reference (30)

[redacted]

APPENDIX D

HIGH TEMPERATURE PLUTONIUM CERMET FUELS

In an efficient, compact, fast reactor, required fuels temperatures may be 2000 °C or higher. Currently, there are two plutonium fuel compounds which have the capabilities of such high temperature operation. These are PuO_2 and PuN. A tabulation of some of the properties of these compounds is given below:

Property	PuO_2	PuN
Theoretical crystal density, g/cc	11.46	14.23
Metal density, g/cc	10.12	13.41
Melting point, °C	2280.	2750.
Coefficient thermal expansion	10.9×10^{-6}	13.8×10^{-6}
Crystal system	FCC (Fluorite)	FCC (NaCl)
Ductility	Brittle	Brittle
Thermal stability	Decomposes near MP to $PuO_{1.62}$	Decomposes at 2600 °C under inert atmosphere

PuN with its higher melting point and decomposition temperature offers the potential of operating at temperatures higher than those obtainable with PuO_2. From the properties of the two compounds and from an analogy to the UO_2 and UN systems, the thermal conductivity of PuN should be significantly higher than that of the PuO_2. In addition, the high metal density of PuN (13.41 g/cc as compared to 10.12 g/cc for PuO_2) allows for more extensive exploitation of plutonium's neutronic properties in reactor and fuel designs.

The summary which follows briefly describes the compatibility of PuN with various matrix and clad materials, some irradiation experiences with PuN-W cermets, and some factors which may tend to affect PuN-W cermet performance.

[redacted]

Compatibility of PuN with Refractory Metals

Tests conducted at BMI, Columbus[42] indicate that PuN is compatible with the common iron base alloys (stainless steels and Inconel) to temperatures of 1300 °C. No reactions were observed after 100 hr under conditions of the test. The test specimens consisted of dense PuN samples encapsulated under pressure in wrought metal containers, thus assuring good contact between metal and nitride.

Two types of tests were conducted with PuN and the metals W, Mo, Ta and Nb. In one type, dense PuN was imbedded in metal powder which was then compacted under pressure; in the other, dense PuN was placed in contact, under pressure, with wrought metal containers. A summary of the results of these tests is presented in the accompanying table.

In general, powdered metals contain significant quantities of gases adsorbed on their surfaces or in the combined state in the form of monolayer type coatings. The oxygen available to the PuN from this source in tests with powdered refractory metals led to the formation of oxide layers (PuO_2 or Pu_2O_3) at the boundaries between PuN and metal particles. Interfacial regions often appeared to be composed of metal oxide-plutonium oxide layers. The most severe reactions occurred between PuN and powdered niobium, with reaction products including several nitride and oxide phases. The tests employing wrought metal containers of W, Ta, Mo, and Nb showed only slight reaction. Wrought niobium and PuN showed no signs of reaction after 50 hr at 1288 °C, but at 1650 °C and 96 hr, a slight reaction was observed between tungsten and PuN.

PuN-W Cermets

PuN–50 vol% cermets have been fabricated at Hanford[43] by pneumatic impaction of mixed powders. The best distribution of PuN in a continuous W matrix was obtained with 44-74 micron PuN particles and 5 micron tungsten particles. An impurity phase identified as PuO_2 was noted in photomicrographs of the cermet material. An irradiation experiment [44] was conducted with these

SUMMARY OF RESULTS OF COMPATIBILITY TESTS OF PuN WITH VARIOUS POTENTIAL CLADDING MATERIALS (42)

Cladding	Condition	Temperature, °C(25)	Time, hr	Results
Iron	Wrought	1300	100	No reaction
Type 304SS	Wrought	1300	100	No reaction
Inconel	Wrought	1300	100	No reaction
Molybdenum	Wrought	1288	50	No reaction
Molybdenum	Powder	1371	200	PuO_{2-x} + molybdenum oxide interface
Molybdenum	Wrought	1650	96	Reaction at interface and precipitation in molybdenum
Tantalum	Wrought	1288	50	No reaction
Tantalum	Powder	1371	200	PuO_{2-x} + tantalum oxide at interface
Tantalum	Wrought	1650	96	Precipitation (Ta_2O_5) in tantalum
Niobium	Wrought	1288	50	No reaction
Niobium	Powder	1371	200	PuO_{2-x} + niobium nitrides at interface
Niobium	Wrought	1650	96	PuO_{2-x} within original PuN particle at interface and precipitation in niobium
Tungsten	Wrought	1288	50	No reaction
Tungsten	Powder	1371	200	PuO_{2-x} at interface
Tungsten	Wrought	1650	96	Reaction at interface and free plutonium in PuN
Platinum—40 wt% rhodium	Wrought	1482	--	Eutectic formation

[redacted]

cermets, reaching a burnup of 13 x 10^{20} fissions/cm^3 at relatively low temperatures. Photomicrographs of the irradiated specimens indicated no change in the tungsten matrix but increased porosity in the PuN particles.

Effect of Dissociation Phenomena on Cermet Performance

It is generally recognized that the major, presently known, weakness of PuN as a fuel material is its relatively high vapor and dissociation pressures. Two schemes are presently being considered as means for reducing the effect of this property.. One scheme is based upon stabilization of PuN by alloying with more stable nitrides. The other involves using PuN in the form of a cermet, wherein discrete particles of the nitride would be completely contained within a continuous matrix of refractory metal. Thus, consideration of PuN as a candidate for high temperature cermet fuels is quite consistent with the effort to minimize the least desirable aspect of the material.

The actual performance of a PuN-refractory metal cermet at high temperatures will depend to a large extent upon the microstructural characteristics of the material. At 2290 ^{o}C a dissociation pressure of about 7 x 10^{-3} atm[45] has been measured for PuN and a partial pressure of plutonium on the order of 5 x 10^{-4} atm[42] can be calculated from thermodynamic data. With small, well confined particles of PuN in a cermet matrix, one would not expect damaging swelling due to the vapor or dissociation products alone. The danger to the integrity of the cermet fuel exists in the possibility of rapid migration of plutonium metal, by means of mass transport mechanisms, and nitriding of the matrix. Grain boundary diffusion mechanisms may be expected to play a dominant role, thus emphasizing the importance of microstructure to cermet performance. Fortunately, plutonium does not form low melting compounds with such refractory metals. If concentrations of free plutonium became available from dissociation reactions and migration, several mechanisms could operate to degrade the cermet. Examples of conceivable destructive mechanisms would be migration of plutonium to the surface of the cermet; development of localized hot spots in concentrations of

Pu metal under reactor operating conditions; and wedging apart of cermet grain boundaries through precipitation of plutonium metal during thermal cycling.

Investigations of the stability of PuN which have so far been reported provide little more than a starting point for more extensive and detailed analyses. This is especially true when considering possible applications of this material, where total performance is usually a function of a number of complex, interrelated parameters. The significant potential advantages of plutonium nitride as a fuel material comprise adequate justification for a thorough investigation of the properties of cermets containing this material.

REFERENCES

1. P. L. Hofmann and L. L. Maas. Nuclear Parameter Survey for Some Compact, Fast Spectrum, Cermet Reactors, HW-78756. August, 1963.
2. J. F. Fletcher. Plutonium Fueling Studies for Fast Compact Reactors, BNWL-10. January, 1965.
3. C. E. Leach. Unpublished Data. (Personal Communication). September, 1965.
4. C. E. Leach. Unpublished Data. (Personal Communication).
5. G. E. Hansen, et al. Los Alamos Group Averaged Cross Sections, LAMS-2941. Los Alamos Scientific Laboratory. July, 1963.
6. 710 Reactor Program, Progress Report No. 10, GEMP-310. General Electric Company, Cincinnati. September, 1964.
7. R. H. Norris. "Concepts of Efficiency of Heat-Transfer and Pressure-Drop Relations in Heat Exchangers," Proc. of 5th International Congress for Applied Mechanics, pp. 585-589. Cambridge, Massachusetts. 1938.
8. J. H. Shapiro. The Dynamics and Thermodynamics of Compressible Fluid Flow, vol. I, The Ronald Press Company. New York. 1953.
9. J. H. Keenan and J. Kaye. Gas Tables, John Wiley and Sons, Inc., 1957.
10. M. E. Davenport, P. M. Magee, and G. Leppert. Heat Transfer and Pressure Drop for a Gas at High Temperature, TID-13485. May, 1961.
11. J. F. Barnes and J. D. Jackson. "Heat Transfer to Air, Carbon Dioxide and Helium Flowing Through Smooth Circular Tubes Uncer Conditions of Large Surface/Gas Temperature Ratio," Journal Mechanical Engineering Science, vol. 3, no. 4. 1961.
12. B. S. Petukhov and V. N. Popov. "Theoretical Calculation of Heat Exchange and Frictional Resistance in Turbulent Flow in Tubes of an Incompressible Fluid with Variable Physical Properties," High Temperature, vol. 1, no. 1. July-August, 1963.
13. M. F. Taylor and T. A. Kirchgessner. Measurements of Heat Transfer and Friction Coefficients for Helium Flowing in a Tube at Surface Temperatures up to 5900 R, NASA-TN-D-133. Cleveland, Ohio. October, 1959.
14. P. J. Schneider. Conduction Heat Transfer, Addison-Wesley Publishing Co., Inc., Reading, Massachusetts. 1957.
15. L. Matter and D. B. Langmuir. "Emissivity and Melting Point of Tantalum," Physics Review, vol. 55, p. 743. 1939.
16. Relation Between Specific Heat and Emissivity of Tantalum at Elevated Temperatures, ASD-TDR-63-371. University of Cincinnati, Cincinnati, Ohio. July, 1963.

[redacted]

17. R. B. Bird, W. E. Stewart, and E. N. Lightfoot. Transport Phenomena, John Wiley and Sons, Inc., New York, 1960.

18. I. Amdur and E. A. Mason. "Properties of Gases at Very High Temperatures," Phys. Fluids, vol. 1, no. 5, p. 370. 1958.

19. C. R. Wilke. "Viscosity Equation for Gas Mixtures," J. Chem. Phys., vol. 18, p. 517. 1950.

20. E. A. Mason and S. C. Saxena. "Approximate Formula for the Thermal Conductivity of Gas Mixtures," Phys. Fluids, vol. 1, p. 361. 1958.

21. R. S. Brokaw. Approximate Formulas for Viscosity and Thermal Conductivity of Gas Mixtures, NASA-TN-D-2502, Lewis Research Center, Cleveland, Ohio. November, 1964.

22. S. C. Saxena and J. M. Gandhi. "Thermal Conductivity of Multicomponent Mixtures of Inert Gases," Rev. Mod. Phys., vol. 35, no. 4, p. 1022. 1963.

23. H. Iwasa and J. Kestin. "The Viscosity of Argon-Helium Mixtures," Physica, vol. 29, no. 12, p. 1345. 1964.

24. J. F. Lee and F. W. Sears. Thermodynamics, Addison-Wesley Publishing Company, Inc., Rading, Massachusetts. 1956.

25. W. Richter. Thermal and Temperature Conductivity of Porous Sintered Materials, NP-TR-1247, UKAEA Research Establishment Translation, Harwell, England.

26. A. E. Wechsler and P. E. Glaser. Investigation of the Thermal Properties of High Tempe rature Insulation Materials, ASD-TDR-63-574, A. D. Little, Inc., Cambridge Massachusetts. 1963.

27. J. C. Maxwell. "On the Motions and Collisions of Perfectly Elastic Spheres," Philosophical Magazine, vol. 19. 1860.

28. Max Jakob. Heat Transfer, vol. 1, John Wiley and Sons, Inc., New York. 1962.

29. G. L. Kulcinski, P. Wagner, and L. R. Cowder. The Effect of Porosity and Pore Interconnection on the Thermal Conductivity and Electrical Resistivity of Tungsten, LADC-6454. Los Alamos Scientific Laboratory. 1964.

30. M. F. Lyons, R. L. Straley, D. H. Coplin, B. Wiedenbaum, and T. J. Pashos. "UO_2 Thermal Conductivity at Elevated Temperatures," ANS Transactions, June, 1963, Meeting, Salt Lake City, Utah.

31. W. M. Pardue, V. W. Storhok, R. A. Smith, P. H. Bonnell, J. E. Gates, and D. L. Keller. Synthesis, Fabrication, and Chemical Reactivity of Plutonium Mononitride, BMI-1693, Battelle Memorial Institute. September, 1964.

32. T. E. Tietz and J. W. Wilson. Mechanical, Oxidation and Thermal Property Data for Seven Refractory Metals and Their Alloys, NP-11106, Lockheed Aircraft, Sunnyvale, California. 1961.

33. Progress Relating to Civilian Applications, BMI-1619. Battelle Memorial Institute. February, 1963.

34. High Temperature Materials Program Progress Report No. 25, Part B, GEMP-25B. General Electric Company, Cincinnati. July, 1963.

35. Personal communication with Don Kizer, Battelle Memorial Institute, Columbus, Ohio. November 18, 1964.

36. Handbook of Chem. and Phy., 44th Ed., Chem. Rubber Pub. 1963.

37. Reactor Handbook, Materials, vol. 1, 2nd. ed., edited by C. R. Tipton, Jr. Interscience, New York. 1960.

38. R. H. Perry, C. M. Chilton, and B. D. Kirkpatrick. Chemical Engineers Handbook, 4th ed., McGraw-Hill, New York. 1963.

39. C. H. Hampel. Rare Metals Handbook. Reinhold, New York. 1954.

40. R. L. Rudkin, W. J. Parker, and R. W. Westover. New Measurement of Thermal Conductivity, Specific Heat and Total Hemispherical Emittance of Tungsten, USNRDL-TR-419, Naval Radiological Defense Laboratory, San Francisco, California. May, 1960.

41. Controlled Atmosphere Sintering of Uranium-Mononitride, PWAC-369. Pratt and Whitney Aircraft, Middleton, Connecticut. May, 1962.

42. W. M. Pardue, V. W. Storhok, R. A. Smith, P. H. Bonnell, J. E. Gates, and D. L. Keller. Synthesis, Fabrication, and Chemical Reactivity of Plutonium Mononitride, BMI-1693. September, 1964.

43. Ceramics Research and Development Operation Quarterly Report, October-December, 1963. HW-76304.

44. Ceramics Research and Development Operation Quarterly Report, July-September, 1964. HW-81602.

45. W. M. Olson and R. N. R. Mulford. Journal of Physical Chemistry, vol. 68, pp. 1048-1051. 1964.

[redacted]